

博士論文

**Surface electromyography controlled steering assistance for
automobiles**

(表面筋電位を用いた自動車用操舵支援)

ナックピル エドリック ジョン クルズ

Nacpil Edric John Cruz

Table of Contents

Acknowledgements	4
Abstract	5
Nomenclature	7
1 Introduction	10
1.1 Motivation.....	10
1.2 Pervious research	10
1.2.1 Drivers with health conditions	12
1.2.2 Superiority of sEMG-controlled steering assistance over alternatives	14
1.2.3 Human-centered automation.....	18
1.2.4 Automotive applications of surface electromyography.....	20
1.3 Problem addressed by research	22
1.4 Steering assistance development challenges	22
1.5 Objective of research	23
1.5.1 Discussion of objective of research.....	23
1.6 Overview of subsequent chapters.....	27
2 Surface Electromyography-Controlled Steering Assistance	29
2.1 Introduction.....	29
2.2 Vehicle dynamics during operation of sEMG-controlled steering assistance.....	29
2.3 Development of surface electromyography-controlled steering	31
2.3.1 Introduction.....	31
2.3.2 Theoretical foundation.....	32
2.3.3 Implementation of surface electromyography-controlled steering	35
3 Experimental Studies with Driving Simulators	49
3.1 Experimental study I: Driving simulator validation of a steering assistance interface using surface electromyography resulting from forearm supination.....	49
3.1.1 Introduction.....	49
3.1.2 Materials	50
3.1.3 Methodology.....	55
3.1.4 Results and discussion	61
3.1.5 Conclusion	67
3.2 Experimental study II: Validation of a surface electromyography-controlled steering assistance interface using isometric contraction of biceps brachii.....	69
3.2.1 Introduction.....	69
3.2.2 Materials	71
3.2.3 Methodology.....	77
3.2.4 Results and discussion	82
3.2.5 Conclusion	86
3.3 Experimental study III: Pedestrian collision avoidance using steering assistance controlled by Myo armband	87

3.3.1 Introduction.....	87
3.3.2 Design of myo armband steering assistance interface for driving simulator	87
3.3.3 Methodology.....	88
3.3.4 Results and discussion	91
3.3.5 Conclusion	98
3.4 Improvement of response times of the sEMG interfaces	99
4 Experiments with an Actual Automobile.....	104
4.1 Experimental study I: Steering assistance of an actual automobile during different low speed turns	104
4.1.1 Introduction.....	104
4.1.2 Materials	105
4.1.3 Methodology.....	109
4.1.4 Results and discussion	111
4.1.5 Conclusions	118
4.2 Experimental study II: Steering assistance during parking of an actual automobile.....	120
4.2.1 Introduction.....	120
4.2.2 Materials	120
4.2.3 Methodology.....	124
4.2.4 Results and discussion	128
4.2.5 Conclusions	131
5 General Discussion	133
5.1 Role of the human driver in the human-centered steering assistance system.....	133
5.2 Limitations and future studies.....	134
6 General Conclusions.....	136
References	137

Acknowledgements

It is a precious opportunity to innovate automotive steering assistance for the benefit of drivers. In order to develop this technology for a production automobile, long hours of planning, discussion, tinkering, experimentation, hardware assembly, software debugging, analysis, writing, and audacity were involved. The process that culminated into this dissertation was seemingly impossible at times, though I am thankful in the utmost to my supervisor, Professor Kimihiko Nakano at The University of Tokyo, whose guidance made the process possible. Our incisive discussions have undoubtedly cultivated our research, even in the most challenging of times.

My sincerest gratitude goes to the following faculty at The University of Tokyo who provided indispensable critiques of my dissertation as defense referees: Professor Yoshihiro Suda, Associate Professor Motoki Shino, Associate Professor Hiroshi Fujimoto, and Dr. Yuji Yamakawa.

I am thankful to current and former members of the K. Nakano Laboratory who were crucial to the realization of the research for my dissertation. As a former project research associate of the K. Nakano Laboratory, Professor Rencheng Zheng at Dalian University of Technology provided many invaluable recommendations towards the implementation of experiments, the drafting of journal manuscripts, and the content of my dissertation. Research Associate, Dr. Tsutomu Kaizuka, also provided recommendations for experiments and manuscripts, in addition to addressing administrative matters such as the filing of ethics committee approval applications for the experiments. As a former doctoral candidate and current project researcher, Dr. Zheng Wang, served as a co-author on one of the first journal articles to be published on our research and assisted with the organization of this dissertation.

As one of the first lab members with whom I had the pleasure to become acquainted, Ms. Atsuko Hasegawa, our laboratory secretary, provided much needed administrative support. Furthermore, current and previous personnel of the K. Nakano Laboratory provided constructive comments and assisted with experimental trials, including Project Researcher, Dr. Bo Yang, Tanat Tunanunkul, Kriditorn Chamniprasart, and Saskia Langsdorf.

In closing, I am ever grateful for the loving support of my family, Eduardo Nacpil, Edward Nacpil, and Elmi Cruz, as well as my closest friend, Michiyo Masukawa, who all encouraged me to complete my doctoral studies in Japan. For my mother, Edna Cruz Nacpil, who is with me even until now – may the years of struggle and hope honor your memory.

January 27, 2020
NACPIL Edric John Cruz

Abstract

Automated vehicles are becoming increasingly advanced with currently available features, such as automatic parking, that allow the driver to temporarily hand over steering, acceleration, or braking to the vehicle. It is expected that highly automated vehicles in the next decade will enable the driver to focus on non-driving related tasks and to resume manual control only if the vehicle is unable to address spontaneous driving conditions such as emergency roadwork. However, despite efforts by multiple automotive manufacturers to develop automated vehicles, numerous technological challenges remain. For example, vision sensors that detect road conditions encounter interference, including extreme lighting conditions and heavy rain. Driving simulator studies demonstrate how drivers who become too reliant on automation could engage in non-driving related tasks, such as watching TV, leading to delayed steering maneuvers. The perception of highly automated vehicles as unsafe could lead to distrust and disuse of automation among drivers.

As a means of addressing overreliance on automated vehicles, human-centered automation allows shared control between the driver and the vehicle. Examples of human-centered steering assistance improve steering feel, reduce driver workload, or improve path following accuracy. Studies are lacking, however, on the applicability of human-centered steering assistance to drivers with health conditions restricting steering wheel operation to one hand. Alternatively, the current research proposes steering assistance controlled by surface electromyography (sEMG) as an instance of human-centered automation for drivers with hemiplegia and unilateral upper limb amputation. Experiments from the current research indicate that sEMG-controlled steering assistance could enable these drivers to safely perform low-speed routine turning maneuvers as well as pedestrian collision avoidance on residential roads.

The objective of the current research is to investigate the feasibility of sEMG-based interfaces as a safe means of steering assistance for drivers with hemiplegia and unilateral upper limb amputation. "Safe" in this context refers to the ability of the steering assistance to provide path following accuracy and vehicle stability to prevent accidents during turning maneuvers. Multiple sEMG-based interfaces were developed to enable the use of healthy arm muscle signals to adjust the steering wheel angle (SWA) at speeds equal to or less than the residential speed limit of 30 km/h in Japan. Drivers who are restricted by disabilities to rapid one-handed steering wheel rotation could use the proposed interfaces to avoid high shoulder joint forces that overload the shoulder muscles of healthy arms. Avoidance of carpal tunnel syndrome resulting from repeated loading of healthy arms during steering is also possible, since the interfaces do not require force input from the driver.

The current research proposed two sEMG-based interface prototypes using custom signal processing circuits and self-adhesive sEMG electrodes with conductive gel. However, in order to practically implement sEMG-based control in an actual automobile, the commercially available Myo armband replaced the prototypes, since the armband employed sEMG input with a comparable response time, as measured from the detection of muscle activation to the initiation of steering.

In low-speed steering and parking studies, the sEMG-based interfaces were comparable, overall, to some steering wheels with respect to path following accuracy. For narrow U-turns with minimum turning radii, the sEMG-based interfaces had significantly higher path following accuracy than the tested steering wheels. Using sEMG-controlled steering assistance also resulted in significantly higher vehicle stability during pedestrian collision avoidance.

By possessing path following accuracy and vehicle stability that is comparable, and in some cases superior to some steering wheel interfaces, the sEMG-controlled interfaces provided steering assistance. Future studies could evaluate the interaction between the sEMG-based interfaces and drivers with regard to workload, sense-of-agency, usability, or other parameters of interest. In the meantime, given the variety of driving scenarios and interfaces that were tested and the statistical significance of the results, the current studies are a major contribution to the development of sEMG-controlled steering assistance for the benefit of drivers with certain disabilities.

Nomenclature

a_Y	Lateral acceleration away from center of turning circle
C	Steering system compliances
d_{left}	Minimum lateral distance from tire wall closest to left parking guideline
d_{right}	Minimum lateral distance from tire wall closest to right parking guideline
e	Error in steering wheel angle of steering system model
K	Unknown parameter of function of steering system
K_O	Selected parameter of function of steering system model
G	Acceleration of gravity
g	Function multiplied by K to obtain function of steering system
g_{actual}	Function of steering system
g_{model}	Function of steering system model
i_S	Steering ratio
I_{sEMG}	Set of surface electromyography signal inputs for steering assistance interface
L	Length of automobile
M	Quintuple of sets for finite state machine control scheme
O	Center of turning circle
O_{SWA}	Set of measured steering wheel angle outputs for steering assistance interface
p	Criterion for statistical significance
Q	Set of steering wheel angles
R	Radius of curvature of turn
S	Set of physical steering wheel angle outputs for steering assistance interface
s	Unique state of steering wheel
t	Time
W_{driver}	Weight of center of gravity of driver
x	Sequence of surface electromyography signal inputs
A	Parameter to stabilize output from steering wheel angle controller
γ	Parameter to tune adaptation rate of steering wheel angle controller

Δ	Transition function for steering wheel angle output
δ_H	Steering wheel angle
δ_{Hmodel}	Steering wheel angle output of steering system model
δ_i	Inner Ackermann steer angle
δ_o	Outer Ackermann steer angle
θ	Voltage setting output for DC motor from steering wheel angle controller
λ	Output function for measured steering wheel angle output
φ	Derivative of error, e , as a function of θ
β	Vehicle slip angle
SNR	Signal-to-noise ratio
V_{sEMG}	Root-mean-square of measured surface electromyography signal
V_{noise}	Root-mean-square of baseline noise in surface electromyography signal

Chapter 1

Introduction

1 Introduction

This chapter provides the motivation for conducting the studies and summarizes the previous work of related studies. Based on this summary, problems to be addressed are presented along with the objective and challenges of the current research

1.1 Motivation

In contrast to some human-centered steering assistance investigations that do not directly address the needs of drivers with disability, the current research developed sEMG-controlled steering assistance for some drivers with disabilities that limit steering wheel operation to one hand. There is an immediate need for this type of steering assistance because common one-handed steering methods, such as steering knobs, joysticks, and one-handed steering wheel operation, require force input to the steering wheel from the driver that could lead to overuse. Even if commercially available power steering is used, some force input will always be required from the driver in order to initiate steering. Some drivers could consequently experience carpal tunnel syndrome or shoulder muscle overload resulting from one-handed steering wheel operation. By using the sEMG interface of a steering assistance system, these drivers could rotate steering wheels with one hand with a reduced risk of overuse, since no force input to steering wheels is required. In order to progress towards the realization of steering assistance that could benefit drivers with disability, studies were conducted to develop and validate sEMG-controlled steering assistance.

1.2 Previous research

Numerous studies have been dedicated to sEMG-controlled devices that rely on electrical muscle activity with the majority of studies pertaining to powered prosthetics that were introduced in the 1940's [1]–[8]. Many studies have developed upper limb prosthetics, whereas other studies developed lower limb prosthetics [9]–[24]. Efforts to develop prosthetics eventually led to commercially produced examples, including prosthetic hands such as Michelangelo and Bebionic by Ottobock SE & Co. KGaA as well as the I-Limb Ultra by Touch Bionics, Inc. [2]. Products for the lower limb include the C-leg by Ottobock SE & Co. KGaA and the Rheo Knee by Össur hf [25]. Researchers have continued to innovate the measurement of muscle activity with the possibility of improving prosthetics as in the case of real-time ultrasound imaging for muscle activity and flexible sEMG sensors [3], [26]. Advances in the outer surfaces of prosthetics have also been made, as exemplified by the work of the Yokoi-Jiang-Togo Laboratory on more realistic and flexible gloves for prosthetic hands [27], [28].

Other applications of sEMG aside from prosthetics have been considered over the years, including powered wheelchairs, flight controls, portable consumer electronics, and robotics [29]–[33]. The advancement of sEMG measurement devices has led to the Myo, the first commercial sEMG-based armband by Thalmic Labs, Inc. In contrast to the current research, which considers the application of the Myo armband for automotive steering control, there is a lack of information

concerning the application of sEMG to automobiles. Figure 1.1 summarizes the history of sEMG-controlled devices, since the 1940's [2].

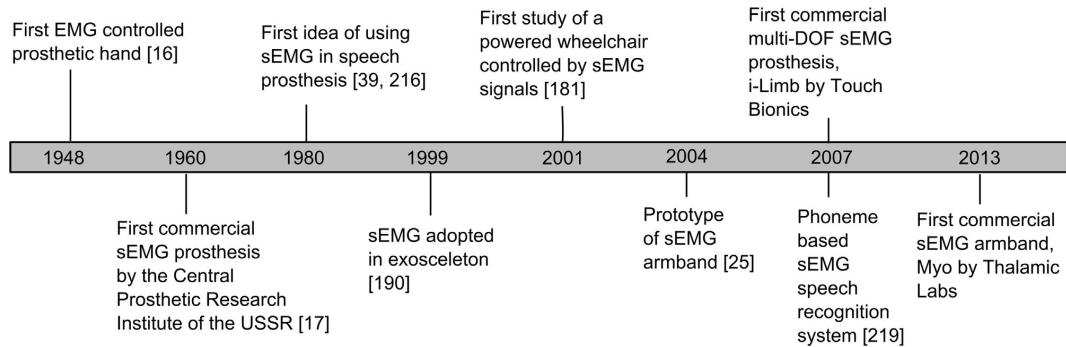


Figure 1.1 Summary of surface electromyography (sEMG) development up to the previous decade [2].

Although the current study pertains to sEMG-based steering assistance, actual automobiles typically employ steering wheels without sEMG control. Predecessors to the modern automobile, such as the steam-powered Locomobile, employed tiller steering interfaces [34]. Subsequent decades saw the advent of devices such as the “twist-wrist,” an alternative to the steering wheel that never made it to production [35]. Originally developed by the Ford Motor Company, the twist-wrist employed a set of two five-inch diameter rings. The left ring was operated by the left hand of the driver, whereas the right ring was operated by the right hand. The rings turned simultaneously so that one or both hands could be used to turn the car. Despite the development of such alternatives, automotive manufacturers continued to implement steering wheels for mass production [36].

With the development of modern autonomous vehicles, there has been some discussion regarding the transfer of steering tasks from the driver to the vehicle control system [36]. Nevertheless, the steering wheel is still a topic of current research. Past studies have addressed various aspects of the steering wheel such as steering feel, driver fatigue, and steering wheel switches [37]–[42]. In order to facilitate the driver’s access to other automobile functions apart from steering, a device known as WheelSense has been developed to recognize a driver’s hand gestures through pressure sensors at the steering wheel surface [43].

Despite the ongoing research and development of steering wheels, there have been challenges with respect to driver safety. It was observed during the 1960’s that head-on collisions resulted in thoracic injuries to the upper bodies of drivers who were not wearing seatbelts [44]. The mechanism for such injuries was the lower rim of the steering wheel that was either bent forward or broken off the hub. With the development of automotive design features such as front airbags along with improved crumple zones and steering columns, aortic ruptures, i.e. bursting of a main artery in the chest, due to steering wheel impacts have become a rare occurrence. An analysis of accidents from 1993 to 2011 revealed that frontal steering wheel deformation occurred in less than 4% of all frontal crashes where drivers wore seatbelts [45].

The possibility of driver injuries resulting from steering wheel collision during crashes has prompted researchers to investigate steer-by-wire joystick control [46]. Joysticks have also been

investigated to assist persons with disability, although some laws require a mechanical connection between the joystick and the steering column [47]. It has been pointed out, however, that replacing the steering wheel with joysticks that are legally restricted for drivers with disabilities could prevent persons without disabilities from operating a vehicle [48]. Thus, steering systems that incorporate conventional steering wheels along with assistive devices such as sEMG interfaces would be beneficial for persons with and without disability.

The rest of this chapter will begin with a discussion of different health conditions that affect driving, followed by assistive technologies that have addressed some of these disabilities. Vehicle automation options that support drivers with health conditions will then be identified and compared. Human-centered automation will be selected from among other options to improve human-automation interaction. It will then be shown how developing sEMG controlled human-centered automation is an opportunity to expand sEMG technology from the common application of driver physiology measurement. A specific research problem that could be addressed by sEMG-controlled steering assistance will then be posed. Challenges to the development of such automation in the current studies will be listed, and the objective of the studies to meet these challenges will be subsequently stated. Finally, an overview will be given on the remaining chapters that detail the theoretical and experimental steps to meet this objective.

1.2.1 Drivers with health conditions

Disability has been defined by the World Health Organization as “the negative aspects of the interaction between an individual (with a health condition) and that individual’s contextual factors (environmental and personal factors) [49].” Elderly drivers with an average age of 59.1 ± 10.4 years sometimes have stroke-induced hemiplegia as a health condition, i.e. paralysis on one side of the body, that restricts steering wheel rotation to one hand [5,6]. Unilateral upper limb amputation involving at least one missing upper limb segment on one side of the body also leads some drivers to steering with the remaining intact limb (Figure 1.2) [50], [51].

Even if drivers who have unilateral upper limb amputations or hemiplegia use one hand to rapidly rotate a steering wheel, shoulder muscle overload could result from existing overuse muscle tears in muscles such as the supraspinatus, due to a history of physical trauma that is linked with heavy labor (Figure 1.3) [52], [53].

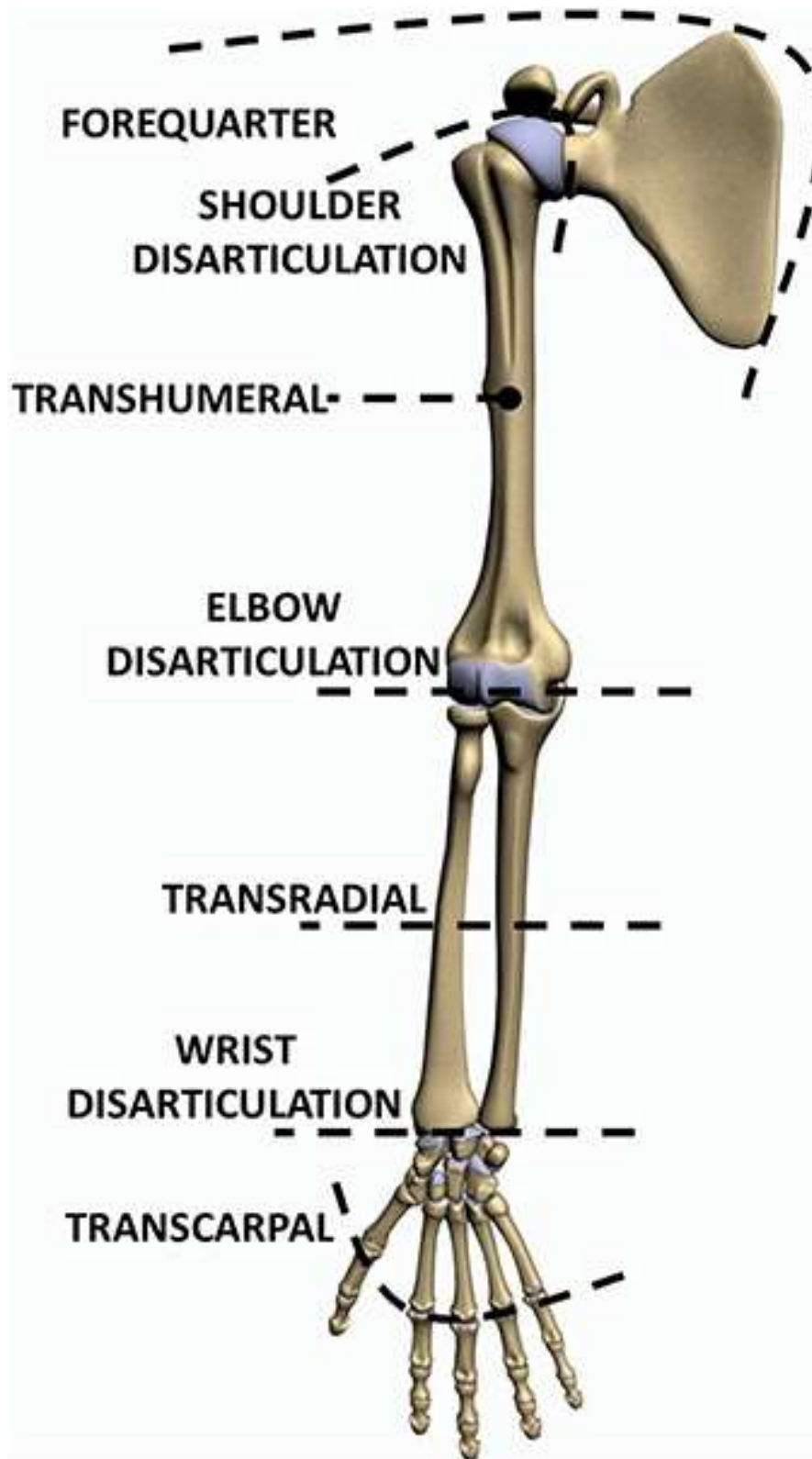


Figure 1.2 Levels upper limb amputation modified from [50].

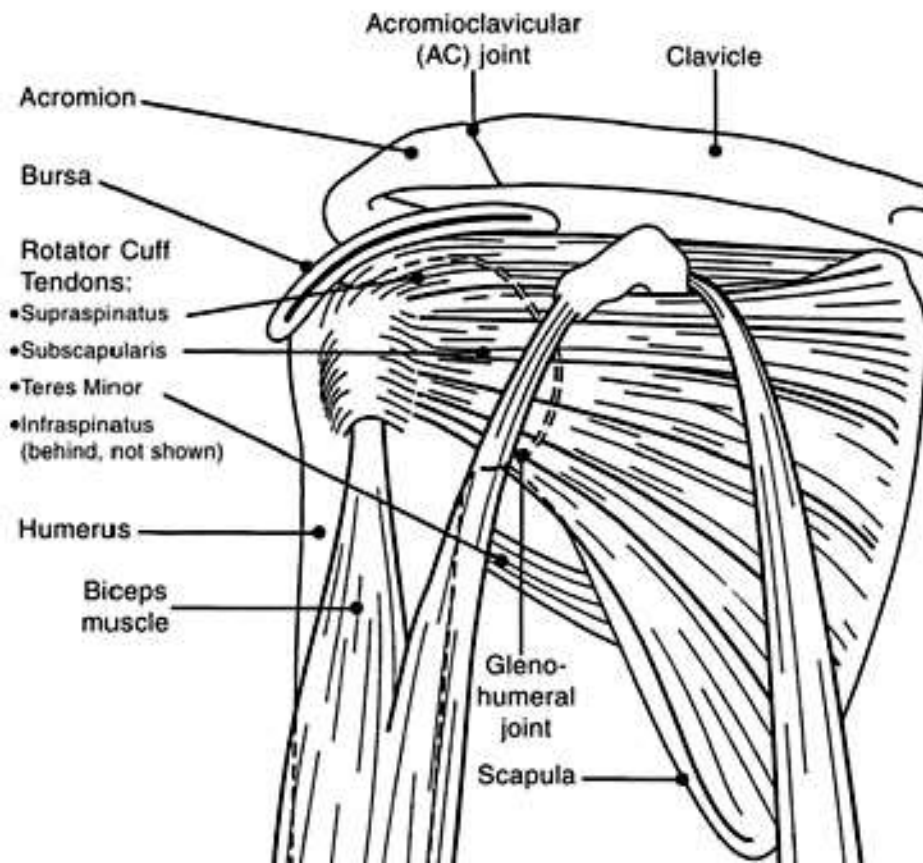


Figure 1.3 Front view of shoulder joint with muscles modified from [54]. Tears in supraspinatus or other shoulder muscles could lead to shoulder muscle overload during rapid rotation of steering wheel [53]. Proposed steering assistance interfaces sometimes relied on biceps muscle, i.e. biceps brachii, at bottom left, to produce surface electromyography signals that controlled steering wheel angle.

1.2.2 Superiority of sEMG-controlled steering assistance over alternatives

Multiple methods exist to enable hemiplegia patients and upper limb amputees to interface with steering wheels. Some drivers rely on knobs that are mounted to steering wheel rims to perform one-handed steering wheel rotation, whereas others rotate the steering wheel directly with unaffected limbs [51], [55]–[58]. Drivers with upper limb amputation may also rely on power steering for increased steering ability [57]. However, nonzero steering input force is always required from the driver to initiate steering wheel rotation. Constant application of force poses a risk of upper limb overuse in the form of carpal tunnel syndrome or shoulder muscle overload. The same problem could arise when using joysticks or other hands-on interfaces that require force input. In contrast, the proposed sEMG-based steering assistance interfaces rely on hand gestures, and therefore do not require force input.

Efficiently addressing the possibility that the driver would suddenly resume manual control is another way in which the sEMG-based interface is superior to some hands-on interfaces. Joysticks have been developed, for example, as alternatives to the steering wheel for people without health conditions and those with disability [46], [123]. As a possible interface for the steering assistance system, a joystick may be installed at a vehicle cabin location such as the center console if there is no space that is adjacent to the steering wheel [47]. When the driver resumes manual control of the steering wheel to avoid a collision, the hand of the driver requires time to traverse the distance between the steering wheel and the joystick. However, the hand would traverse a shorter distance during the operation of the sEMG-based interface as long as the hands of the driver are closer the steering wheel than the possible location of a joystick. Users could be trained to hold their hands close to the steering wheel without interfering with its automatic rotation. This problem could be avoided with accelerometers that measure forearm supination because the hands could be held close to the steering wheel. Nevertheless, accelerometry is subject to noise from vehicle vibrations and unintentional driver movement [128]. Whether the frame of reference for an accelerometer is located inside or outside of the vehicle, relative movement between the frame of reference and the accelerometer caused by vehicle acceleration could be a source of considerable noise that would render accelerometry impractical.

Other alternative interfaces that rely on motion tracking devices, such as the leap motion controller, can detect gestures such as forearm supination, thereby providing hands-free steering wheel rotation [126], [127]. As in the case of joysticks, however, the sensor for the motion tracking device may be installed in a location that adds more distance between the hands of the driver and the steering wheel, in comparison to the sEMG-based interface. Furthermore, motion sensors have limited mounting locations in the vehicle cabin, with some consumer grade sensors positioned at least 50 cm from a detectable gesture [59]. Gyros mounted on the limbs of drivers, on the other hand, could be used in the confines of a vehicle cabin, but gyro signals are subject to drift, in addition to interference resulting from vehicle vibrations [59]–[61]. Strain gauges mounted on the hands of drivers are unaffected by vehicle vibrations or drift when detecting hand gestures [60]. Thorough testing has not been performed, however, apart from driving an automobile along a straight path.

Electroencephalogram (EEG) signals could also be considered as input for steering assistance. However, an EEG-based brain–computer interface (BCI) would be subject to noise, in addition to BCI illiteracy that affects about 20% of users [129], [130]. “BCI illiteracy” refers to low user performance and the inability to operate BCIs that prevented a driver in one study from steering a farm tractor with EEG signals [131]. The neuroheadset that measured the EEG was repurposed so that the driver was able to steer the tractor with sEMG signals from the scalp. The sEMG-based interface was almost as accurate as the tractor steering wheel with respect to path following.

Steering control without limb movement may be enabled by eye gaze tracking, but the “Midas touch problem” has to be addressed so that algorithms can distinguish gazes that convey commands from gazes that merely obtain visual information [62], [63]. The current sEMG interface avoids this problem by accepting myoelectric signals rather than eye gaze input. Similarly, voice recognition could also be unable to distinguish voice commands from other types of speech.

Since sEMG electrodes could be individually mounted in selected locations, the proposed steering assistance interface could be readily adjusted to measure residual muscles from amputated limbs as in the case of sEMG-controlled prostheses [2], [64]. If an amputee prefers to grip the handle with an unaffected limb, it would be possible to measure sEMG input signals from the affected limb, provided that the myoelectric activity of residual muscles could be detected with electrodes [65]. The interface could also be used by drivers, such as patients with stroke-induced hemiplegia, with one paralyzed arm and one unaffected arm that provides sEMG signals [55], [56]. Even though spinner knobs could be mounted to steering wheels to enable one-handed operation in place of the proposed interface, some drivers with disabilities choose not to use spinner knobs [51]. Furthermore, it seems that further research needs to be conducted to determine whether or not the use of spinner knobs could cause overuse, as in the case of shoulder muscle overload that was observed when steering wheels were directly rotated with one hand [53].

Interfaces with sEMG sensors have their own set of challenges. Inaccurate measurement could result from motion artifacts due to the movement of electrode wires and relative motion between electrodes and skin surfaces [66]. Inaccuracy could also result from electromagnetic interference originating from body tissue and environmental sources, such as power lines and electronic devices [66]. However, signal filtering, bipolar electrode configurations, and non-polarized electrodes could mitigate electromagnetic interference [2], [66]. Wireless sEMG signal transmission, as featured on the Myo armband, could also reduce noise and prevent driver movements from being impeded by electrode wires [66]–[68].

Although sEMG technology is subject to its own set of potential problems, considering advantages and disadvantages of various prospective interfaces has identified sEMG-based interfaces as the most practical alternative to steering wheels. Advantages and disadvantages for interface alternatives discussed above are summarized in Table 1.1.

Table 1.1 Comparison of steering assistance interfaces with respect to advantages and disadvantages for drivers with disabilities.

Interface Type	Advantages	Disadvantages
Power steering	<ul style="list-style-type: none"> • Readily available. • Safely operated in many automobiles. • Can feature power steering or haptic guidance. 	<ul style="list-style-type: none"> • Needs to be modified for one-handed operation. • Could cause overuse injury to upper arm, even with reduced input force. • Haptic guidance force could overwhelm elderly drivers
Steering knob	<ul style="list-style-type: none"> • Easy to install. • Simple design. 	<ul style="list-style-type: none"> • Could cause shoulder muscle overload. • Repeated motion and force applied with one hand could cause carpal tunnel syndrome or rheumatoid arthritis.
Joystick	<ul style="list-style-type: none"> • Available in some countries for persons with disability. • Less upper limb movement required in contrast to steering wheel 	<ul style="list-style-type: none"> • Mounting location could increase time to resume manual control of steering wheel, if joystick fails. • Repeated motion and force applied with one hand could cause carpal tunnel syndrome or rheumatoid arthritis.
Motion sensor	<ul style="list-style-type: none"> • Touchless operation requires no force input from driver. 	<ul style="list-style-type: none"> • Requires space in cabin for driver to perform gestures.
Electroencephalography (EEG)	<ul style="list-style-type: none"> • Touchless operation requires no gestures from driver. 	<ul style="list-style-type: none"> • 20 % of users unable to operate brain-controlled interfaces.
Eye gaze tracking	<ul style="list-style-type: none"> • Touchless operation requires no force input from driver. 	<ul style="list-style-type: none"> • Difficult to design algorithm to distinguish eye movement or speech as a steering command. • Recognition depends on visibility of eyes under different lighting conditions, opening and closing of eyes, etc.
Voice recognition	<ul style="list-style-type: none"> • Touchless operation requires no force input from driver. 	<ul style="list-style-type: none"> • Slower eye movement and speech of elderly users could increase error rate. • Difficult to distinguish voice commands from other forms of speech.
Accelerometry, gyros, and strain gauges	<ul style="list-style-type: none"> • Can be used in compact space of vehicle cabin. • Touchless operation requires no force input from driver. 	<ul style="list-style-type: none"> • Gyros and acceleration signals highly sensitive to noise. • Strain gauges not tested for steering.
sEMG	<ul style="list-style-type: none"> • Touchless operation requires no force input from driver. 	<ul style="list-style-type: none"> • Highly sensitive to noise from electromagnetic interference and bodily movement.

1.2.3 Human-centered automation

SAE (Society of Automotive Engineers) International categorizes driving automation into five levels (Figure 1.4) [69]. With the exception of the experiment for pedestrian collision avoidance, the proposed sEMG interfaces are intended for vehicles with Level 1 automation, meaning that the driver shares steering control with the automated driving system. The driver issues steering commands to the system through sEMG signals generated by arm gestures, while the system automatically adjusts the steering wheel angle (SWA), i.e. the position of the steering wheel. For pedestrian collision, an sEMG interface was designed with Level 2 automation so that the vehicle controls speed, in addition to steering wheel angle.

SAE Level	Name	Description
0	No automation	Human driver always in control of driving task.
1	Driver assistance	Steering or acceleration/deceleration performed by vehicle. Driver monitors environment and takes control, if necessary.
2	Partial automation	Both steering and acceleration/deceleration performed by vehicle. Driver monitors environment, and takes control, if necessary.
3	Conditional automation	Vehicle completely controls all aspects of driving task. If necessary, vehicle requests driver to take control.
4	Higher automation	Vehicle completely controls all aspects of driving task. If necessary, driver control input can be overridden by vehicle.
5	Full automation	Vehicle completely controls all aspects of driving task. Not controlled by humans.

Figure 1.4 Levels of driving automation established by SAE international [69].

At Level 3, the drivers can allow the automated driving system to perform steering, acceleration, and braking, giving the driver freedom to focus on non-driving related tasks such as checking e-mail or reading a book. If there is a situation that cannot be addressed by the system such as manual roadwork or obscured traffic signals, the driver may be requested to intervene through visual and auditory cues provided by the system. Recent driving simulator trials have shown, however, that drivers may steer a vehicle inaccurately after manually taking over or may be delayed in response to requests to intervene [70]. Failed takeovers are therefore a potential issue for highly automated vehicles that allow the driver to be removed completely from the control loop of a steering system.

Failed takeovers could be a result of deficiency in the design of the automated driving system. Rather than keeping the driver “in the loop” by giving the driver direct control and feedback for some or all of the driving tasks, automation could lead to the isolation of the driver from feedback, since the driver may rely too much on the system by only paying attention to non-driving related tasks [71]. Since Level 4 to Level 5 automation have yet to be realized in production automobiles, drivers of contemporary automated vehicles are requested to intervene with possibly insufficient

feedback to respond appropriately to driving conditions. Consequently, as driving simulator trials have demonstrated, drivers who resume manual takeover from the non-driving related task of watching internet TV were sometimes unable to adjust steering wheels when changing lanes [70].

Negative interactions between drivers and vehicles could result from automation that is not centered on humans at Level 3 or higher. The driver is usually outside of the control loop unless the driver takes over during an emergency situation through a conventional driving interface, as shown in Figure 1.5. In contrast, conventional human-centered automation that is implemented at Level 2 trades control between the driver and the system during routine and emergency situations so that the driver always makes final driving decisions [72]. However, as demonstrated by experiments in this thesis, using a steering wheel could introduce a delay during turns requiring rapid steering wheel rotation or reduce vehicle stability through abrupt collision avoidance trajectories. In order to safely realize smooth and prompt interaction between vehicle automation and drivers with and without disability, inclusive human-centered automation is proposed. The driver always makes final driving decisions that can be transmitted to the vehicle through bio-signals, such as sEMG.

Human-centered automation = Driver always makes final driving decisions

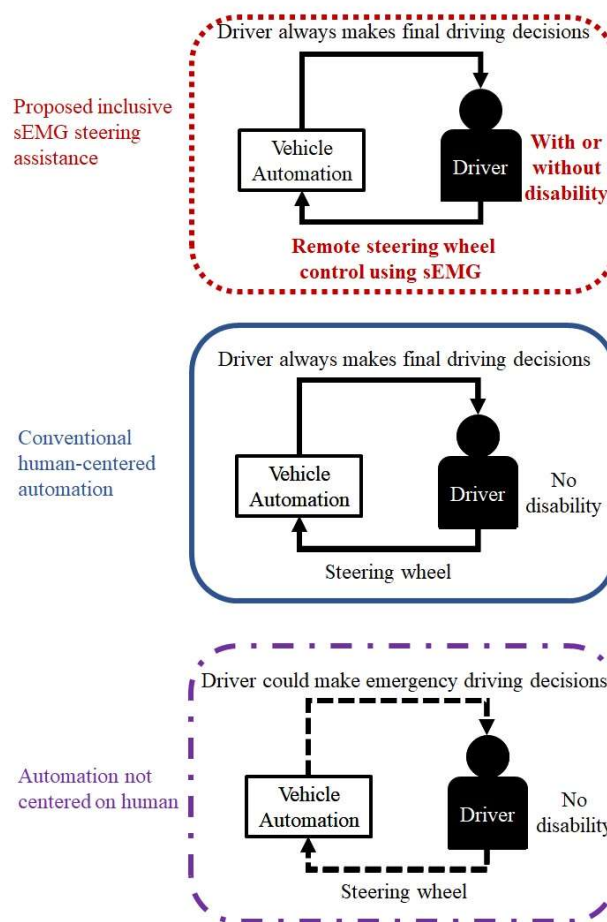


Figure 1.5 Differences between conventional steering interfaces and proposed inclusive human-

centered sEMG-based steering assistance.

There have been a few investigations into human-centered automation for steering, although the applicability of such systems to persons with disability was not discussed [73]–[75]. Nevertheless, disabilities currently affect how drivers steer actual automobiles, and thus there is an immediate need for human-centered automation that is inclusive of drivers with health conditions. Since sEMG interfaces could be developed to assist drivers with disabilities through remote steering wheel rotation, it is possible to integrate such interfaces into automation systems to provide inclusive human-centered steering, as shown in Figure 1.5.

1.2.4 Automotive applications of surface electromyography

Studies involving sEMG measurement during driving typically aim to assess the muscle activation of the driver or human factors. Examples of measured variables include: muscle activation during steering to derive steering torque, comparison of muscle activation among healthy drivers and drivers with hemiplegia, driver stress, and steering comfort [41], [55], [76]–[78].

In the past few years, some studies conducted by investigators from the current study have considered different sEMG sensor configurations for automotive control. One study proposed that multiple sEMG electrode configurations are possible to enable a driver to control steering for a driving simulator. A subsequent study selected a particular configuration of electrodes to measure biceps brachii muscles on the left and right arms. This configuration was intended to enable drivers with bilateral transhumeral amputations above the elbows to control acceleration, braking, and steering in driving simulator trials. The data generated by human participants in these trials associated the sEMG interface with path following accuracy along a circular 270° turn that was comparable to game steering wheel and pedals interface.

Path following accuracy was also measured in the current research for a sEMG-controlled steering assistance interface that was developed to reduce the risk of shoulder muscle overload from rapid steering wheel rotation and to avoid reduced steering portability. Electrical muscle signals from the biceps brachii of both arms of the driver were measured with disposable silver–silver chloride (Ag/Ag-Cl) electrodes that would eventually be converted into dry electrode armbands, if the electrode configuration was associated with path following accuracy that was comparable to a game steering wheel. Rightward supination, i.e. rightward twisting, of the right forearm produced biceps brachii sEMG signals to rotate the steering wheel to the right at a fixed steering wheel rate (SWR). The left forearm supinated, i.e. twisted leftward, to produce left arm biceps brachii sEMG signals that rotated the steering wheel to the left at the same SWR. 24 test drivers used the interface with a driving simulator to execute a U-turn, 90° turn, and 45° turn. All these rightward turns involved a change in the direction of the vehicle from a linear path to a circular path by steering to the minimum turning radius of the vehicle. If the SWR of the sEMG interface was set to 720 deg/s, which was the maximum possible value of some commercially available steering actuators, it took 0.1 s for the vehicle to transition to a circular path [79]. The sEMG interface, together with an accelerator and brake pedal, was found at the set SWR to be

comparable in path following accuracy to a game steering wheel and pedals for the 90° turn and 45° turn. On the other hand, the sEMG interface was significantly more accurate in the case of the U-turn.

For the sake of investigating alternative sEMG signal generation and to eliminate the need for hand gestures, a subsequent study redesigned the interface to accept isometric contraction of the biceps brachii as input. While acceleration and braking were controlled by pedals, the drivers operated the sEMG interface through isometric contractions of the right arm biceps brachii, i.e. the arm was held stationary at the side of the torso by grasping a handle near the location of the steering wheel with the elbow at 90° of flexion. Stroke-induced hemiplegia patients or other drivers with at least one functional arm could operate the interface. In the study with the sEMG interface that relied on forearm supination, the U-turn indicated the greatest difference between the sEMG interface and the game steering wheel. Hence, the investigators validated the path following accuracy of the redesigned sEMG interface with 16 drivers who performed two U-turns with differing radii of curvature. One U-turn had a radius equal to the minimum turning radius of the virtual car, whereas the other U-turn radius was twice as long. Since the sEMG interface maintained a constant SWA throughout the turns, steering correction through SWA adjustment was not allowed. Furthermore, steering correction with the game steering wheel was not allowed for the U-turn with the minimum turning radius, since the game steering wheel had to be turned to the maximum SWA. In order to determine if steering correction was necessary to attain path following accuracy comparable to the game steering wheel, the larger radius of the wider U-turn allowed the drivers to perform steering corrections with the game steering wheel. Since it was expected that rotations of the game steering wheel were similar in duration to steering wheels in actual cars, and therefore slower than the SWR of 720 deg/s for the sEMG interface, the SWR of the sEMG interface was reduced, in accordance with existing steering correction data from actual automobiles and driving simulations, to approximate the average SWR of steering wheels. This approximation translated to a duration of 0.5 s to steer from a linear trajectory to a circular U-turn trajectory. Any significant difference between the two interfaces would be due primarily to the fixed SWA of the sEMG interface rather than a combination of the SWR and fixed SWA. As expected, the game steering wheel had comparable path following accuracy relative to the sEMG interface for the wider U-turn. Furthermore, as expected from the previous study, the sEMG interface was significantly more accurate than the game steering wheel in the case of the U-turn with the minimum radius, since the SWR of the sEMG interface was set to 720 deg/s.

The next study conducted by the investigators builds upon the vehicle dynamics of the driving simulator experiments. All of the previously simulated driving scenarios involved circular turning trajectories performed at speeds below the residential limit of 30 km/h in some countries [80]. If these circular trajectories are followed at a constant parking speed close to 0 km/h and a constant SWA, a fully functioning steering system can be optimally designed to execute circular turns without oversteer or understeer caused by tire slippage or cornering compliances, i.e. undesired internal forces in the steering system [81], [82]. This type of vehicle motion is referred to as Ackermann steering [83], [84]. For the previously validated interfaces, path following accuracy at the minimum turning radius of a vehicle could be maximized through Ackermann steering. As explained in the next section, the most recent sEMG interface employs the Myo armband to

perform Ackermann steering when parking an actual automobile. Similar to other instances of automated parking, the maneuvers were circular paths at speeds close to 0 km/h with the front road wheels steered to their respective Ackermann steer angles to maximize path following accuracy [84]–[86]. The current study also addresses static steering at zero speed by validating a steering wheel angle controller for the sEMG interface. In contrast, the sole focus of the driving simulator studies was on dynamic steering at nonzero speed.

In order to confirm the extent to which results from the first two driving simulator studies were applicable to an actual automobile, a small-scale electric vehicle was used to replicate the steering maneuvers from the previous studies. Unlike the previous studies, however, the Myo armband was used by five test drivers instead. Overall, the Myo armband was comparable to the steering wheel with respect to path following accuracy, although the Myo armband was superior in the case of the narrow U-turn, as predicted by the previous driving simulator studies.

For another study conducted by the investigators, the Myo armband was used to steer a simulated car in two pedestrian collision avoidance scenarios. One of the scenarios had a simulated pedestrian cross the road in front of the simulated vehicle at a pedestrian crosswalk, whereas the other scenario had the same pedestrian cross the road without using a crosswalk. Results from the participation of 10 test drivers indicate that use of the Myo armband resulted in significantly greater vehicle stability, in contrast to conventional steering wheel operation and manual takeover during Level 2 vehicle automation.

1.3 Problem addressed by research

Most actual automobiles are not designed for drivers with disability. Vehicle automation could assist these drivers with driving tasks such as steering, although overreliance on automation could lead to safety issues such as failed takeovers. Human-centered automation could improve safety by giving the driver ultimate control over steering, although there are only a few studies involving human-centered automation that meets needs of drivers with disability. The current research addresses this problem by conducting experiments to validate of human-centered automation in the form of sEMG-controlled steering assistance.

1.4 Steering assistance development challenges

- Noise in the sEMG signal

Noise could result especially from the movement of electrode wires and electromagnetic sources such as power lines, neighboring muscles at the measurement site, and nearby electrical equipment [66]. Although it is possible to employ wired wet electrodes for interface prototypes, as in the case of the first two experimental studies, the wired electrodes could be improved or replaced with alternatives such as stainless-steel or capacitive electrodes with equivalent or superior measurement accuracy [87]. Therefore, the last driving simulator study and the experiments with an actual automobile utilized a commercially available Myo armband that: mounts on the forearm with an elastic band rather than adhesive, features stainless-steel electrodes

to eliminate the need for conductive gel, and relies on wireless signal transmission for improved noise reduction [67], [88].

- Design of the sEMG control scheme

Given that sEMG controlled devices have existed for decades, multiple sEMG control schemes are available, some of which originated from the development of powered prosthetics [1], [89]–[91]. As detailed in Chapter 2, the control scheme for the current studies was designed according to the driving scenarios in which the sEMG interface was applied. For the tested scenarios completed below residential driving speeds of 30 km/h with a minimum speed of 0 km/h, finite state machine (FSM) control that divides the SWA into states was chosen over other methods because FSM can be readily implemented to allow for large, rapid changes in the SWA to maximize path following accuracy in confined areas such as parking lots.

- Application of the sEMG controlled steering assistance

Given the lack of literature concerning sEMG controlled automobiles, selecting the most appropriate application for the steering assistance interface in terms of path following accuracy and safety was an open-ended endeavor. Possibilities ranged from high-speed freeway lane changes to low-speed parking. Since the motivation for developing the sEMG interfaces was to benefit drivers with health conditions that impede or prevent safe and rapid steering wheel rotation at low speeds, the interfaces were applied to rapid steering wheel rotation during residential driving, parking, and pedestrian collision avoidance.

1.5 Objective of research

The objective of the current research is to determine the feasibility of inclusive sEMG-controlled steering assistance as a form of safe human-centered automation with the following specifications:

- a) In order to prevent collision accidents during turning maneuvers, steering assistance provides path following accuracy and safer vehicle motion that are comparable or superior to steering wheel operation.
- b) Steering assistance is applicable to static and dynamic steering at vehicle speeds less than or equal to the speed limit of 30 km/h for residential roads in Japan.
- c) The inclusive interface assists drivers at age 20 and above without disabilities and with disabilities restricting steering wheel operation to one healthy arm. The steering assistance enables remote one-handed steering to address the following health conditions:
 - Hemiplegia
 - Transradial or more severe amputation affecting one arm, i.e. unilateral amputation

1.5.1 Discussion of objective of research

Hemiplegia is identified as a condition that only affects one side of the body. In contrast, upper limb amputation could affect both arms, although it is more common for upper limb amputation to affect one arm [52], [57].

Even though it is possible for drivers in the target user group to operate steering wheels directly with only one arm, use of one arm to perform everyday tasks could lead to: shoulder muscle overload, rheumatoid arthritis in hemiplegia patients, or carpal tunnel syndrome in those with upper limb amputation [53], [92], [93].

Given the above specifications for users of the proposed steering assistance, elderly drivers could also use sEMG-based interfaces. Although muscle activation could vary with age, past research has demonstrated that sEMG interfaces for devices such as robots could be feasibly operated by elderly users [94], [95]. Elderly drivers usually have characteristics that limit the ability to use alternatives to sEMG-controlled steering, and thus sEMG-based interfaces are more suitable for elderly drivers in the target user group. As listed in Table 1, these characteristics include:

- i. Speech-related issues such as increased breathing, slowed speaking pace, and increased or decreased speaking volume; results in higher recognition error rates in voice recognition interfaces [92], [93].
- ii. Slower eye movement that could increase recognition error of eye gaze tracking interfaces [94].
- iii. Decreased motor skills due to problems such as rheumatoid arthritis in one or both arms [94], [95]; lowered manual control could lead to decreased ability to interact with power steering systems or to respond to forces from haptic guidance systems [69].

In order to determine the feasibility of sEMG-controlled steering assistance, sEMG interface development was carried out according to the sequence in Figure 1.6. Experiments were conducted to confirm comparability of sEMG-controlled steering assistance to steering wheel interfaces with respect to vehicle stability and path following accuracy. The relationships between the experiments and the achievement of the research objective are described in Table 1.2.

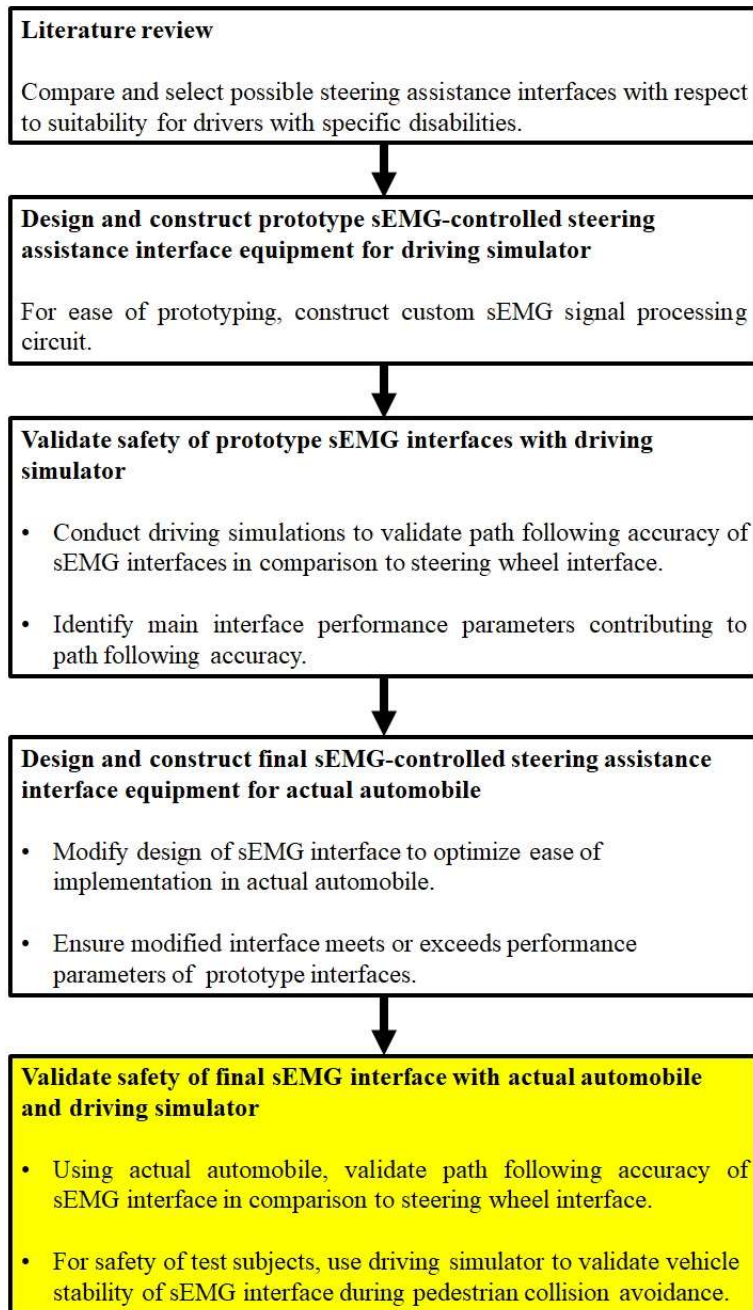
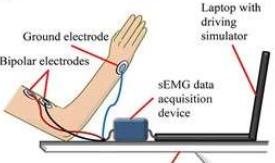
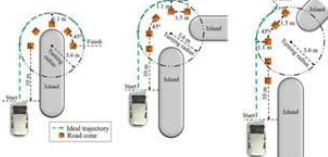
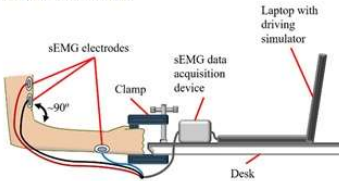
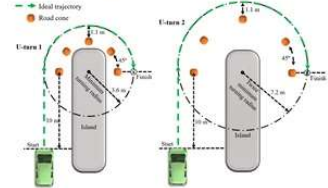
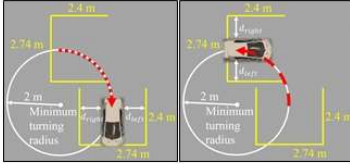
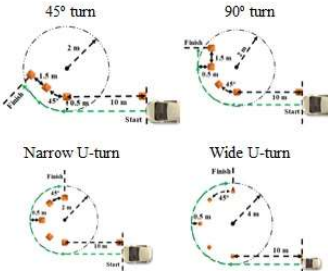
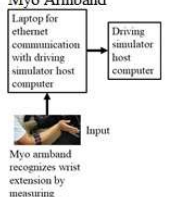
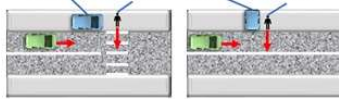


Figure 1.6 Sequence to achieve objective of current research.

Table 1.2 Summary of experiments to validate safety of sEMG-based interfaces.

Type of sEMG Interface	Driving Conditions	Significance for Research Objective	Advantages of sEMG Interfaces	Disadvantages of sEMG Interfaces
<p>Custom Interface Using sEMG from Twisting of Forearm</p>  <p>1st Experiment</p>	<p>Turning with laptop driving simulator.</p> <p>Narrow U-turn 90° turn 45° turn</p> 	<ul style="list-style-type: none"> Designed and constructed prototype sEMG-controlled steering assistance interface equipment for driving simulator. Using driving simulator, validated safety of prototype sEMG interface with regard to path following accuracy. 	<ul style="list-style-type: none"> Fast-turning sEMG-based interface had higher overall path following accuracy than steering wheel. Fast-turning sEMG-based interface significantly more accurate than steering wheel with regard to path following accuracy during narrow U-turns. 	<ul style="list-style-type: none"> Slow-turning sEMG-based interface had less accurate steering trajectories than fast-turning interface and steering wheel. Slow-turning sEMG-based interface had significantly less accurate path following accuracy than steering wheel with respect to narrow U-turn. Wet self-adhesive electrodes not as easy to put on as dry electrodes of Myo armband.
<p>Custom Interface Using sEMG from Isometric Muscle Contraction</p>  <p>2nd Experiment</p>	<p>Turning with laptop driving simulator.</p> <p>Narrow U-turn Wide U-turn</p> 	<ul style="list-style-type: none"> Design and constructed prototype sEMG-controlled steering assistance interface equipment for driving simulator. Validated safety of prototype sEMG interface with respect to path following accuracy in driving simulator. 	<ul style="list-style-type: none"> sEMG-based interface with same steering wheel rate from previous driving simulator study had highest overall path following accuracy. sEMG-based interface significantly more accurate than steering wheel with regard to path following accuracy during narrow U-turns. Hand gestures eliminated due to isometric contraction sEMG as input, instead of sEMG from forearm twisting in previous experiment. 	<ul style="list-style-type: none"> sEMG-based interface did not allow for steering for steering corrections due to fixed steering wheel angle throughout turn, but manual operation of steering wheel allowed for steering corrections. Therefore, sEMG-based interface was comparable, but not better than steering wheel with respect to path following accuracy during wide U-turn. Wet self-adhesive electrodes same as sEMG-based interface from first experiment; electrodes not as easy to put on as dry electrodes of Myo armband.
<p>Myo Armband</p>  <p>Myo armband controls steering wheel angle.</p> <p>3rd Experiment</p>	<p>Forward and reverse parking with actual automobile.</p> 	<ul style="list-style-type: none"> Designed and constructed practical human-centered sEMG-controlled steering assistance interface equipment for actual automobile. Validated feasibility of Myo armband as safe human-centered interface due to acceptable path following accuracy with actual automobile. 	<ul style="list-style-type: none"> Myo armband had dry stainless-steel electrodes that were easier to wear than wet self-adhesive electrodes of prototype interfaces. Myo armband comparable replacement for prototype interfaces, since difference in response time, as measured from muscle signal activation to initiation of steering, was negligible at 0.005 s. Acceptable path following accuracy during parking indicated Myo armband contributed to safe steering. 	<ul style="list-style-type: none"> Control algorithm to adjust steering wheel angle with Myo armband only validated for static steering. Consequently, driver had to hold steering wheel manually during, while vehicle was moving.
<p>Myo Armband</p>  <p>Myo armband controls steering wheel angle.</p> <p>4th Experiment</p>	<p>Turning with actual automobile.</p> <p>45° turn 90° turn</p> <p>Narrow U-turn Wide U-turn</p> 	<ul style="list-style-type: none"> Successfully designed control algorithm to enable dynamic steering of actual automobile with Myo armband as final version of sEMG-based steering assistance. Based on path following accuracy that was comparable overall to steering wheel, Myo armband validated as a safe form of human-centered automation. 	<p>Myo armband had significantly higher path following accuracy than steering wheel during narrow U-turn with actual moving vehicle.</p>	<p>Unlike driving simulations with prototype interface in first experiment, Myo armband had significantly lower path following accuracy than steering wheel for 90° turn due to delayed initiation of steering. However, possible to modify steering wheel angle controller. Also, drivers could be trained through formal instruction or experience to initiate turn sooner.</p>
<p>Myo Armband</p>  <p>5th Experiment</p>	<p>Pedestrian collision avoidance with large driving simulator.</p> 	<p>With respect to vehicle stability during avoidance of pedestrians, validated feasibility of Myo armband as a safe human-centered interface.</p>	<p>Myo armband enabled drivers to avoid simulated pedestrian with significantly higher vehicle stability than conventional operation of steering wheel and manual takeover from fully automated driving.</p>	<p>Control algorithm of Myo armband could be refined to improve response time with respect to initiation of steering, while maintaining superior vehicle stability relative to manual takeover and conventional steering wheel operation.</p>

1.6 Overview of subsequent chapters

The chapters that follow provide an account of the experimental methodology and results of the current research, in addition to theoretical underpinnings. Chapter 2 pertains to the vehicle dynamics and control theory that underly sEMG-controlled steering assistance during low-speed path following and vehicle stability. Chapter 3 concerns validation and experimental outcome estimation studies with driving simulators. Chapter 4 is structured in the same way to describe validation studies with an actual automobile. Finally, Chapter 5 discusses limitations, prospects for future work, and conclusions based on the results of the studies.

Chapter 2

Surface Electromyography-Controlled Steering

2 Surface Electromyography-Controlled Steering Assistance

2.1 Introduction

This chapter concerns the vehicle dynamics and control of the proposed sEMG-controlled steering assistance. Validation of the sEMG interfaces was conducted at low speeds during driving simulations and field tests. In addition to defining vehicle stability, the vehicle dynamics of oversteer and understeer are presented in Section 2.2 to explain the path following accuracy of the sEMG interfaces. A relationship is then elaborated in Section 2.3 between path following accuracy and the SWR that is controlled by the sEMG interfaces. Sections 2.2 and 2.3 provide a theoretical framework for interpreting the experimental results.

2.2 Vehicle dynamics during operation of sEMG-controlled steering assistance

With the exception of the pedestrian collision avoidance experiment, the need to rapidly rotate a steering wheel to optimize path following accuracy was observed from the low-speed dynamic steering scenarios in the current studies. Such low-speed steering scenarios involved steady-state turning, where speed, SWA and the smallest turning radius are constant. This type of vehicle motion is referred to as Ackermann steering, as illustrated in Figure 2.1 [83]. The outer and inner Ackermann steer angles relative to the center of a turn, O , with a radius of curvature, R , are designated as δ_o and δ_i , respectively [82], [83], [96]. In the case of the laptop driving simulator, the Ackermann steer angles are approximately equal. Since the steering ratio is 1:1, both angles are approximately equal to the SWA, δ_H .

There is a transient phase prior to steady-state turning in which the steering wheel rotates from the neutral position to a desired SWA. As rigorously demonstrated in Section 2.3, a briefer transient phase leads to attainment of the Ackermann steering angle in less time. Therefore, the SWRs of a steering wheel or a sEMG-based interface could be maximized to reduce the transient phase and to optimize path following accuracy. Aside from the Ackermann steer angle, a vehicle characteristic that is relevant to path following is the steering-wheel angle gradient [82]:

$$\text{steering - wheel angle gradient} = \partial\delta_H/\partial a_Y \quad (2.1)$$

A vehicle that follows a circular path at increasing speed generates centrifugal force on the vehicle that alters the turning circle and increases the lateral acceleration, a_Y , away from the center of the turning circle. Consequently, the SWA, δ_H , is adjusted to maintain a circular path. The changes in SWA and lateral acceleration constitute the steering-wheel angle gradient expressed by Equation 2.1. This equation is modified to account for two steering phenomena that affect path following accuracy, namely, oversteer and understeer. Dividing Equation 2.1 by the steering ratio of the vehicle yields the understeer gradient [82]:

$$\text{understeer gradient} = \partial \delta_H / \partial a_Y \times 1 / i_s \quad (2.2)$$

For the laptop driving simulator studies, the steering wheel ratio, i_s , for the game steering wheel is 1:1, and therefore Equation 2.2 reduces to Equation 2.1. For studies with the large-scale moving platform driving simulator and the actual vehicle, the steering wheel ratio is not 1:1, and thus Equation 2.2 applies to those studies.

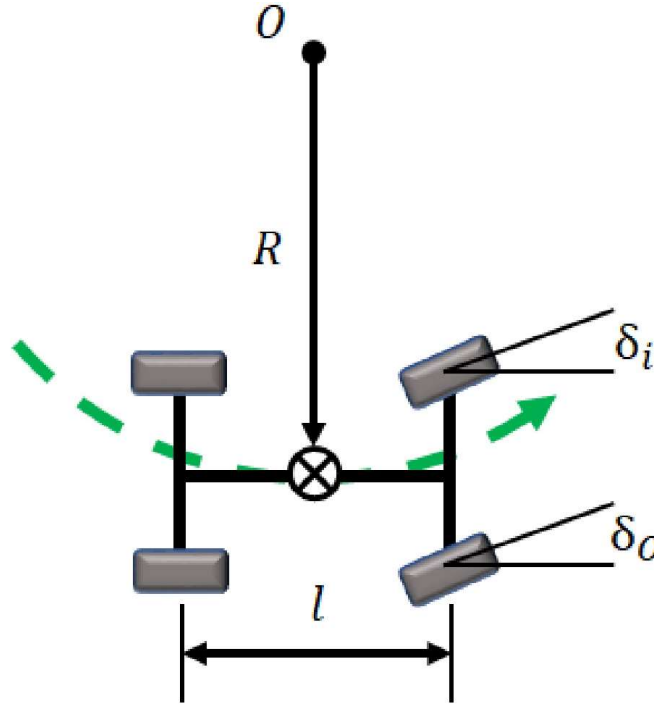


Figure 2.1 Overhead view of Ackermann steering geometry for front steering automobile [96].

Understeer can occur when the radius of the circular path increases because of increasing lateral acceleration, a_Y . Because empirical testing demonstrates that δ_H and a_Y are positively associated, the driver should increase δ_H in the direction of the turn to correct for understeer and to restore steady-state steering [83]. On the other hand, oversteer can occur when the radius of the circular path decreases because of decreasing lateral acceleration. Thus, δ_H is decreased by the driver in accordance with Equation 2.2 to restore steady-state steering. Whereas Equation 2.2 applies to the game steering wheel, the understeer gradient is modified to apply to the sEMG-based interfaces. As the steering assistance system maintains a constant SWA during steady-state steering, the understeer gradient becomes [82]:

$$\text{understeer gradient} = l \times \partial \frac{1}{R} / \partial a_Y \quad (2.3)$$

The understeer gradient is determined by the length of the vehicle, l , lateral acceleration, a_y , and the radius of curvature, R , of the circular path. Because empirical data typically indicate a negative association between $1/R$ and a_y , a decrease in a_y results in an increase in $1/R$ and thus a decrease in R [83]. In the case of oversteer, the decrease in R can be mitigated by pressing the accelerator to increase lateral acceleration, a_y . As understeer increases R , the driver corrects by releasing the accelerator or braking to decrease lateral acceleration. In summary, even though the steering wheel is held at a fixed angle, the driver could correct understeer and oversteer by longitudinally decelerating or accelerating the vehicle, respectively.

As a measure of vehicle stability, the vehicle slip angle, β , was measured by the driving simulator during the pedestrian collision avoidance experiment. The vehicle slip angle is defined as the angle between the longitudinal trajectory of the vehicle, i.e. the trajectory parallel to the x-axis in Figure 2.2, and the axis parallel to the vehicle length that intersects the center or gravity of the vehicle. Relative to the vehicle slip angle, the Myo armband was compared to steering wheel operation and manual takeover from Level 2 vehicle automation.

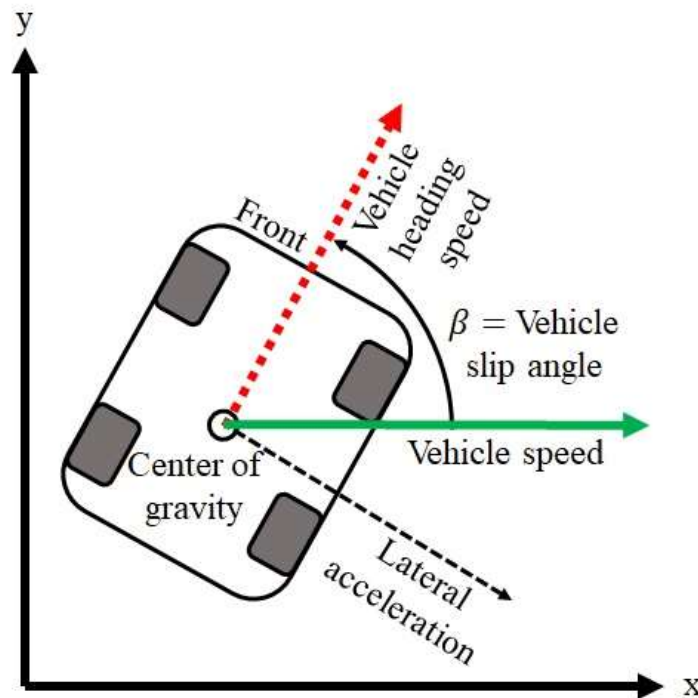


Figure 2.2 Vehicle slip angle, β , relative to center of gravity of simulated vehicle.

2.3 Development of surface electromyography-controlled steering

2.3.1 Introduction

This section begins with a discussion on the theoretical foundation for sEMG-controlled

steering based on concepts from prosthetics control and vehicle dynamics. Details are then conveyed on the implementation of sEMG-controlled steering interfaces for driving simulators and for an actual automobile.

2.3.2 Theoretical foundation

Electrical muscle signals, i.e. myoelectric activity, has been utilized over the years for various instances of myoelectric control, especially in the case of powered prosthetics [1], [30], [32]. Multiple myoelectric control schemes have been developed for sEMG controlled prosthetics (Figure 2.3). Since the current research developed steering assistance for rapid steering wheel rotation, the adaptation of a myoelectric control scheme that allows for quick transitions between SWAs was determined to be optimal. A finite state machine (FSM) control scheme was chosen from among other alternatives because it can be readily implemented by programming SWAs as states between which the steering wheel could rapidly rotate.

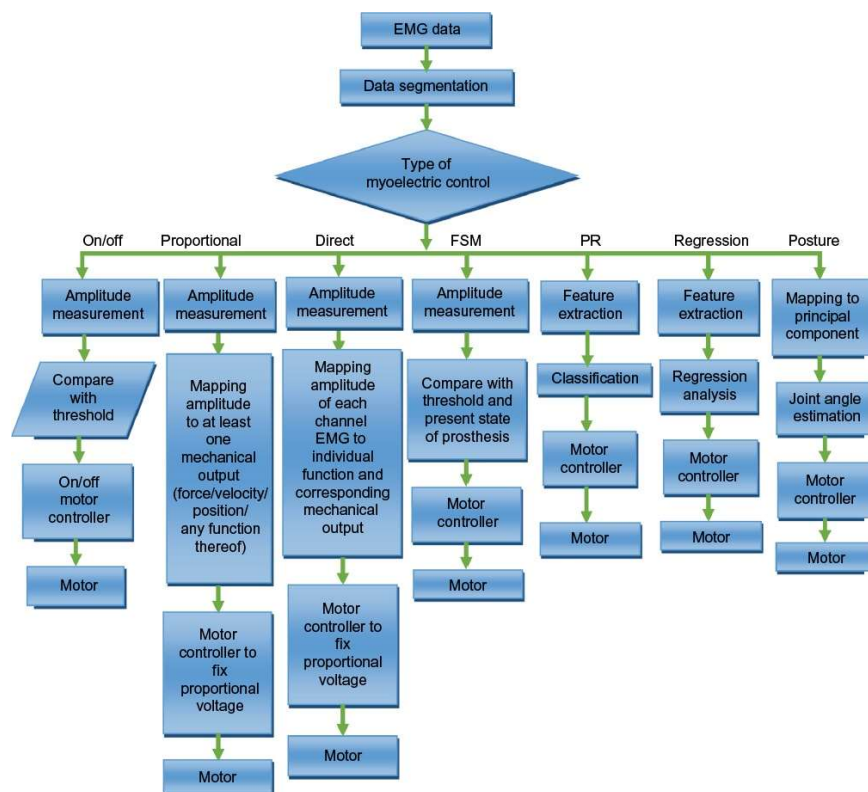


Figure 2.3 Myoelectric control schemes originally developed for powered prosthetics. Modified from [90].

The myoelectric control scheme for steering assistance can be expressed by the following quintuple sequence [97]:

$$M = (I_{sEMG}, O_{SWA}, S, \delta, \lambda) \quad (2.4)$$

where I_{sEMG} is a set of sEMG signal inputs, O_{SWA} is a set of measured SWAs provided by an encoder that is driven by the steering column, S is set of physical SWA outputs, δ is a transition function corresponding to I_{sEMG} and S , and λ is the output function corresponding to I_{sEMG} and O_{SWA} . If Q is a set of SWAs and x is a sequence of sEMG signal inputs, then δ is expressed as

$$\delta(Q, x) = \{\delta(s, x) | s \in Q\} \quad (2.5)$$

and λ is expressed as

$$\lambda(Q, x) = \{\lambda(s, x) | s \in Q\} \quad (2.6)$$

where s is a unique state of the SWA output. Take for example the sEMG interface of the first study described in Section 3.1. I_{sEMG} would consist of two elements: a left arm biceps brachii signal corresponding to left forearm supination and a right arm biceps brachii signal corresponding right forearm supination (Figure 2.4). The output, O_{SWA} , is the set of steady-state SWAs measured by the encoder, and S consists of three unique SWA states: the neutral position at 0° , the maximum leftward SWA, $-\delta_{max}$ and the maximum rightward angle δ_{max} . As indicated by the steering wheel diagram in Figure 2.4, the transition function δ indicates that the steering wheel rotates to one of the three states given the current SWA. Consequently, the output, λ , from the encoder would reflect the steering wheel rotation sequence specified by δ .

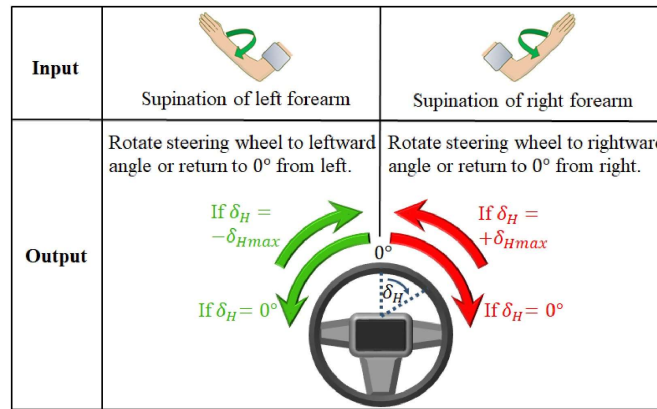


Figure 2.4 Relation between muscle contraction input and steering wheel angle output for sEMG interface that receives forearm supination as input [96].

The SWR of the FSM control scheme in Figure 2.4 is the derivative of the transition function as stated by

$$d\delta_H/dt = d\delta(Q, x)/dt \quad (2.7)$$

As hypothesized in Section 2.2, path following accuracy would increase by raising the SWR for the sEMG interface. It is possible to arrive at this hypothesis analytically by considering the steering-wheel gradient in the context of turning maneuvers that were performed for some of the studies. As described in Section 4.2, one of the maneuvers is performed during parking with Ackermann steering at a fixed SWA. The vehicle trajectory is a circular path with a radius of curvature equal to the minimum turning radius of the vehicle. For the other maneuver described in Sections 3.1 and 3.2, a vehicle transitions from a linear trajectory to a circular trajectory. The steering wheel angle increases in the direction of a circular turn as the lateral acceleration increases. Based on previously reported empirical observations of this maneuver and Equation 2.2, the steering wheel angle during Ackermann steering is linearly determined by the length of the vehicle wheelbase, the radius of the turn, cornering compliances in the vehicle steering system, and lateral acceleration on the vehicle [82], [98]:

$$\delta_H/i_S = 57.3l/R + C a_Y/G \quad (2.8)$$

where C represents empirically observed steering system compliances, G is the acceleration of gravity, and 57.3 is an empirical constant. Given that the wheelbase, l , and the radius of the turn, R , are constant, the change in SWA, δ_H , and lateral acceleration, a_Y , over time can be expressed as follows:

$$d\delta_H/i_S dt = C da_Y/G dt \quad (2.9)$$

Since an FSM control scheme controls the SWA, Equation 2.7 and 2.9 can be combined to produce

$$d\delta(Q, x)/dt = i_S C da_Y/G dt \quad (2.10)$$

As implied by Equation 2.10, rapid changes in lateral acceleration, require rapid changes in the SWA output of the steering assistance system to maintain Ackermann steering that maximizes path following accuracy along a circular path. If lateral acceleration decreases rapidly, the SWR would also have to decrease rapidly in order to prevent oversteer. On the other hand, if a rapid increase in lateral acceleration were to occur, the SWR would have to increase rapidly in order to prevent understeer. Hence, the relationship between increases in SWR and lateral acceleration over time is critical to explaining path following accuracy. Since the proposed steering assistance interfaces rely on a fixed SWA to perform parking maneuvers with an actual car, it was expected that Ackermann steering would result in negligible steering system compliances. Hence, Equation 2.8 could be modified as follows:

$$\delta_H/i_S = 57.3l/R \quad (2.11)$$

Since a FSM control scheme was used to change the SWA, Equations 2.7 and 2.8 could be

combined as follows:

$$\delta(Q, x) = i_5(57.3l/R) \quad (2.12)$$

In order to maintain Ackermann steering, Equation 2.12 states that the SWA output of the FSM control scheme must be adjusted to a constant steering wheel angle to maintain a constant turning radius.

Equations 2.10 and 2.12 respectively represent the dynamic and static relationships between the proposed sEMG-controlled steering assistance systems and the dynamics of front steering vehicles. As a result of the integration of previous work on vehicle dynamics and powered prosthetics, these equations contribute to the theoretical framework underlying sEMG-based vehicle control. Applications of this type of control are exemplified by the Ackermann steering studies in the next chapter. However, since the vehicle stability of sEMG-controlled steering assistance was validated through a study involving dynamic steering for pedestrian collision avoidance in a driving simulator, as described in Chapter 3.3, Equations 2.10 and 2.12 do not apply to this study.

2.3.3 Implementation of surface electromyography-controlled steering

The subsections that follow describe the progression from prototype sEMG equipment used for controlling the steering of a driving simulator to commercially available sEMG equipment that controlled an actual automobile. General consideration is given to designing a sEMG-based steering interface. Accounts are then given about the data acquisition methods of the prototype and production sEMG interface devices.

2.3.3.1 Designing a surface electromyography-based interface

Designing a sEMG-based interface involves the assignment of specific gestures to operations of controlled devices. Gestures are associated with sEMG signals that serve as user input for the interface. Past studies have used sEMG resulting from particular gestures to control the operation of different types of devices [30], [89], [99]. Researchers in one study decided to assign 26 different movements of the hand and arm to keyboard functions [89]. With regard to the operation of a model vehicle, pronation and supination of the right forearm corresponded to left turns and right turns, respectively [99]. The control systems for the model vehicle and the keyboard utilized matrix-type electrodes in conjunction with the Monte Carlo Method to select the optimum quantity and position of the electrodes. Therefore, knowledge of physiology or anatomy is not required to mount the electrodes onto test subjects. The tradeoffs are: the time and effort involved in the fabrication of the electrode matrix, the acquisition or construction of a multichannel sEMG DAQ (data acquisition device), and the development of signal processing algorithms to carry out the Monte Carlo Method calculations.

For the prototype sEMG interfaces used in the first two experiments of the current research, such tradeoffs are not necessary to achieve rapid steering wheel rotation, and thus the more

traditional approach involving physiological and anatomical knowledge is used, as shown in Figure 2.5. Two differential electrodes and one ground electrode measure the sEMG signal of an arm muscle. Electrode placement is determined under the guidance of recommendations from SENIAM (Surface Electromyography for the Non-Invasive Assessment of Muscles) [100].

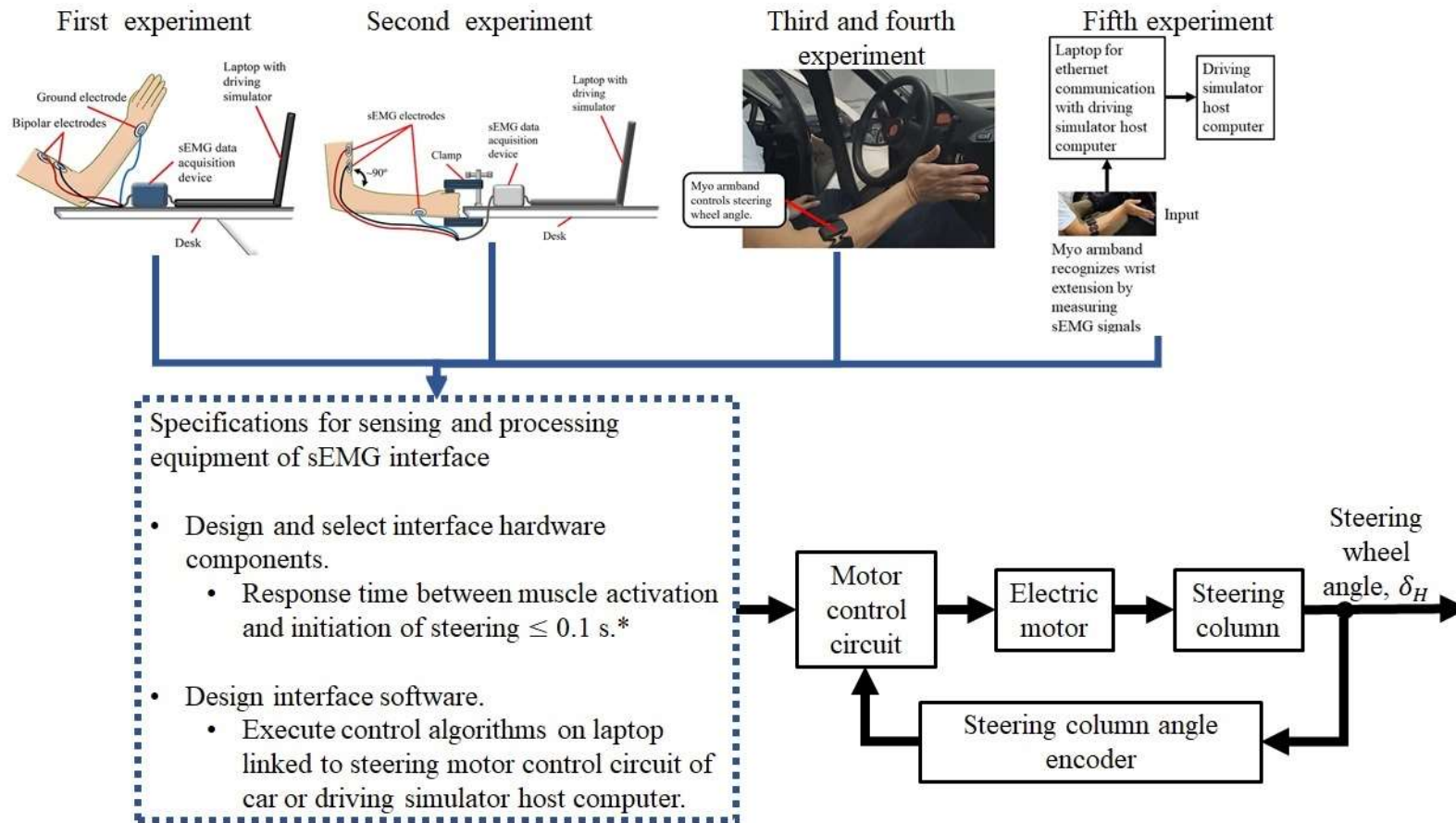


Figure 2.5 Design process of sEMG-controlled interface. *Maximum response time of interface based on recommendation by [101].

Regardless of the method used in optimizing electrode number and quantity, previous studies involving sEMG-machine interfaces vary with respect to the selection of gestures, measured muscles, and device operations [4]. Test drivers in the current driving simulator studies utilized sEMG signals generated by arm gestures to steer a virtual car. Multiple combinations of gestures and steering directions are possible. One combination is to have a test subject perform supination, i.e. twisting away from the body, with the left forearm to steer the virtual car to the left, whereas supination with the right arm would steer the car to the right. The sEMG of the biceps brachii would serve as a control signal. Table 2.1 includes this and other possible configurations.

Table 2.1 Several possible surface electromyography-based interface configurations.

Configuration	Steering Direction	Gesture	Measured Muscle
1	Left	left forearm supination	biceps brachii of left arm
	Right	right forearm supination	biceps brachii of right arm
2	Left	left forearm supination	biceps brachii of left arm
	Right	left forearm pronation	pronator teres of left arm
3	Right	right forearm supination	biceps brachii of right arm
	Left	right forearm pronation	pronator teres of right arm

Further configurations are possible, and thus Table 2.1 is not an exhaustive list. An optimal set of configurations could be determined through empirical observations gained from driving simulations or field tests with actual automobiles. Note that the first configuration was used in the first driving simulator study in Chapter 3.

Based on the first prototype interface for the first experiment with a laptop-based driving simulator, a second prototype interface was developed for the second laptop-based driving simulator experiment. The advantage of the second interface over the first prototype was the ability was the elimination of hand gestures for ease of use. Upon further investigation, the Myo armband was chosen to replace the first and second prototypes as the final interface for use with an actual automobile and with a large scale driving simulator because the Myo armband was capable of providing the same response time, from muscle activation to the initiation of steering. Specifically, the Myo armband measured sEMG signals at 200 Hz [88], meaning that the response time was 1/200 Hz or 0.005 s. In comparison, the prototype interfaces captured at 81 Hz or a response time of 0.01 s. Since the difference between the response times is 0.005 s or 0.5 % of the maximum allowed response time of 0.1 s, the Myo armband and the prototype interfaces provide similar response times. Although the Myo armband used a proprietary sEMG signal processing algorithm that was unreported in previous literature, the armband still used electrodes to measure muscle activity, as in the case of the prototype interfaces. Therefore, as a replacement for the prototype interfaces, the Myo armband was a comparable replacement with respect to the type of signal measured and the response time.

2.3.3.2 Surface electromyography-controlled interface prototypes

The sEMG-based interface represented in Figure 2.4 is an example of a steering interface that was used to control a driving simulator in the first study. Since the sEMG-based interface in the second experiment used sEMG signals from isometric contraction of the right arm biceps brachii, the same interface equipment was used, but a clamp was attached to the desk so that the drivers could grip the clamp to restrain their arms during operation. The experimental equipment includes a commercially available PC laptop that runs the driving simulator software, Digital Battlespace 2™ by Bohemia Interactive. Since the laptop is powered by a battery, line noise resulting from an AC power source for the laptop is eliminated along with the risk of a high current electric shock caused by accidental short-circuiting of the laptop. Avoiding line noise reduces the electrical interference encountered by the sEMG measurement equipment.

Commercially available self-adhering Ag/AgCl electrodes are mounted on the skin surface of the test subject in order to measure sEMG signals. In order to improve muscle signal transmission at the skin-electrode interface, conductive gel is applied to the adhesive side of the electrodes during the electrode manufacturing process. The sEMG DAQ amplifies the sEMG signals so that they are detected by a commercially available, Arduino™ Uno R3 microcontroller by Arduino S.r.l. (Figure 2.6). The microcontroller is the component of the DAQ that converts sEMG signals from analog to digital waveforms. After the analog-to-digital conversion, the microcontroller performs a smoothing function on the digital waveforms in order to reduce undesired effects on the sEMG signals such as pull artifacts and electromagnetic interference. The microcontroller transmits processed sEMG signals to the laptop via a USB connection. Then the driving simulator software on the laptop utilizes these signals to control the steering of a virtual car. Foot pedals control the braking and acceleration of the car.

The DAQ employed in the driving simulator studies was recently developed in the past couple of years, although it was used to complete hundreds of experimental trials involving dozens of test subjects. It was possible to use commercially available bio-signal measurement equipment such as the Polymate AP1132 by Miyuki Giken, Inc. However, in contrast to the open source microcontroller that was used for the current DAQ, proprietary software and hardware made the Polymate AP1132 less modifiable for the laptop driving simulator. For example, since the laptop executes programs in Windows 10, the laptop is not compatible with the Polymate AP1132 software, which is only supported up to the previous operating system, Windows 7.

The peak-to-peak voltage of sEMG signals ranges from 0 mV to 10 mV [102]. However, the resolution of the microcontroller is 4.9 mV, and consequently sEMG signals with lower amplitudes will not be adequately detected [103]. In order to ensure that the microcontroller can detect the sEMG signals, the investigators have designed and constructed an amplifier circuit that is represented in Figure 2.7.

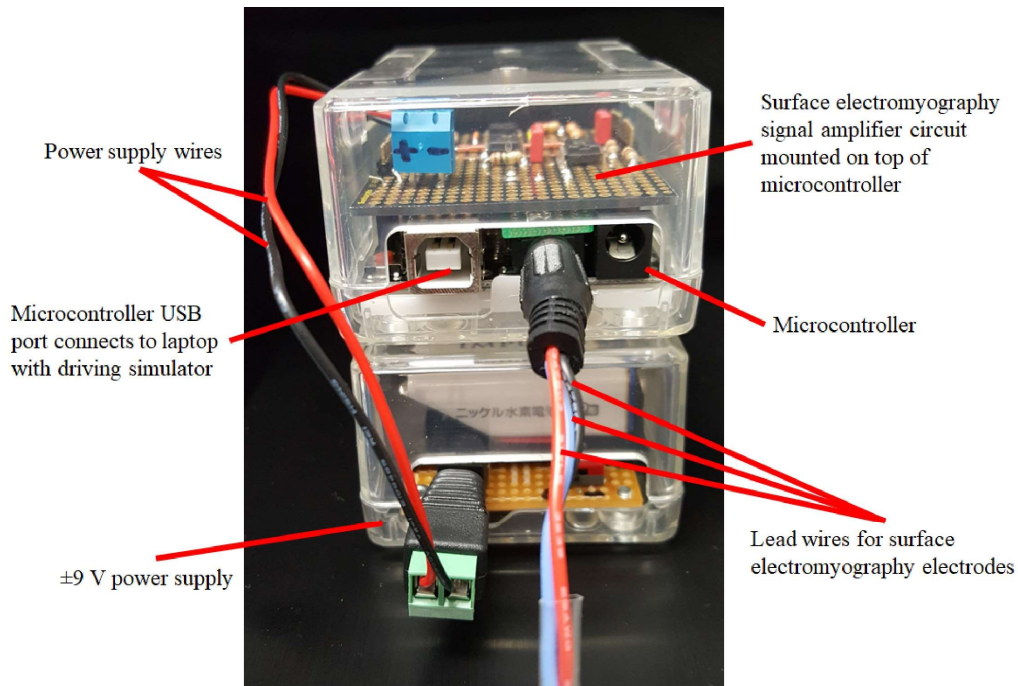


Figure 2.6 Custom surface electromyography data acquisition device used for driving simulator.

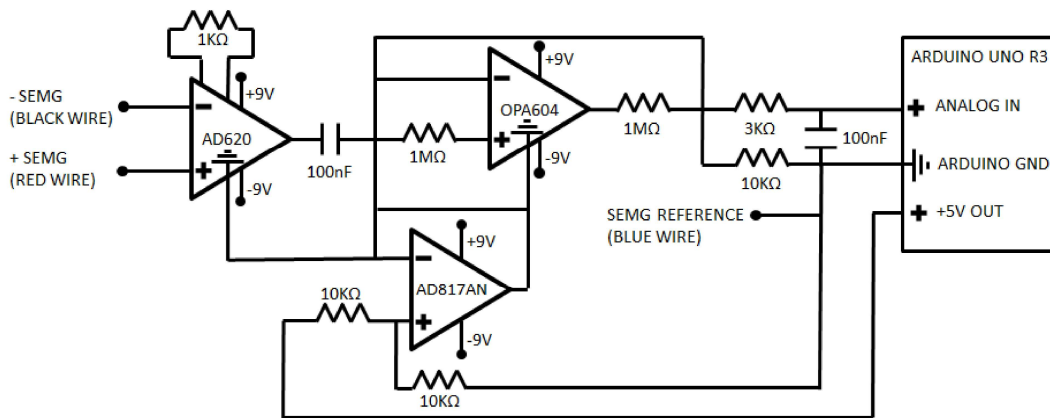


Figure 2.7 Diagram of surface electromyography signal amplifier circuit for driving simulator. Note: ± 9 V DC power supply provided by two 9 V alkaline batteries connected in series; batteries not shown to improve readability of circuit diagram

Since the operational amplifier, OPA604, in Figure 2.7 could be readily purchased at low price relative to other amplifiers, it was selected to amplify sEMG signals from the driver. However, the OPA604 could not efficiently amplify the signals with the ± 9 V DC (direct current) power supply consisting of two commercially available 9 V alkaline batteries connected in series to the amplifier circuit. Rather than purchasing larger, more expensive batteries or an AC-to-DC power supply that increases the risk of electric shock, the AD620 operational amplifier, which was powered by the 9 V batteries, was chosen to provide preamplification for the OPA604. Connecting

the lead wires from the positive and negative sEMG electrodes to the AD620 allowed for differential amplification to reject common mode noise resulting from the transmission of signals through the lead wires. The gain of the AD620 was set to 50 by connecting a 1 K Ω resistor. On the other hand, the gain of the OPA604 was set to 100 with a 1 M Ω resistor. Given that the total gain is the product of the gains for the OPA604 and AD620, the amplifier circuit provided a total gain of 5000 so that the Arduino™ Uno R3 microcontroller could detect the sEMG signals.

Recording of sEMG signals is partly influenced by the signal-to-noise ratio [102]. Noise can be produced from numerous sources such as: electronic components in the DAQ, external appliances such as light bulbs and computer monitors, and pull artifacts resulting from the movement of sEMG lead wires and sEMG electrodes relative to the skin surface. By connecting a 100 nF capacitor and 1 M Ω resistor in series at the voltage output terminal of the AD620, a high-pass filter was created to exclude low frequency noise, such as lead wire movements, below 2 Hz (Figure 2.7). On the other hand, frequencies above 531 Hz were excluded with a low-pass filter consisting of a 3 K Ω resistance and a 100 nF capacitor that respectively had series and parallel connections to the microcontroller. Since the usable energy of sEMG signals is between 0 Hz and 500 Hz, the microcontroller received most of the sEMG signal components [102]. As a means of preventing aliasing, the microcontroller was programmed to acquire the signal at 10 KHz, which is more than twice the maximum signal frequency of 531 Hz [104]. The microcontroller used a 10-bit analog-to-digital converter to digitize the sEMG signal [103].

Consistent sEMG signal acquisition was enhanced by having the sEMG signals share a common ground with the DAQ. This was accomplished by connecting the lead wire for the reference sEMG electrode to the ground for the microcontroller (Figure 2.7). The influence of electromagnetic interference on the grounding of the microcontroller and amplifier circuit was reduced with a floating ground that was constructed from an AD817AN operational amplifier. Other amplifiers could have been used, although the affordability and availability of the AD817AN made it a viable option. The pair of 10 K Ω resistors connected to the positive terminal of the AD817AN divided the conveniently utilized 5 V supply from the microcontroller in half so that a 2.5 V offset was added to the sEMG signal.

Some undesired effects remain in the sEMG signal, even if it undergoes filtering during the amplification stage. Ambient line noise, motion artifacts, and the firing rate of motor units in the muscle can influence the signal [102]. In order to reduce this influence, the microcontroller performs a smoothing function, in the form of arithmetic averaging, on the digital sEMG signal. The additional benefit of this process is a more gradual change in amplitude that translates to less erratic steering control in the driving simulator.

A summary of the processing sequence for sEMG signals obtained by the custom DAQ are shown in Figure 2.8. For experiments involving a driving simulator executed on a laptop, UnoJoy!, a firmware and software package developed for the Arduino™ Uno, mapped the averaged sEMG signals from the right arm biceps brachii to a universal serial bus (USB) joystick control scheme so that an amplitude of 0 mV was assigned to the centered joystick position, while a peak amplitude was assigned to an extreme rightward joystick position [105]. Since the steering of the driving simulator, Digital Battlespace 2™ (DBS2™, Bohemia Interactive), was controlled by keyboard commands, the laptop (Panasonic CF-LX6 laptop, 14 inch 1920 × 1080 resolution

screen) executed JoyToKey software to convert maximum rightward joystick input into the keyboard command to steer rightward at a set SWR [106]. Whenever a test subject is connected to the DAQ, the game controller calibration software in Windows 10 was executed so that the center joystick position and maximum rightward joystick position could be set. Then, in order to mitigate sEMG signal interference and to calibrate for the maximum sEMG amplitude of a given test subject, the threshold for sEMG control signals was set in JoyToKey from a minimum of 10% to a maximum of 30% of the peak joystick input signal, i.e., the maximum peak average rectified sEMG signal resulting from isometric contraction lasting up to 1 s. For some test subjects, it was less likely for the JoyToKey software to recognize sEMG input at thresholds above 30%, and thus the threshold was not increased beyond this percentage during training or experimental trials.

Graphical representations of the acquired raw sEMGs from one user, and the corresponding averaged sEMGs, are shown in Figure 2.8. For the first driving simulator experiment discussed in this paper, the right arm biceps brachii sEMG resulting from the supination, i.e. rotation, of the right forearm was acquired, whereas the second experiment utilized the right arm biceps brachii signal resulting from isometric contraction, as the right hand grips a handle attached to a stationary table. Since the objective of developing the custom sEMG acquisition device was to utilize sEMG signals for steering assistance rather than the mere observation or evaluation of muscle activity, the accuracy of the custom device, as a physiological measurement tool, was not assessed.

The quality of the sEMG signals in Figure 2.8 was validated with respect to the signal-to-noise ratio (*SNR*) in dB, as adopted from [107]:

$$SNR = 10 \log_{10}(V_{sEMG}/V_{noise})^2 \quad (2.13)$$

where V_{sEMG} is the root-mean-square (RMS) voltage for measured sEMG and V_{noise} is the RMS of the baseline noise when no electrodes are attached to the DAQ. The RMS was calculated from the ensemble averages of the amplified sEMG waveforms in Figure 2.8 and the raw baseline noise signal. Table 2.2 summarizes the *SNR* from the biceps brachii sEMGs resulting from forearm supination and isometric contraction. Using a previously reported *SNR* of 3.284 for healthy biceps brachii sEMG signals as a minimum criterion for validation, the larger *SNRs* of the current research are more than adequate with respect to signal quality.

Table 2.2 Signal-to-noise ratios (*SNRs*) for measured biceps brachii sEMG signals.

sEMG Signal Type	Signal-to-noise Ratio (dB)
Forearm supination	6.57
Isometric contraction	4.00

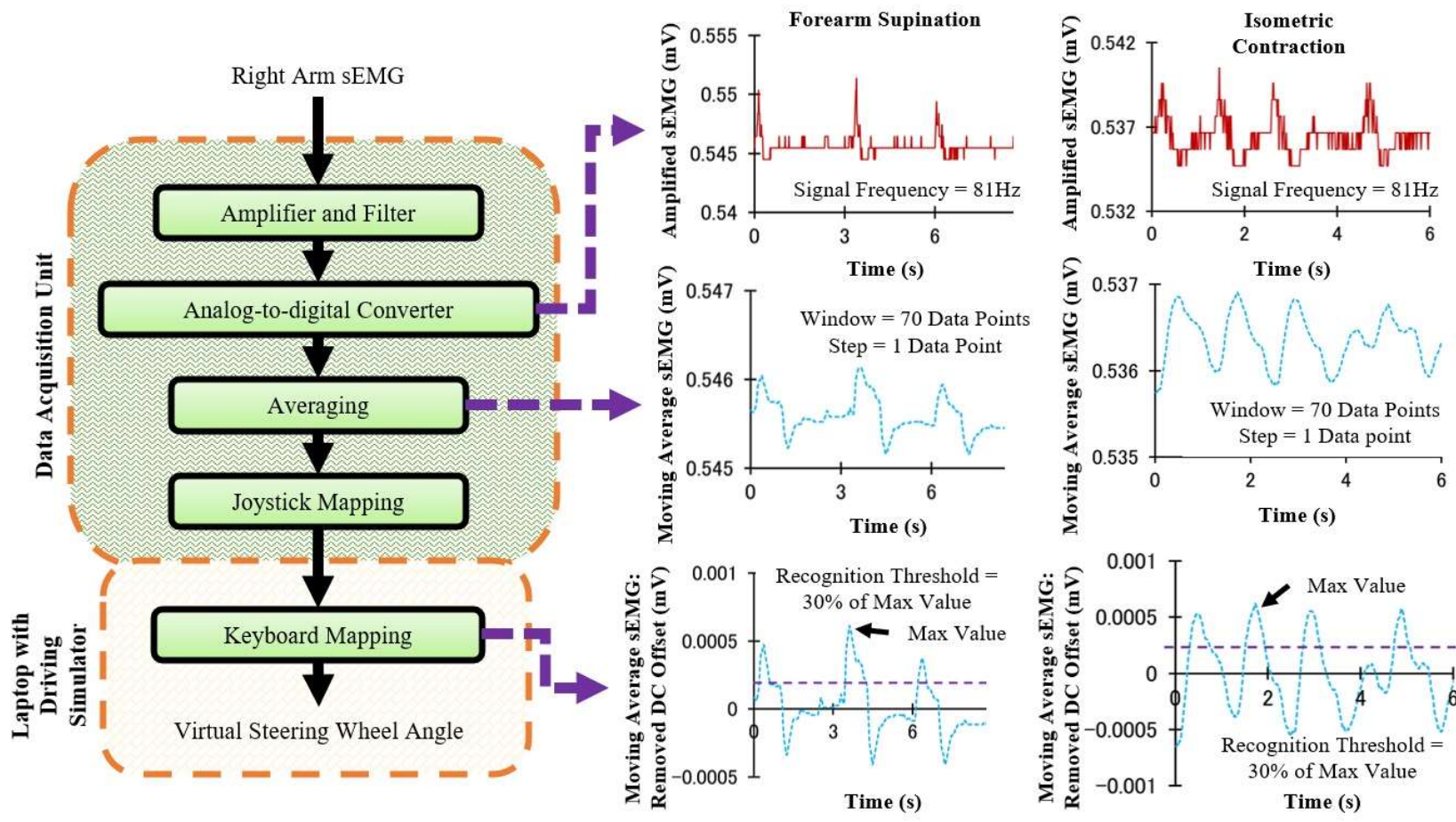


Figure 2.8 Signal processing scheme for sEMG signals recorded with custom data acquisition unit.

In order to explain the relatively large *SNRs* in Table 2.2, power spectral densities (PSDs) were generated for each type of sEMG signal and for the baseline noise (Figure 2.9). The power of the noise is consistently lower than the largest power values for the sEMG signals. To a lesser extent, the power of the noise is also less than the powers of the sEMG signals above 70 Hz. Consequently, as expected from the PSDs, all the *SNRs* are greater than 1 in Table 2.2.

Although sEMG signals can be measured at frequencies above the sampling frequency 81 Hz for the prototype sEMG interfaces, the PSDs indicate that higher frequencies are not necessary to represent the activation of the biceps brachii during forearm supination or isometric contraction. Since most of the power of the sEMG signals is associated with frequencies below 10 Hz, the sampling frequency of 81 Hz sufficiently captures most of the content of the sEMG signals.

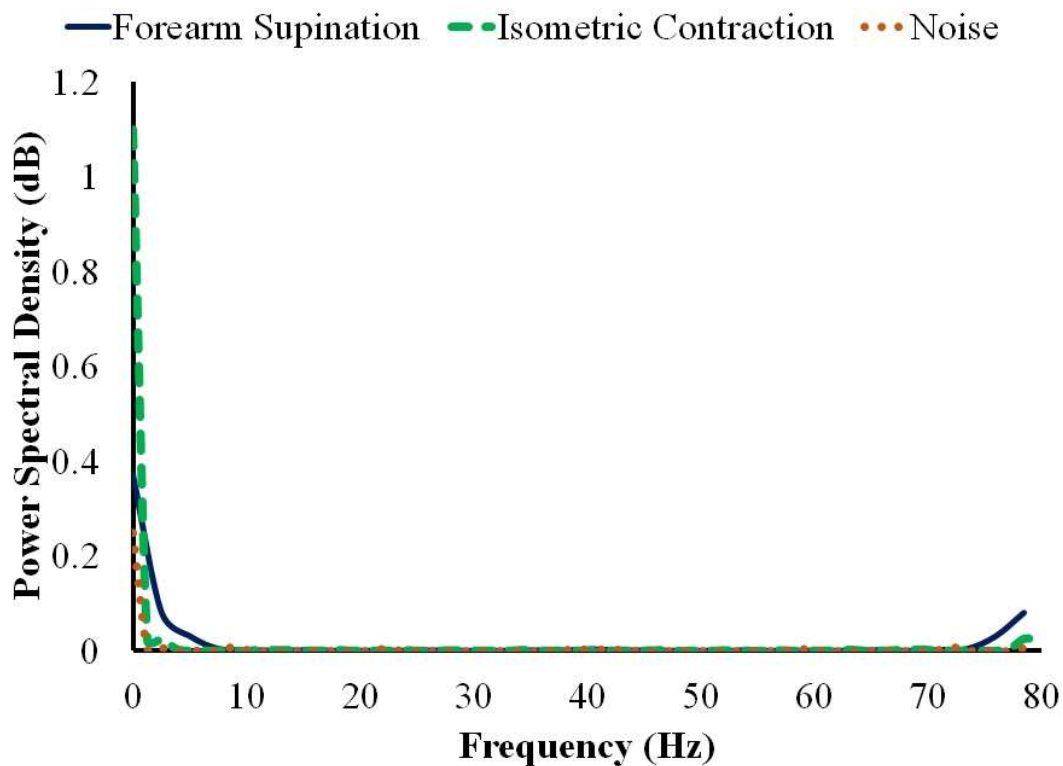


Figure 2.9 Comparison of power spectral densities of measured sEMG interface input signals and baseline noise.

In order to serve as input signals for the prototype interfaces, the measured sEMGs corresponding to isometric contraction of the biceps brachii and forearm supination were averaged in real time. With window of 70 data points to minimize sEMG signal noise, a moving average was applied to obtain the averaged sEMG that underwent joystick mapping. Similar to previous research related to sEMG signal filtering, the step of the window was set to 1 data point so that the detection algorithm outputted one averaged data point every 0.01 s [108]. The step setting is implemented through an iterating moving average program on the Arduino that stores measured data points in an array consisting of 70 sEMG data point values. At a frequency of 81

Hz, i.e. 0.01 s, the program adds data points to the array. If no array positions are available, the oldest data point is removed, and the positions of the remaining data points are shifted so that a new data point is added. Whether the array is completely or partially full, the program will output a new moving average value every 0.01 s based on values in the array. If the array is completely empty, then no output is provided. However, in the driving simulator experiments that utilized the prototype sEMG-based interfaces, the array will be full when steering is initiated because the moving average program was running for longer than 1 s before the beginning of each turn.

As mentioned previously, a maximum threshold of 30 % was applied to the maximum averaged sEMG, as indicated by Figure 2.8. Since the raw sEMG was acquired at 81 Hz and the window was 70 data points with a step of one data point, the minimum response time from the moment of muscle activation, as represented by a nonzero raw sEMG amplitude above the threshold, to a nonzero averaged sEMG value was 0.1 s. Not including the miniscule latency time for the custom sEMG measurement device to communicate with the laptop, the combined minimum response time from moment of muscle activation to the maximum steering wheel angle of the simulated automobile was 0.2 s. This total response time was lower than the previously reported average steering response time of 0.268 SD (standard deviation) 0.065 s for a human to rapidly rotate a steering wheel with two hands from 0° to 65° [53].

2.3.3.3 Surface electromyography-controlled steering with Myo armband

In the course of developing an sEMG interface for an actual automobile, it was determined that the Myo armband by Thalmic Labs, Inc. could be used for recognizing muscle activation during driving (Figure 2.10). The Myo armband was a mass-produced sEMG interface device that was introduced in 2013 [2]. Although the potential of the Myo armband as method for automotive steering had not been previously investigated, researchers recognized the potential of the armband beyond its original purpose as an entertainment device by successfully controlling devices for daily living such as robotic assistants and prosthetic limbs [29], [88], [109], [110]. In the absence of comparable sEMG interface products in the same price range, the Myo armband was readily chosen to assess mass-produced sEMG technology as a feasible method for controlling an actual automobile. If the prototype interfaces developed by the investigators for the driving simulator had been chosen instead of the Myo armband, then it would not have been possible to directly assess mass-produced sEMG technology.

The Myo armband is worn on either the left or right forearm to recognize a set of six default hand gestures (Figure 2.11) [111]. Although it is not required, calibration for these gestures can be performed for each user using the proprietary software included with the armband. The software also allows the gestures to be mapped to custom commands such as steering wheel rotations. Although a software developer package has been provided by Thalmic Labs, Inc. to allow other gestures to be recognized, the default gestures were enough to readily realize automotive steering control for the current research. For example, wrist flexion of the right hand rotated the steering wheel leftward, whereas wrist extension of the same hand resulted in rightward rotation. Furthermore, default gestures were used to facilitate experimental replicability for other studies. Details regarding the correspondence between gestures and steering wheel

commands are found in Section 3.3.2.1.

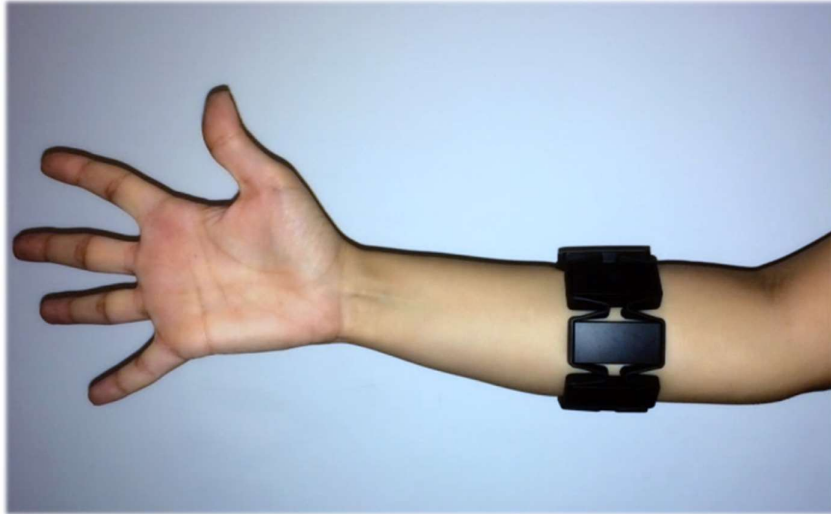


Figure 2.10 Myo armband worn on right forearm to recognize hand gestures. Armband can also be worn on left arm [112].

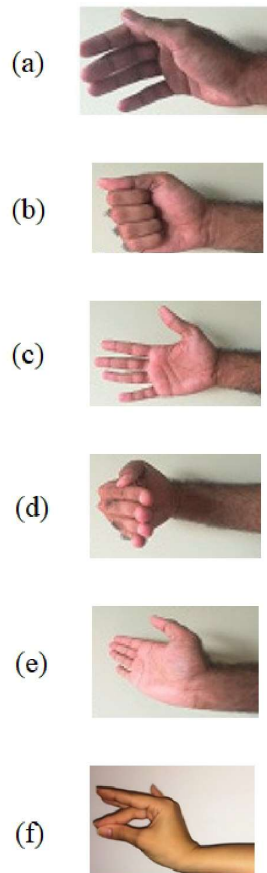


Figure 2.11 Myo armband recognizes six default hand gestures: (a) Hand relaxed, (b) fist, (c) spread fingers, (d) wrist flexion, (e) wrist extension, and (f) tap middle finger and thumb [111]–[113].

The Myo armband wirelessly communicates with computers via Bluetooth connectivity. Arm acceleration can be detected through an onboard nine-axis inertial measurement unit (IMU), although the IMU was not necessary for the current research [113]. Vibrotactile haptic feedback indicates events to the user such as gesture detection and armband deactivation or activation. Each of the eight stainless-steel electrodes mounted radially along the longitudinal axis of the forearm provides one channel for sEMG measurement [88]. It has been determined that the 200 Hz sEMG sampling frequency at 8-bits is a limitation of the device, since the classification accuracy of sEMG signals decreases at frequencies below 400 Hz [109], [114]. Multiple studies involving classification with other sEMG devices have accordingly sampled above 200 Hz [115]–[119]. Nevertheless, the Myo armband demonstrated classification accuracy at 200 Hz that was comparable to conventional sEMG equipment with a higher sampling frequency of 2 kHz [88]. Experiments testing prosthetic hand control have also demonstrated the comparable classification accuracy of a dual Myo armband setup to Delsys Trigno and Cometa Wave setups that are 30 times more expensive [109]. Thus, the Myo armband was chosen as an affordable option that could provide accurate classification accuracy for automotive steering control.

Chapter 3

Experimental Studies with Driving Simulators

3 Experimental Studies with Driving Simulators

Two types of sEMG-controlled interfaces were developed and validated across three studies. The earliest interface discussed in Section 3.1 employed prototype sEMG equipment with disposable wet electrodes to control the SWA of a driving simulator with sEMG signals resulting from forearm supination [120]. This chapter also includes a subsequent study in Section 3.2 utilizing the same sEMG equipment for a driving simulator, although sEMG signals from isometric contractions of the biceps brachii are measured instead [121]. The final driving simulator study in Section 3.3 expands the application of sEMG-controlled steering assistance to pedestrian collision avoidance. In place of either of the aforementioned prototype sEMG-based interfaces, the Myo armband was used because it also received sEMG input and had equivalent response time, from the moment of muscle activation to steering initiation. Collectively, the first three driving simulator experiments demonstrate the safety of sEMG-controlled steering assistance with respect to path following accuracy during dynamic steering and vehicle stability during pedestrian collision avoidance.

Although the results of the first three driving simulator studies were promising with respect to vehicle safety, it was observed that the steering angle response time of the proposed interfaces could be improved. In order to investigate the improvement of the interfaces, the final section concerns driving simulator studies that estimate the outcomes of faster response with respect to path following and vehicle stability.

3.1 Experimental study I: Driving simulator validation of a steering assistance interface using surface electromyography resulting from forearm supination

3.1.1 Introduction

Sometimes drivers have to steer sharply and rapidly at low vehicle speeds to maneuver in confined spaces such as narrow roads and crowded parking lots [122]. However, rapid, two-handed steering subjects the shoulder of the driver to high forces that may cause overuse injury. If the steering wheel is rotated to the right with two hands from 0° to 65° , with an average time of $0.268 \text{ SD (standard deviation) } 0.065 \text{ s}$, healthy supraspinatus and deltoid muscles are subjected to forces that could lead to muscle overload [53].

The risk of injury is a consequence of another issue at low speeds, namely, a decrease in the ability of the driver to turn a steering wheel, i.e. decreased steering portability. Primarily because of the reaction forces between the tires and the road, the torque required to steer the road wheels is maximized when an automobile is moving slowly or at a full stop [123], [124]. Thus, when the steering wheel is manually rotated from the neutral position, the ability of the driver to rotate the steering wheel decreases towards the maximum SWA [123].

As a means of preventing decreased steering portability and reducing the risk of shoulder injury, a steering assistance interface that relies on surface electromyography (sEMG) input from the biceps brachii muscles has been developed to produce rapid, hands-free steering wheel rotation

for low speed, nonemergency driving tasks. Because the interface was designed to rotate steering wheels faster than healthy drivers, the major driving task of curve negotiation could have been significantly affected [81]. The path following accuracy of the interface during curve negotiation was thus validated by driving simulator trials at different steering wheel rates (SWRs). The fastest SWR setting was associated with path following accuracy that was comparable overall to a game steering wheel. This setting also resulted in more efficiently executed U-turns.

The details of this study are presented in the following subsections. Section 3.1.2 offers an overview of the design of the steering assistance system and the adaptation of the system interface to a driving simulator. Section 3.1.3 describes how drivers performed turning maneuvers with the interface so that the resulting trajectories could be used to determine path following accuracy. A comparison in Section 3.1.4 is conducted between the interface and the game steering wheel with respect to path following accuracy. Although the results of this comparison validate the accuracy of the steering assistance interface, there are limitations in this study that are conveyed in Section 3.1.4. Nevertheless, the results warrant further interface development, as recommended in Section 3.1.5.

3.1.2 Materials

One design objective of the steering assistance system is to enable hands-free steering wheel rotation to prevent decreased steering portability when a vehicle travels at low speeds of 30 km/h or less or at parking speeds near or equal to 0 km/h [80], [124]. Hands-free rotation also meets the design objective to reduce the risk of shoulder injury resulting from rapid two-handed steering [53].

Considerations regarding the control design and operation of the steering assistance interface are provided in Section 3.1.2.1. Although the steering assistance system was intended for an actual automobile, path following accuracy was validated with a driving simulator for the safety of the test subjects and to identify how the interface could be improved prior to further development. The adaptation of the interface to a driving simulator is discussed in Section 3.1.2.2.

3.1.2.1 Steering assistance interface

Consideration was given to the possible ways in which myoelectric signals could be measured. There are multiple gestures with corresponding sEMG signals that could be assigned to steering maneuvers [125]. In a previous study, a radio-controlled model vehicle was successfully steered to the right by supinating the right forearm [99]. Because the biceps brachii is one of the most active muscles when the forearm supinates with the elbow flexed at 90°, the sEMG of the biceps brachii was selected to readily control the steering wheel angle (SWA) of the simulated vehicle [126].

If the proposed steering assistance system were to be implemented in an actual automobile, the steering control system design would use sEMG data acquisition equipment, as shown in Figure 3.1.1. Gesture-sensing technology that is functionally similar to commercially available technologies, such as the Myo Armband, would be worn on the left and right arms of the driver

and would consist of dry electrodes that sense sEMG signals from the biceps brachii muscles [88]. Twisting the forearms through supination produces biceps brachii sEMG signals that are wirelessly transmitted by the armbands to signal processing equipment so that the signals are rectified and averaged. The signals are then converted to steering motor commands by the onboard vehicle computer. The signals are then converted to steering motor commands by the onboard vehicle computer.

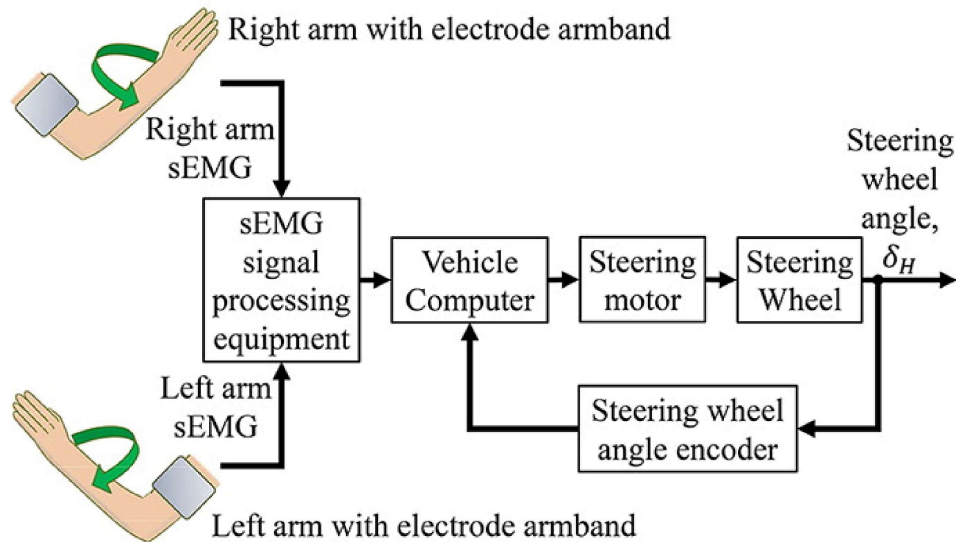


Figure 3.1.1 Overall steering assistance control design.

For a steer-by-wire system, hydraulic power assistance at low vehicle speeds enables the steering motor to meet the increased steering torque demand at the front road wheels [127]. If the steering wheel is mechanically linked to the road wheels with a steering column, some commercially available steering motors can meet the increased demand for torque by providing more steering wheel torque than human drivers [79], [124]. Whether a mechanical or steer-by-wire connection is implemented, the SWA resulting from the steering motor would be relayed by an encoder to the vehicle computer so that steering motor commands are adjusted with respect to the measured SWA.

The flowchart in Figure 3.1.2 provides an overview of the operation scheme for the proposed steering assistance interface. The relation between the sEMG input of the driver and the rotational output of the steering wheel depends on the SWA. If the steering wheel is at the neutral position, supination of the left forearm results in leftward steering wheel rotation until the maximum leftward SWA is reached. On the other hand, supination of the right arm results in rightward steering wheel rotation up to the maximum rightward SWA. The steering assistance system uses a FSM control scheme that converts sEMG input to the rotational output of the steering wheel.

If the amplitude of the average rectified sEMG from the driver exceeds a specified threshold, e.g. 30% of the signal peak that is determined during the calibration of the sEMG armband to the driver, the vehicle computer determines which arm generated the sEMG signal (Figure 3.1.2). Based on the current SWA of the steering wheel, the vehicle computer then changes the state of

the steering wheel by sending a command to the steering motor.

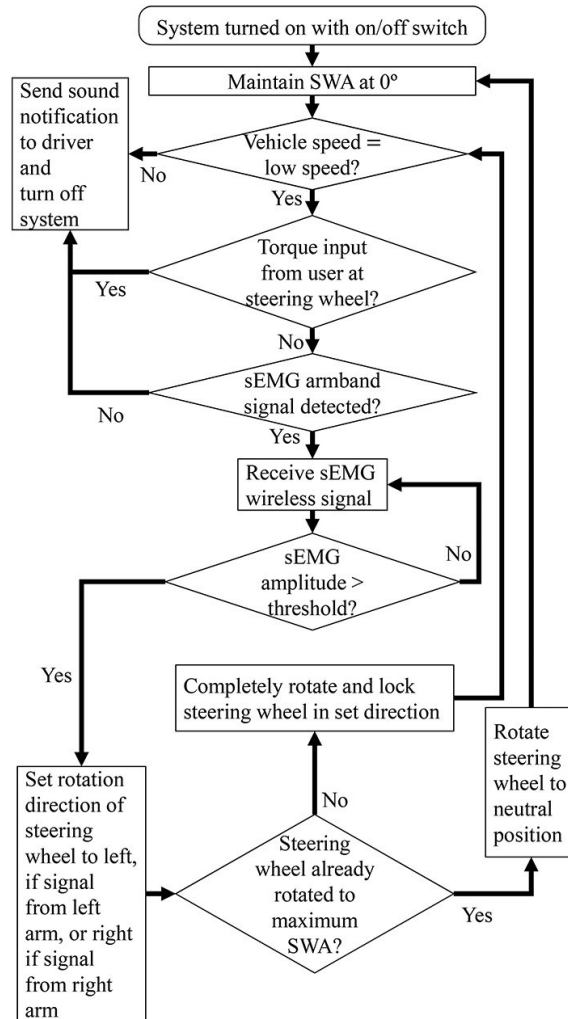


Figure 3.1.2 Operation scheme of steering assistance interface.

Visual feedback is provided by the position of the driver relative to the surroundings of the vehicle [128], [129]. When performing turns with small radii of curvature, for example, visual feedback from the road is used to maintain lateral distance between the driver and the lane marking of a curve. Because this visual feedback is available in the simulated driving scenarios of the current study, other methods of steering feedback, such as vibrotactile devices, are not incorporated into the design of the steering assistance interface [130].

Because the proposed steering assistance is intended for controlling steering wheel states at low speed or parking speed, the maximum vehicle speed at which states can transition or be maintained without losing steering control is determined through simulation or actual vehicle testing [82], [83], [131]. As a safety measure, if the maximum speed is exceeded when the steering assistance system is on, a sound notification is sent to the driver, such as a tone lasting several

seconds so that the driver can resume manual control of the steering wheel (Figure 3.1.2). Note that the same notification would be sent if no signal is provided from the armband.

Before the steering assistance system is turned on, the driver confirms that the SWA is at or close to 0° and the vehicle is stationary. Thus, it would not be recommended to turn on the system in emergency situations, such as the instant before a collision, where there is no time to stop the vehicle and move the steering wheel toward the neutral position. When steering assistance is turned on, the driver lets go of the steering wheel so that the vehicle computer maintains the SWA at 0° (Figure 3.1.2). The driver could then supinate the forearms to rotate the steering wheel.

During the operation of the interface, there is a possibility that arm gestures intended for other tasks, such as the operation of the stereo, may produce sEMG signals that would inadvertently cause steering wheel rotation. Therefore, when the driver wishes to perform another task besides the rotation of the steering wheel, steering assistance can be deactivated by pressing an on/off switch at a convenient location such as the dashboard.

While steering assistance is active, the driver may suddenly need to control the steering wheel manually, as in the case where a collision avoidance task cannot be sufficiently addressed by the steering assistance system. Therefore, as a safety precaution, a torque sensor that is similar in function those found on production vehicles would be installed in the steering wheel to allow the driver resume manual control through torque input [132] (Figure 3.1.2). A sound notification lasting several seconds would then inform the driver that steering assistance has been deactivated. Note that sound notification and torque sensing were not included in the current study because the simulated driving scenarios did not involve manual takeover.

3.1.2.2 Adaptation to a driving simulator

The sEMG-based HMI was adapted to a laptop-based driving simulator with a focus on ease of implementation. Components that comprise the sEMG acquisition equipment of the interface were chosen based on affordability and, in cases where the components had to be designed and constructed, component complexity was minimized. Such a strategy was appropriate because the objective of the experiment was the validation of path following accuracy rather than the complete implementation and testing of all HMI components.

An armband consisting of electrodes was to serve as the sEMG-based HMI for an actual automobile. However, before investing time and effort in the development of the armband, a readily available and affordable substitute for the armband was used. Disposable Ag/Ag-CL bipolar electrodes were attached to the biceps brachii longhead, and a ground electrode was mounted on the wrist in accordance with the recommendations of SENIAM [100]. Because the lateral portion of the biceps brachii belly provided a peak signal with the least variability in comparison to the medial and central portions, bipolar electrodes were placed along the lateral portion [133]. Bipolar electrodes were selected because they were more resistant to noise than other sensors such as monopolar electrodes [2].

Given that one design objective of the steering assistance system is to reduce the risk of shoulder injury to the driver during sudden two-handed rotation of the steering wheel to the right, all the simulated driving scenarios involved the rapid execution of rightward turning maneuvers

(Figure 3.1.3) [53]. Consequently, only sEMG input from the right arm was used because the right arm exclusively controlled rightward steering.

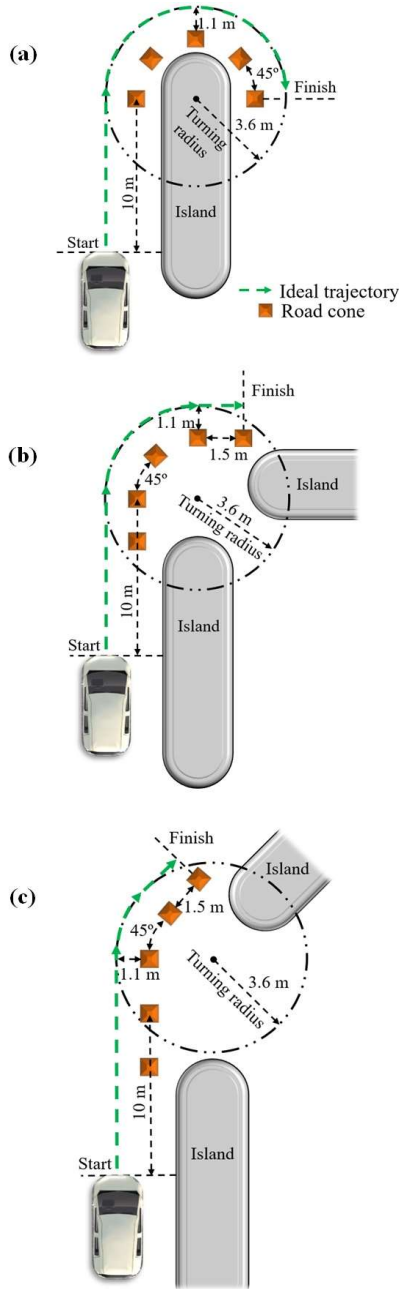


Figure 3.1.3 Three driving simulator scenarios: (a) U-turn, (b) 90° turn, (c) 45° turn.

In previous studies involving males and females, the median electromyography reaction time for the sEMG signal of the right arm biceps brachii was faster than that of the left arm by 3-4% [134], [135]. Because supination of the left arm rather than the right arm would add a negligible

increase to the steering response time, it was expected that there would be a correspondingly negligible effect on path following accuracy. Therefore, performing turns with the right arm alone was sufficient for path following validation.

A custom DAQ, as described in a previous chapter, was developed for the sEMG-based HMI. Control signals were processed with the DAQ and a Windows 10 platform laptop. Because the driving simulator accepted keyboard commands, the laptop executed software to convert joystick commands into keyboard commands so that the steering of the driving simulator could be controlled. Whenever a test subject initially connected or reconnected to the DAQ, calibration of the DAQ was performed by using the game controller calibration software included with Windows 10. Based on this calibration, the threshold for sEMG control signals was set from 10 to 30% of the peak signal resulting from forearm supination lasting up to 1 s. This setting prevented the detection of inadvertent sEMG signals and other interferences below the threshold.

As the test subjects operated the sEMG-based HMI, acceleration and braking were controlled with a set of foot pedals that originally came with the commercially available game steering wheel (Driving Force™ GT). The game steering wheel had force feedback and a steering ratio of 1:1 (Figure 3.1.4a). As the steering of the driving simulator could be controlled without input from the game steering wheel, sEMG input controlled the steering in the simulator rather than the rotation of the game steering wheel.

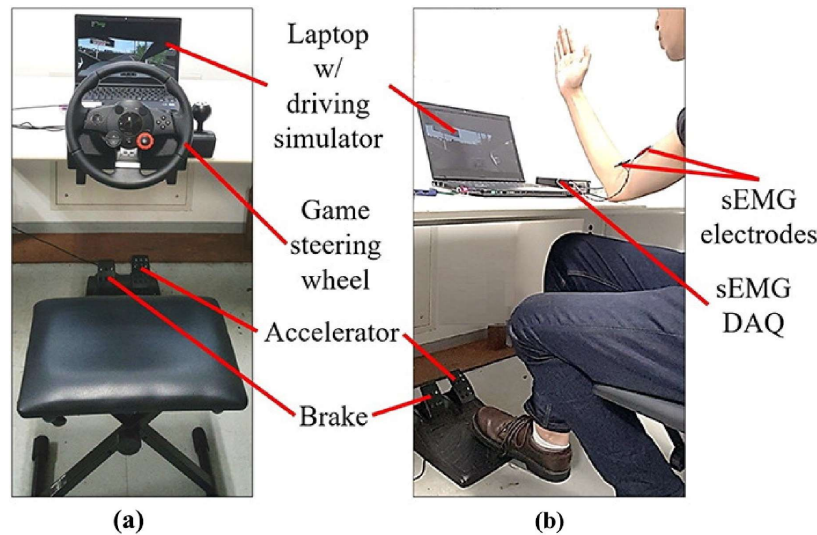


Figure 3.1.4 Experimental setup for (a) game steering wheel and (b) steering assistance interface.

In addition to using the steering assistance interface to complete the driving scenarios, the test subjects repeated the scenarios with the game steering wheel as a basis for comparison.

3.1.3 Methodology

The objective of the experiment was to validate the path following accuracy of the sEMG-

controlled interface with a driving simulator. If the use of the interface was associated with a path following accuracy that was at least comparable to the use of the game steering wheel, then the sEMG-based HMI would be successfully validated.

Driving scenarios that were simulated in the experiment were constructed to test the interface with rapid SWRs at vehicle speeds below 30 km/h. The design of the scenarios and a general strategy for completing the scenarios with maximized path following accuracy are detailed in Section 3.1.3.1. An experimental protocol for validating path following accuracy is provided in Section 3.1.3.2.

3.1.3.1 Driving scenarios

Since the steering assistance system was designed to reduce the risk of shoulder injuries posed by rapidly rotating the steering wheel to the right from 0° to 65° , all the simulated driving scenarios were designed to necessitate rapid SWRs and steering wheel rotation up to 65° to maximize path following accuracy [53]. As a means of ensuring that this SWA would be necessary, the ideal trajectory in each scenario had a radius of curvature corresponding to the SWA. Given that the SWA corresponded to the smallest turning radius of the virtual car, the test subjects were instructed to only rotate the steering wheel up to the SWA. On the other hand, when test subjects used the sEMG-based interface, the virtual car would be steered to the turning radius at a constant SWR.

The need to rapidly rotate the steering wheel to optimize path following accuracy was determined by the driving scenarios. Distance was allotted between the starting line in each scenario and the cone at the beginning of each turn (Figure 3.1.3). Test subjects were instructed to accelerate from the start line without braking or decelerating so that the speed at the beginning of the turn was nonzero. Because the ideal trajectory of the turn in each scenario had a radius of curvature equal to the smallest turning radius of the virtual car, it was possible to optimize path following accuracy, if the steer angle of the road wheels corresponded to the smallest turning radius.

Based on transient and steady-state steering, a general strategy can be devised to maximize path following accuracy for the driving scenarios (Figure 3.1.3). As mentioned previously in Section 2.2, there is a transient phase at the beginning of a turn involving the steering of the front road wheels to the Ackermann steer angle. When steady-state steering begins, the game steering wheel or, in the case of the sEMG-based interface, the accelerator can be adjusted to correct oversteer and understeer. Hence, based on Section 2.2, the general strategy can be executed in the following sequence:

- (1) Maintain a constant low speed before and throughout the turn to prevent oversteer and understeer. This can be accomplished by constantly pressing the accelerator and not pressing the brake before and during the turn.
- (2) At the beginning of the turn, rotate the game steering wheel to 65° as soon as possible, or in the case of the sEMG-interface, supinate the right arm as soon as possible.

- (3) If oversteer should occur during the turn, rotate the steering wheel to the left, if applicable, or press the accelerator further.
- (4) If understeer should occur during the turn, rotate the steering wheel to the right, if applicable, or reduce accelerator depression. If the steering wheel is already rotated to the maximum SWA of 65°, understeer cannot be corrected with the steering wheel.
- (5) Do not return the vehicle to a longitudinal trajectory until the vehicle reaches the last road cone along the ideal circular trajectory.

Items (1)-(5) were demonstrated through training videos for drivers who participated in experimental trials.

3.1.3.2 Experimental procedure

Experimental trials with the driving simulator were completed by a group of 24 healthy drivers, consisting of two females and 22 males. One test subject was left-handed and the rest were right-handed. The ages of test subjects ranged from 20 to 45 years, with an average age of 23. Thirteen test subjects had previous driving simulator experience. All test subjects had between six months and seven years of driving experience, and the test subjects all had standard driver's licenses issued by the Government of Japan. The test subjects were recruited through referrals from persons at The University of Tokyo who were not involved in conducting this research and by response to recruitment flyers that were posted on the university campuses. Ethical approval for this experiment was obtained from the ethics committee of the Interfaculty Initiative in Information Studies within the Graduate School of Interdisciplinary Information Studies at The University of Tokyo (No. 14 in 2017).

Test subjects completed driving scenarios with the sEMG-based HMI and the game steering wheel (Figure 3.1.3). Acceleration and braking of the car were performed with a set of pedals. A turning maneuver was completed only if the center of the front bumper of the car passed the first and last road cones along the turn without running into an island. Furthermore, the test subjects were instructed not to press the brake pedal until the car cleared the last road cone so that the execution of a turn would not be influenced by the operation of the brake pedal. However, releasing the accelerator was allowed, as this operation was included in the strategy outlined in Section 3.1.3.1.

Operation of the sEMG-based HMI followed the steps shown in Figure 3.1.5. First, the accelerator was pressed to move the virtual car forward, and then the test subject supinated the right forearm to begin turning to the right. The test subject then supinated the right forearm again to exit the right turn before pressing the brake pedal to stop the virtual car. The same procedural structure was repeated with the game steering wheel in place of the sEMG-based HMI.

Throughout the execution of a right turn, the elbow of the test subject rested on a desk (Figure 3.1.5). This assisted with the maintenance of elbow flexion at 90° and flexion of the right arm at

90° from the anatomical position. When the virtual car was not turning, the surface of the palm of the right hand was held nearly parallel to the sagittal plane. Given that the virtual car was moving forward along a linear trajectory, supination of the right forearm steered the front road wheels of the virtual car to the rightward Ackermann steer angle. Supinating the forearm again returned the front wheels to their original positions so that the virtual car could continue moving forward along a linear trajectory.

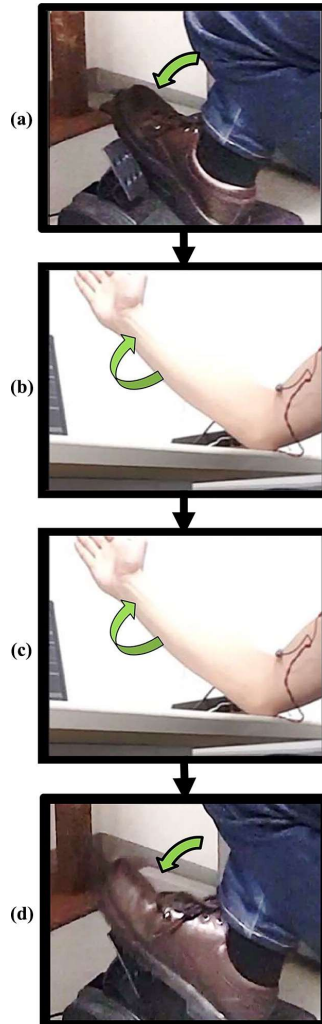


Figure 3.1.5 Test drivers operated sEMG-based HMI as follows: (a) Press accelerator. (b) Supinate right arm to initiate turn. (c) Supinate right arm to terminate turn. (d) Press brake.

Training of the test subjects involved the viewing of a slide presentation that included written interface operation instructions as well as videos of an expert user demonstrating the operation of each interface for each driving scenario. Test subjects who viewed the presentation went on to complete driving simulator training for the sEMG interface equipment, followed by driving simulator training for the game steering wheel. Training for a given interface consisted of the

completion of driving scenarios in the following order: U-turn, 90° turn and 45° turn (Figure 3.1.3). Each scenario had to be successfully completed twice before a test subject could move on to the driving simulator trials for data collection.

Two simulated SWR settings for the sEMG-based HMI were used during the experimental trials to observe the effect SWR on path following accuracy. Some commercially available steering motors could provide maximum SWRs that ranged from 720 to 1,300 deg/s [79]. However, the driving simulator was only capable of providing a maximum simulated SWR of 720 deg/s. Given that all the driving scenarios were designed to require the SWA to transition between 0° and 65°, the transient steering phase was determined by dividing 65° by 720 deg/s to get 0.1 s. This was the transient phase of the fast-turning sEMG-based HMI. A considerably longer transient phase of 1 s for the slow-turning sEMG-based HMI was also tested to confirm an a priori observation derived from the discussion in Section 2.1 – that prolonging the transient phase reduces path following accuracy. According to this observation, the fast-turning interface would be more accurate than the slow-turning interface. Furthermore, as previous driving simulator testing has shown that the transient phase for two-handed steering wheel rotation was 0.268 SD 0.065 s, the fast-turning interface would be more accurate than the game steering wheel, whereas the slow-turning interface would be less accurate [53]. Hence, it was anticipated that the experiment would confirm the following:

- (H1) For most of the tested driving scenarios, the slow-turning sEMG-based HMI has a lower path following accuracy than the game steering wheel.
- (H2) For most of the tested driving scenarios, the fast-turning sEMG-based HMI has a higher path following accuracy than the game steering wheel.

The experiment was structured to test these hypotheses by evenly dividing the test subjects into two groups, shown in Table 3.1. Group A consisted of 12 test subjects who completed the three driving scenarios with the game steering wheel and the fast-turning sEMG-based interface. Therefore, each member of Group A participated in a total of six experimental conditions that are listed as 1 to 6 in Table 3.1. Conditions 1 to 3 were compared to conditions 4 to 6, respectively, to assess hypothesis (2). Group B consisted of another 12 test subjects who followed the same procedure as Group A, but the slow-turning sEMG-based interface was used instead of the fast-turning counterpart. Each member of Group B participated in another set of six experimental conditions that are listed as 7 to 12 in Table 3.1. Conditions 7 to 9 were compared to conditions 10 to 12, respectively, to assess hypothesis (1).

Within-subject randomization for the conditions of Group A was carried out by dividing the group into two subgroups of six and applying a balanced 6×6 Latin square to each subgroup [136]. The same randomization was applied to the conditions of Group B.

Each test subject was allowed five attempts per condition. Given that the sEMG-based HMIs fell under the category of sEMG interfaces and the game steering wheel fell under the category of steering wheel interfaces, the number of experimental trials was calculated as follows:

$$3 \text{ driving scenarios} \times 5 \text{ attempts} \times 24 \text{ test subjects} \times 2 \text{ interface categories} = 720 \text{ trials} \quad (3.1)$$

As a means of reducing the risk of insufficient data from each test subject, only the first three successful attempts for each experimental condition were used for data analysis.

The shortest distance between the ideal trajectory and the edge of a given road cone in any attempted scenario was 1.1 m (Figure 3.1.3). The lateral error of the actual trajectory was calculated by finding the absolute value of the difference between 1.1 m and the shortest distance between the actual trajectory and the edge of the road cone. Because there are five cones per scenario, the lateral error was calculated five times for each trial. For each condition in Table 3.1, the median lateral error was calculated across trials. The data spread about the median lateral error was expressed as the interquartile range (IQR) [137].

Table 3.1 Experimental conditions.

Test subject group	sEMG-based interface type	sEMG-based interface conditions	Game steering wheel conditions
Group A	Fast-turning	Condition 1: U-turn	Condition 4: U-turn
		Condition 2: 90° turn	Condition 5: 90° turn
		Condition 3: 45° turn	Condition 6: 45° turn
Group B	Slow-turning	Condition 7: U-turn	Condition 10: U-turn
		Condition 8: 90° turn	Condition 11: 90° turn
		Condition 9: 45° turn	Condition 12: 45° turn

Data used to calculate path following accuracy were also used to generate two-dimensional plots of the median trajectories for each interface. Data from Group A and Group B were used to plot the median trajectories for the fast and slow-turning sEMG interfaces, respectively. The median trajectory for the game steering wheel was plotted from the data of both groups. Observations were made from the driving trajectories regarding the relation between the driving scenarios and path following accuracy (Section 3.1.4). Associations between driving trajectories, path following accuracy, and the efficiency of turning maneuvers were also observed on the basis of recorded durations for each experimental trial.

Statistical significance tests were the criteria for confirming hypothesis (1) and hypothesis (2) and for determining any differences in efficiency among the interfaces. Some data sets did not have a normal distribution as indicated by Shapiro–Wilk tests, where $p < 0.05$ [138]. Thus, the nonparametric Wilcoxon signed-rank test was used to calculate statistical significance with a significance level of $p < 0.05$ [139]. If there was a statistically significant difference in the sense that the game steering wheel had higher path following accuracy than the slow-turning sEMG-based HMI for most of the tested driving scenarios, then hypothesis (1) would be confirmed. Similarly, hypothesis (2) would be confirmed if the fast-turning sEMG-based HMI had a lower median lateral error than the game steering wheel, and this difference was statistically significant

for most of the tested driving scenarios. Given that the minimum criterion for validation of the sEMG-based HMI is equivalency to the game steering wheel with respect to path following accuracy, even if hypothesis (2) was not confirmed, the path following accuracy of the steering assistance system would be validated if there was at least no statistically significant difference between the game steering wheel and the fast-turning sEMG based interface.

3.1.4 Results and discussion

Based on data from the experimental trials, the path following accuracy of a simulated automobile was calculated for a U-turn, 90° turn and 45° turn (Figure 3.1.6). Drivers in Group B used the game steering wheel and the slow-turning sEMG-based HMI to complete the scenarios (Table 3.1). The results for Group B showed a statistically significant difference, namely, that the slow-turning sEMG-based HMI was significantly less accurate than the game steering wheel when performing a U-turn (Figure 3.1.6b). There was no significant difference, however, in the case of the 90° and the 45° turns. Therefore, hypothesis (1) was rejected because the sEMG-based HMI was comparable to the game steering wheel in most of the scenarios (Section 3.1.3.2).

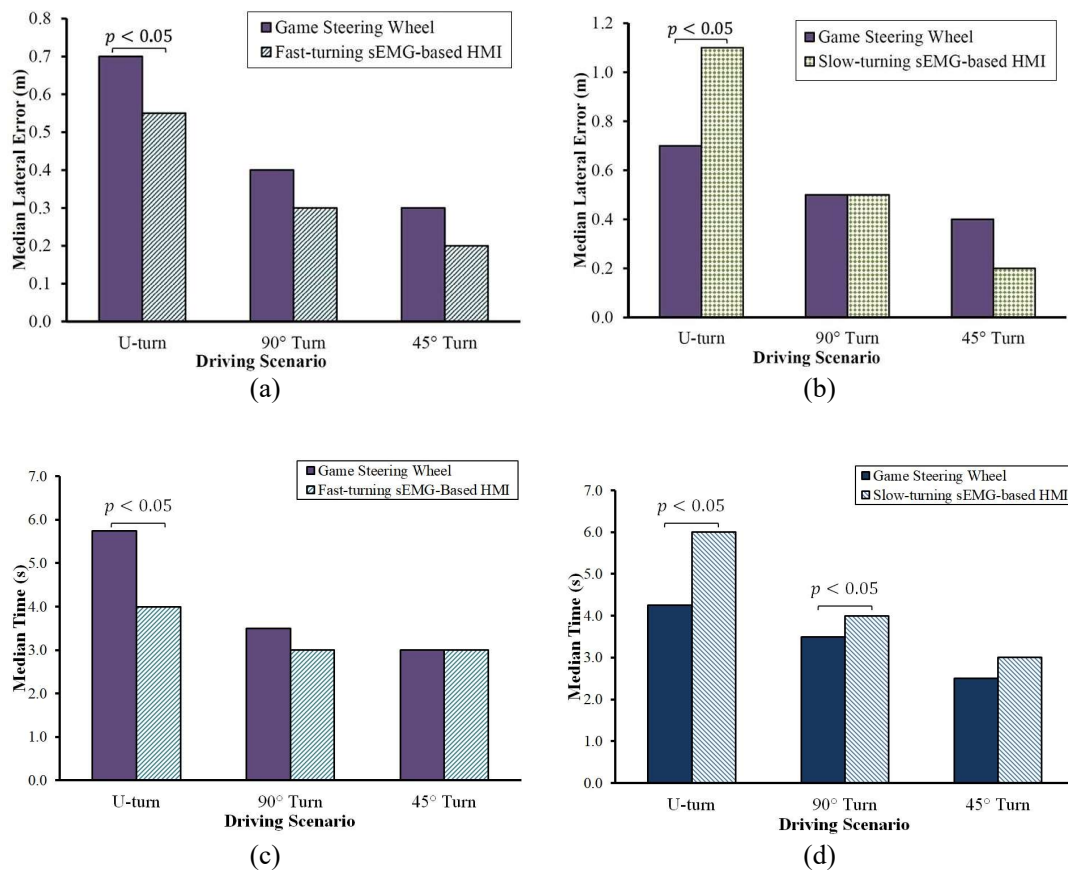


Figure 3.1.6 Comparison of steering interfaces with respect to median lateral error: (a) game steering wheel versus fast-turning sEMG interface. (b) game steering wheel versus slow-turning

sEMG interface. Comparison also made with respect to median time: (c) game steering wheel versus fast-turning sEMG interface. (d) game steering wheel versus slow-turning sEMG interface.

Drivers in Group A completed the driving scenarios with the game steering wheel and the fast-turning sEMG-based HMI (Table 3.1). The drivers steered with greater accuracy in all scenarios with the fast-turning sEMG-based HMI than with the game steering wheel (Figure 3.1.6a). Because the U-turn was the only scenario where the difference between the interfaces was statistically significant, hypothesis (2) was rejected (Section 3.1.3.2). Nevertheless, the fast-turning sEMG interface was at least comparable to the game steering wheel across all tested scenarios, and therefore the path following accuracy of the fast-turning sEMG interface was validated.

Path following accuracy varies between trials as indicated by the data summary in Table 3.2. The IQR values for the slow-turning sEMG-based HMI are all higher than those of the other interfaces, meaning that the accuracy of the slow-turning sEMG-based HMI has the highest variability. In contrast to the other interfaces, the accuracy of the fast-turning sEMG-based HMI varies the least with IQRs that are consistently low across all scenarios. The fast-turning sEMG-based HMI is therefore associated with more repeatable path following.

Table 3.2 Summary of path following accuracy data.

Test subject group	sEMG-based interface type	Driving scenario	Median lateral error (m)	IQR (m)
Group A	Fast-turning	U-turn	0.55	0.8
		90° turn	0.3	0.8
		45° turn	0.2	0.8
	Game steering wheel	U-turn	0.7	0.9
		90° turn	0.4	1.0
		45° turn	0.3	0.8
Group B	Slow-turning	U-turn	1.1	1.8
		90° turn	0.5	1.4
		45° turn	0.2	1.4
	Game steering wheel	U-turn	0.7	1.0
		90° turn	0.5	1.2
		45° turn	0.4	1.0

One pattern that is associated with all the interfaces, is the decrease in the median lateral error as the angle of the turning maneuver decreases from the U-turn angle to 45° (Table 3.2). A possible reason for this pattern pertains to the median trajectories shown in Figure 3.1.7. The U-turn trajectories for all interfaces have the lowest error at the first road cone along the ideal trajectory because the longitudinal trajectory of the simulated car at the beginning of the scenario is enough to follow the ideal trajectory at the first road cone (Figure 3.1.7a). A longitudinal trajectory of the

virtual car provides the highest accuracy before reaching the third road cone in the 90° turn and before reaching the fourth road cone in the 45° turn (Figure 3.1.7b and c). It is therefore expected that driving scenarios involving longer longitudinal trajectories are associated with higher path following accuracy, as evidenced by Table 3.2. In contrast, scenarios involving longer circular paths are associated with lower path following accuracy. The median trajectories account for this lower accuracy by indicating that lateral error tends to progressively increase with the length of a turn. Notice that all the median trajectories terminate at the finish lines with lateral distances from the final road cones that are greater than the lateral distances from the initial road cones (Figure 3.1.7).

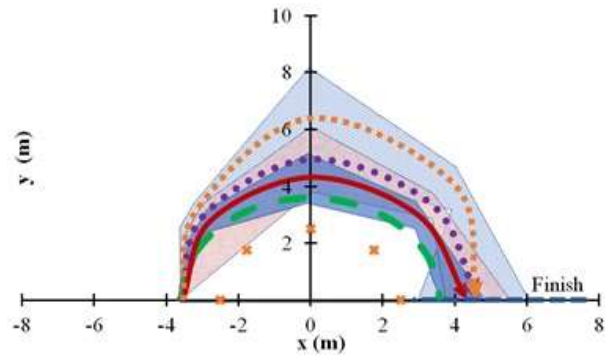
There are potential explanations for the lateral error in Table 3.2. Although it may be a cause of lateral error, understeer does not explain why the median trajectory of the fast-turning sEMG interface tends to be the closest to the ideal trajectory, whereas the median trajectory of the slow-turning sEMG interface tends to be the farthest. Because these two interfaces only differ with respect to the duration of their transient steering phases, perhaps there is a relation between transient steering phases and lateral errors. As opposed to the 1 s transient steering phase of the slow-turning sEMG interface, the fast-turning sEMG interface has a transient steering phase of 0.1 s. This shorter period allows steady-state steering to begin earlier in the turn, resulting in a median trajectory with higher path following accuracy. Since a previously tested steering wheel for a driving simulator has an mean intermediate transient time of 0.268 SD 0.065 s, the median trajectory of the game steering wheel in the current study would hypothetically have the second highest path following accuracy [53]. This expectation is confirmed because the median trajectory with the second largest lateral distance from the ideal trajectory tends to belong to the game steering wheel (Figure 3.1.7).

Although Figure 3.1.7 shows that the median trajectories of the interfaces differ with respect to path following accuracy, only the U-turn is associated with statistically significant differences between the interfaces (Figure 3.1.6a and b). The U-turn thus appears to be the most effective of the simulated scenarios at distinguishing the path following accuracy of the interfaces.

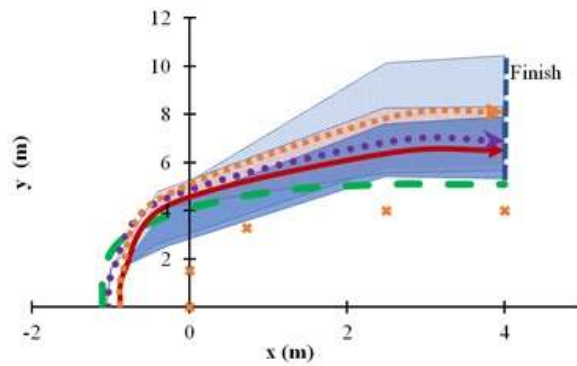
Path following accuracy is affected by the speed of the simulated vehicle. Figure 3.1.8 shows that the fast-turning sEMG interface was associated with higher and more consistent average vehicle speed corresponding to lower average time. This correspondence is especially apparent in the case of the U-turn. The more consistent speed of the fast-turning sEMG interface, as in the case of the U-turn, is necessary for lower vehicle acceleration. Based on the previous section in this chapter on the vehicle dynamics of the current experiment, changes in vehicle speed result in deviation from Ackermann steering, where vehicle speed is constant. As indicated by the average vehicle acceleration plots in Figure 3.1.8, the fast-turning sEMG interface is associated with acceleration that tends to be closer to zero than the other interfaces. Lower average vehicle acceleration enables the vehicle to more effectively achieve Ackermann steering, thereby allowing for higher path following accuracy.

Notice in Figures 3.1.8c and 3.1.8d that the standard deviations for the fast-turning sEMG-based interface increased noticeably at the end of the 45° turn. This increase in the standard deviations was a result of some drivers slowing down at the end of the turn. However, since this deceleration occurred at the end of the turn, there was no significant effect on path following

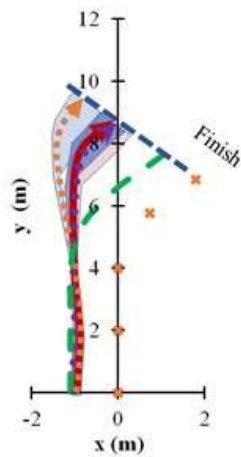
accuracy



(a)



(b)



(c)

Figure 3.1.7 Median and ideal trajectories for (a) U-turn, (b) 90° turn, and (c) 45° turn.

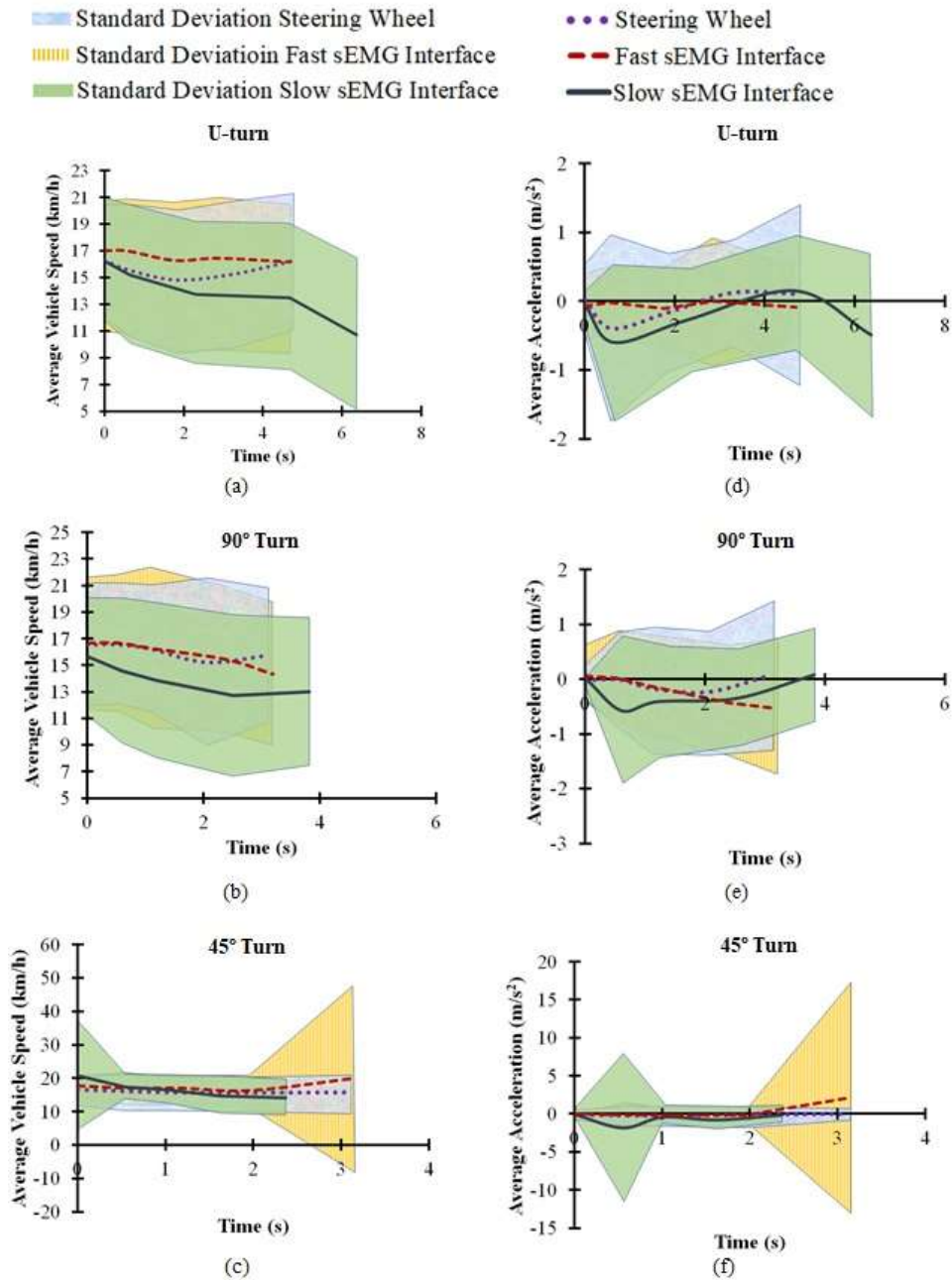


Figure 3.1.8 Average vehicle speed for (a) U-turn, (b) 90° turn, and (c) 45° turn. Average acceleration also shown for (d) U-turn, (e) 90° turn, and (f) 45° turn

Given that the average age of the test subjects was 23 years, the results were relevant to regular driver's license holders between the ages of 20 and 24 years, who comprised about 51% of the nearly 9,000,000 regular driver's license holders in Japan as of 2015 [140]. Given that some age groups were not represented by the test subjects, the total population of regular driver's license holders in Japan could have been more accurately represented by recruiting a group of test

subjects with an age distribution that was close to that of the total population.

Two females and 22 males participated in the experimental trials. Based on data from a previous study that measured the range of motion and velocity of forearm supination, females supinated their left and right forearms 6 to 8% faster than males, and therefore the results may not have accurately reflected biomechanical differences between males and females [141]. Because the inclusion of more female participants may decrease the median time to perform supinations, and consequently the total time to steer from a longitudinal trajectory to the turning circle may also decrease, it was expected that the median lateral error of the sEMG-based HMI would decrease, if not remain approximately the same. Thus, the results may have conservatively estimated the accuracy of the sEMG-based HMI.

Setting the SWR of the sEMG-based interface to a transient steering phase of 0.1 s resulted in more accurate U-turns than those of the game steering wheel. As the differences between these interfaces were only statistically significant for the U-turn, further studies that only adjust the SWR could include the U-turn as a driving scenario to observe any statistically significant differences in path following accuracy. For example, U-turns could be executed to determine different accuracies for transient steering phases between 0.1 s and 1 s. Based on these accuracies, the relationship between path following accuracy and transient steering phases would be quantified in further detail.

Given that the steering assistance system was validated with a fixed-base driving simulator, steering feedback in the form of lateral vehicle acceleration and other aspects of an actual vehicle environment were not simulated. Furthermore, unlike the virtual car in the driving simulator, actual cars had cornering compliances such as steering system deflections that alter the Ackermann steering angle [82]. Nevertheless, the design optimization of actual automobile steering systems could minimize the effect of cornering compliances on the Ackermann steering angle, and therefore the results of the current study could closely approximate vehicles with optimized steering systems [81].

3.1.5 Conclusion

An sEMG controlled steering assistance interface with a maximized SWR of 720 deg/s was found to have path following accuracy that was at least comparable to a game steering wheel. The validation of this accuracy was conducted with a driving simulator that enabled drivers to complete a U-turn, 90° turn and 45° turn. The median lateral errors of the game steering wheel and the sEMG-based HMI indicated that a faster SWR was associated with greater path following accuracy. The difference in path following accuracy between the interfaces was statistically significant in the case of the U-turn, with the sEMG-based HMI being more accurate and more efficient. Thus, future studies could incorporate the U-turn as a means of distinguishing the accuracies of interfaces with varying SWRs.

Acceptable path following accuracy indicated by the results warrants further development of the sEMG-based HMI for an actual automobile. In place of the wet electrode setup in the current study, a wireless electrode armband consisting of dry electrodes would be configured to provide comparable signal measurement accuracy [2]. In contrast to wet electrodes, dry electrodes do not

need conductive electrolyte gel at the skin-electrode interface, and thus drivers would not need to clean the gel after using the electrodes. Another potential improvement would be a vibration device in the wireless sEMG armband to indicate the state of the steering wheel. Other devices could be realized as well, including untested components that were previously proposed, e.g. sound notifications during manual takeover and a motorized steering wheel that can sense torque input from the driver.

3.2 Experimental study II: Validation of a surface electromyography-controlled steering assistance interface using isometric contraction of biceps brachii

3.2.1 Introduction

On confined residential roads or parking areas where sharp turns are rapidly executed at or below the speed limit of 30 km/h, a primary task for automobile drivers is to be safe by keeping their “eyes on the road and hands on the steering wheel” [36], [80], [122]. However, using one or both hands to rotate the steering wheel rightward from 0° to 65° with an average time of 0.268 SD 0.065 s, results in dangerously high shoulder joint forces that could overload the supraspinatus shoulder muscle [53], [82], [142]. Although the risk of muscle overload is applicable to a large population of 38 million regular drivers in the United Kingdom, drivers continue to operate steering wheels frequently in modern actual automobiles [53]. A further issue with some steering wheels is an increasing amount of torque input from the driver as the maximum steering wheel angle (SWA) is approached. This reduction in steering ability, i.e. reduced steering portability, mainly results from reaction forces between tires and the road and is most pronounced when an automobile is at a full stop [123], [124].

Some steering wheel users who may experience shoulder muscle overload or reduced steering portability are restricted to one-handed steering wheel operation due to hemiplegia, i.e. paralysis on one side of the body, or an amputated upper limb [55]–[57], [143]. In order to reduce the risk of shoulder injury to these drivers and to avoid reduced steering portability, a steering assistance interface was developed to enable remote steering wheel rotation. The interface included a handle to stabilize the unaffected arm of the driver and a set of surface electromyography (sEMG) electrodes positioned on the upper arm by an armband (Figure 3.2.1).

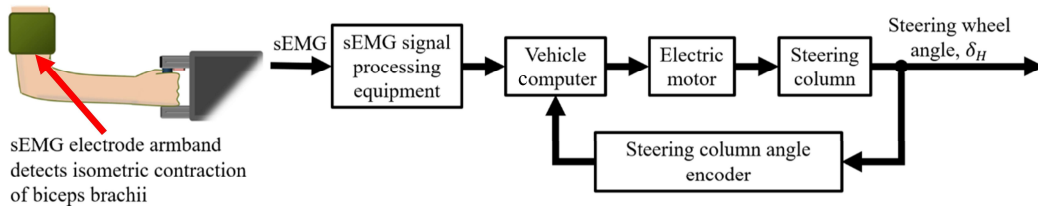


Figure 3.2.1 Overall steering assistance control design.

In an actual automobile, an onboard vehicle computer would rely on the sEMG electrodes to detect electrical muscle activity, i.e., myoelectric activity, resulting from isometric contractions of the biceps brachii (Figure 3.2.1) [144]. The computer converts the myoelectric activity into control signals for an electric motor. A steering column is rotated by the motor at a constant steering wheel rate (SWR) to change the SWA.

Although sEMG electrodes have been used to reliably control prosthetic limbs and to objectively evaluate the muscle burden, steering comfort, and the time for drivers to apply force on steering wheels during vehicle turning maneuvers, few studies have investigated sEMG controlled steering as a means of assisting drivers with disability [1], [15], [32], [77], [90], [125],

[145]–[149]. In contrast, other sensors such as joysticks, strain gauges and motion detectors have been developed [47], [59], [60], [150], [151]. Past sensor interfaces have often required force or motion input from limbs, as in the case of joysticks and gyros. However, some health conditions such as upper limb amputation and hemiplegia inhibit or preclude this input. In contrast, sEMG electrodes are more versatile because they can detect muscle signals from amputated limbs and a variety of other body parts [2]. The proposed sEMG interface could thus be readily adjusted to accommodate sEMG input from amputated limbs, in addition to intact limbs [1], [2], [13], [15], [31], [32].

Since the safety of the test subjects was of the highest priority during the study, the proposed steering assistance interface was tested with a driving simulator as a safer alternative to an actual automobile. A further advantage over an actual automobile was the ability to use the driving simulator to execute turning maneuvers more consistently for each test subject. Myoelectric activity was measured by individual self-adhesive electrodes to provide steering control signals. If the mounting configuration of the electrodes was at least experimentally comparable to a game steering wheel, with respect to path following accuracy, the configuration would be adapted to an automobile as an electrode armband for more efficient mounting (Figure 3.2.1).

Since path following is the primary task of conventional automobile steering, the sEMG interface was subjected to driving simulator trials to evaluate path following accuracy in comparison to a game steering wheel [152]. Drivers used the game steering wheel and the sEMG interface to perform rightward U-turns with differing radii of curvature. U-turns allow the simulated automobile to reach steady-state cornering conditions under which SWA, turning radius, and vehicle speed are constant [82]. Therefore, U-turns were chosen as driving scenarios to clearly observe any effects from the steady-state phenomena, understeer or oversteer, that reduce path following accuracy [83].

One driving scenario involved a right U-turn with a radius of 3.6 m, which was equal to the minimum turning radius of the simulated automobile. The trajectory of this U-turn required the SWA to change from 0° to 65° to evaluate the accuracy of the sEMG interface in a driving scenario associated with high shoulder joint forces in steering wheel users [53]. Since the trajectory of this U-turn corresponded to the maximum SWA, it was not possible to perform understeer correction through rightward steering. The radius of the other right U-turn was two times longer at 7.2 m with a smaller corresponding SWA that allowed for understeer correction. U-turn trajectory data generated by human participants confirmed the hypothesis that, for a radius of 3.6 m, the sEMG interface would be comparable or greater in path following accuracy to the game steering wheel. It was also confirmed, for a radius of 7.2 m, that the accuracy of the sEMG interface was at least comparable to the game steering wheel interface, even if no steering wheel correction was used with the sEMG interface.

The rest of this section is structured as follows: Section 3.2.2 describes the design of the sEMG interface, the selection of steering input sensors for the interface, and the adaptation of the interface to a driving simulator. The experimental setup and methodology for evaluating the path following accuracy of the interface are described in Section 3.2.3. Section 3.2.4 presents and discusses experimental results. Finally, Section 3.2.5 provides conclusions about the experiment, including implications for future studies.

3.2.2 Materials

The steering assistance interface design integrates sEMG sensors into an automobile. The justification for the selection of sEMG electrodes over other steering input sensors is provided in Section 3.2.2.2. In order to evaluate the path following accuracy associated with sEMG electrodes, driving simulator trials were conducted. Consequently, Section 3.2.2.2 describes how interface features relevant to sEMG measurement were adapted to a driving simulator. Finally, the overall experimental setup for driving simulator trials is detailed in Section 3.2.2.3.

3.2.2.1 Steering assistance interface

The steering assistance interface in Figure 3.2.2 enables remote steering wheel rotation to prevent decreased steering portability as the SWA increases, while reducing the risk of shoulder injury during rapid steering [80]. Unlike conventional steering wheels, the interface only needs to be operated with one hand. Thus, drivers with disabilities, such as amputees with at least one fully functioning arm, could readily operate the interface. Input from the driver is provided through sub-second sEMG signal pulses resulting from the isometric contraction of the biceps brachii [153]. A handle that is gripped to stabilize the arm during isometric contraction could be installed on the dash or at another convenient cabin location to allow left-handed or right-handed operation.

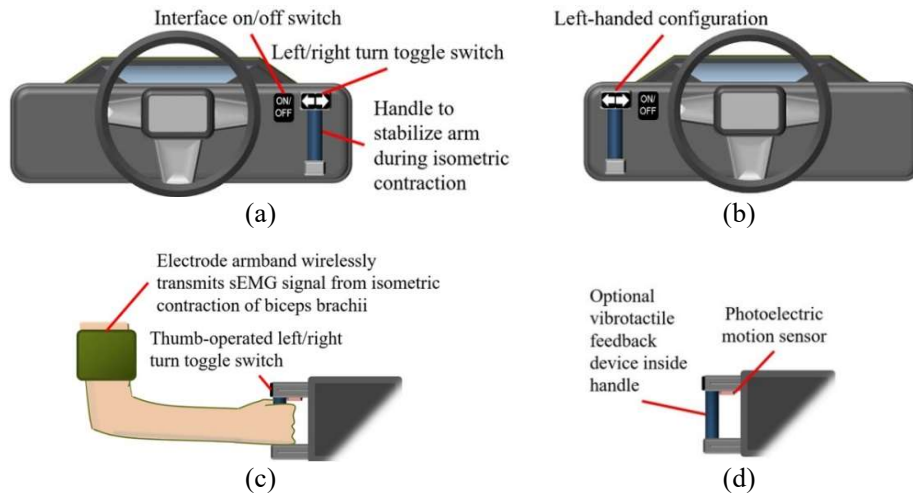


Figure 3.2.2 Steering assistance interface for (a) right-handed operation and (b) left-handed operation. (c) Steering direction selected with toggle switch before steering is initiated by surface electromyography (sEMG) signals from isometric contraction of biceps brachii. (d) Holding handle causes photoelectric motion sensor to activate reception of sEMG signals by steering assistance system, whereas releasing handle deactivates signal reception.

In order to prevent steering caused by inadvertent myoelectric activity or sEMG signal noise,

the handle could be released to cause a photoelectric sensor on the handle to deactivate sEMG signal reception [154]. Alternatively, the on/off toggle switch could be pressed to shut down the steering assistance system. The on/off toggle switch is also used to turn off steering assistance so that the driver can resume manual control of the steering wheel. The driver could also manually rotate the steering wheel so that a torque sensor located in the steering wheel could turn off steering assistance.

Turning maneuvers are executed through a finite state machine (FSM) control scheme that divides the SWA of the steering wheel into three states (Figure 3.2.3) [90]:

(State 1) Rightward steering wheel angle = $+\delta_{Hset}$

(State 2) Leftward steering wheel angle = $-\delta_{Hset}$

(State 3) Neutral position = 0°

The parameters, $+\delta_{Hset}$ and $-\delta_{Hset}$, refer to the rightward and leftward SWAs that are programmed into the vehicle computer according to the health conditions of drivers. If drivers require assistance with turns involving maximum steering wheel rotation, then maximum SWA values for $+\delta_{Hset}$ and $-\delta_{Hset}$ are programmed. Assistance with partial steering wheel rotation is provided by setting lower SWA values for $+\delta_{Hset}$ and $-\delta_{Hset}$. Lower SWA values allow drivers to correct for understeer by resuming manual control of the steering wheel before steering further in the direction of the turn.

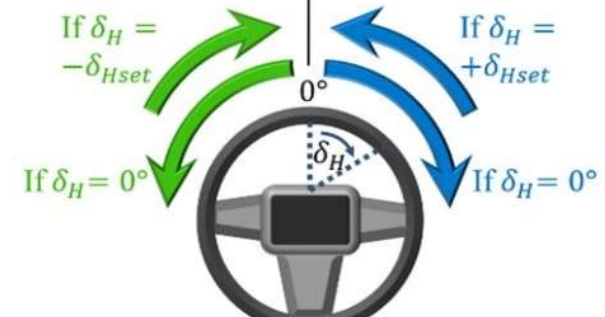
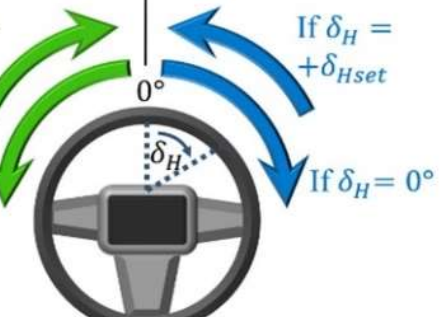
Input	Isometric contraction of biceps brachii on left/right arm with left turn selected via toggle switch.	Isometric contraction of biceps brachii on left/right arm with right turn selected via toggle switch.
Output	Rotate steering wheel to leftward angle or return to 0° from left. 	Rotate steering wheel to rightward angle or return to 0° from right. 

Figure 3.2.3 Relation between muscle contraction input and steering wheel angle output.

When a rightward turning direction is selected with the left/right turn toggle switch (Figure

3.2.2c) and the biceps brachii of the preferred arm undergoes a sub-second isometric contraction, i.e., the arm is static as the biceps brachii maintains a constant length during a contraction lasting less than one second, the steering wheel is rotated rightward, i.e., clockwise from the perspective of the driver, if the initial SWA is equal to the neutral position of 0° (Figure 3.2.3) [155]. If the steering wheel is already rotated rightward to the set SWA, the same muscle contraction returns the steering wheel to the neutral position. Selecting the leftward turning direction, on the other hand, causes the steering wheel to rotate towards the left instead of the right. Regardless of the direction of rotation, the steering wheel rotates at a constant SWR. The SWR depends on the chosen steering actuator with commercially available specifications ranging from 720 to 1300 deg/s [79]. Since some steering actuators produce more steering wheel torque than human drivers, increased steering wheel torque required at low vehicle speeds could be provided by the actuators [123], [124].

The driver is made aware of the SWA throughout a turn by receiving visual feedback from the position of the vehicle in relation to roadside curbs, painted road lines, and other surrounding objects. Although visual feedback is sufficient for turning, supplementary feedback could be obtained by observing the physical rotation of the steering wheel or through a vibrotactile feedback device inside the handle of the interface (Figure 3.2.2d). An existing example of a vibrotactile feedback device preferred by some prosthetic hand users, as opposed to a lack of vibrotactile feedback, has a mass of less than 1 kg that is spun by a small DC motor to provide a mechanical vibration to the user between 10 to 500 Hz [156], [157]. Given the preference of this device among some prosthesis users, the device could be employed by the sEMG interface so that a vibration could occur for a brief period, e.g., 1 s, when the SWA completely transitions to any of the three control scheme states (Figure 3.2.3).

The operation of the steering assistance interface in an actual automobile is shown as a diagram in Figure 3.2.4. After confirming that the steering wheel is at or near the neutral position, the driver turns on the steering assistance system so that the vehicle computer maintains the SWA at 0° . Since the interface is intended for steering on residential roads in Japan, where the legally prescribed speed limit for safely driving on residential roads is 30 km/h, steering assistance is automatically turned off if the vehicle speed exceeds 30 km/h [80]. The cutoff speed may be adjusted on the basis of empirical tests to determine the highest speed at which a vehicle can stably turn at the set SWR [83]. When steering assistance is turned off due to the exceeded cutoff speed or the lack of a wireless signal from the electrode armband, a sound notification such as a constant 1 s tone would alert the driver to resume manual control of the steering wheel.

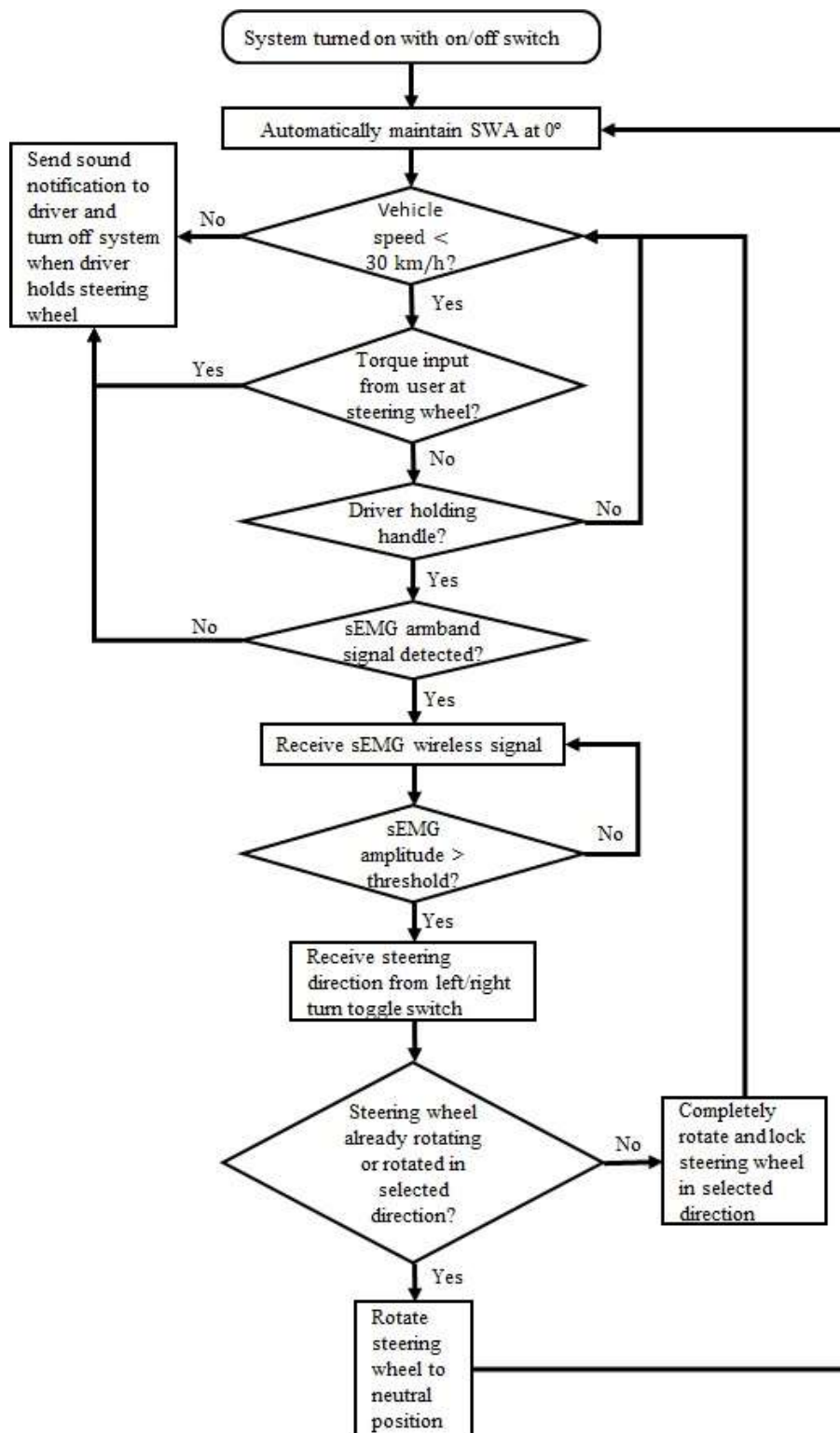


Figure 3.2.4 Operation flowchart of steering assistance interface.

According to Figure 3.2.4, if the vehicle is traveling below the cutoff speed and no input from the driver is detected at the steering wheel by a torque sensor similar to those found on automated vehicles, the interface handle could be grasped so that a photoelectric motion sensor would detect the hand of the driver and activate sEMG signal reception (Figure 3.2.2d) [132]. Before providing muscle contraction input, the steering direction is selected with a toggle switch (Figure 3.2.2c). If the sEMG signal resulting from the isometric contraction of the biceps brachii is greater than a preset threshold, e.g., 30% of the maximum sEMG amplitude, then the steering column of the vehicle is rotated in accordance with the control scheme shown in Figure 3.2.3.

The steering assistance operation shown in Figure 3.2.4 is an instance of Level 1 automation, as defined by SAE (Society of Automotive Engineers) International [69]. In contrast to higher levels of automation that assign control of acceleration, deceleration, and steering to the vehicle, the user of the steering assistance interface controls acceleration and deceleration with the option to share steering control with the vehicle. Although higher levels of automation would relieve persons with disability from the task of driving, there are a number of challenges for highly automated vehicles, including: sampling mismatch among different automated driving sensors, high manufacturing cost, susceptibility of networked automation computers to hackers, high vehicle power consumption by automation hardware, and the reduced ability of advanced driver assistance systems (ADASs) to detect road obstacles under rainy or extreme lighting conditions [150], [158]–[160]. Since the sEMG interface is at Level 1, such challenges could be avoided by implementing the sEMG interface over other more highly automated control schemes.

3.2.2.2 Steering assistance interface

Recently developed sEMG sensors for research and commercial applications utilize wireless transmission [29], [88], [161]. Unlike conventional wet electrodes that require conductive gel at the skin–electrode interface, emerging sensor technology can detect myoelectric activity without gel, and in the case of capacitive electrodes, without skin contact [26], [87], [161], [162]. However, unlike some emerging sEMG sensors, disposable Ag/Ag-Cl wet electrodes are relatively affordable and readily available [87]. Thus, wet electrodes were used in the current study to facilitate experimental replicability and the iteration of electrode mounting configurations (Figure 3.2.5) [2]. If the mounting configuration of the conventional electrodes corresponded to path following accuracy that was comparable to a game steering wheel, the configuration would be finalized for conversion to an armband that uses dry electrodes with comparable measurement accuracy [87].

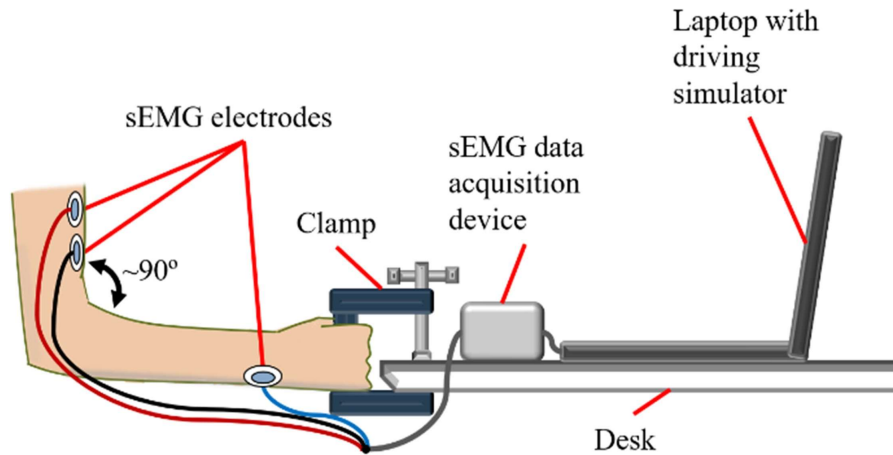


Figure 3.2.5 Steering assistance interface adapted to driving simulator.

Electrode placement for the driving simulator trials was performed in accordance with the recommendations of SENIAM [100]. The ground electrode was mounted on the wrist (Figure 3.2.5), while a set of two bipolar electrodes was placed on the belly of the biceps brachii with the elbow flexed to approximately 90°, since prior testing has shown that the muscle belly is more active at 90° of flexion than other mounting locations on the biceps brachii [163]. As the biceps brachii contracts isometrically, the hand grips a clamp that substitutes for the original handle depicted in Figure 3.2.2. Controls from the original interface design, such as a left/right turn toggle switch and photoelectric sensor, were not incorporated into the clamp, since simulator trials only included right turns that required the clamp to be held continuously (Section 3.2.2.3); isometric contractions only initiated and terminated right turns.

Relocating the ground electrode from the wrist to a location above the elbow, such as the lateral side of the upper arm, could accommodate some amputees [164]. Whereas the buttons of the interface could be pushed with an intact arm or prosthetic limb, transradial amputees with residual muscles above the wrist could choose to provide steering input with sEMG signals from the residual biceps brachii, although residual forearm muscles that commonly control prosthetic hands may be more preferable to the user [165]. On the other hand, transhumeral amputees could typically provide sEMG signals with residual muscles above the elbow, including biceps brachii, that are capable of isometric contraction [19], [22]. Both types of amputations account for a significant portion of amputees that could control the interface with affected limbs [57], [143].

Similar to the majority of studies on sEMG-controlled prosthetics, nondisabled drivers in the current study performed isometric contractions that could represent sEMG signals from the affected limbs of transhumeral amputees [20], [21], [23], [166], [167]. Consequently, the results of this study are relevant to the operation of the sEMG interface with intact or affected limbs. Regardless of the presence or absence of health conditions, anatomical and physiological differences across drivers could affect the measurement of sEMG signals [168]. In order to detect sEMG amplitudes that vary across a range of drivers, the sEMG input threshold of the steering assistance interface would have to be calibrated for each driver (Section 3.2.2.1) [169]–[171]. Hence, the calibration process for driving simulator trials is described in the next section.

3.2.2.3 Experimental setup

Rather than controlling a physical steering wheel, sEMG signals control the virtual SWA of the driving simulator in order to facilitate the implementation of the interface. Consequently, in contrast to the original operation of the sEMG interface (Figure 3.2.4), the steering wheel torque sensor, sound notification, and other features associated with manual takeover of the steering wheel were not included in the control system as shown in Figure 3.2.6.

The experimental setup for the force feedback game steering wheel (Driving Force™ GT) consists of: a laptop that runs the driving simulator, the steering wheel assembly, and the brake and accelerator pedal assembly (Figure 3.2.6a). In the case of the steering assistance interface, braking and acceleration were controlled by the same pedal assembly, but the steering wheel assembly was replaced by the clamp and sEMG equipment (Figure 3.2.6b).

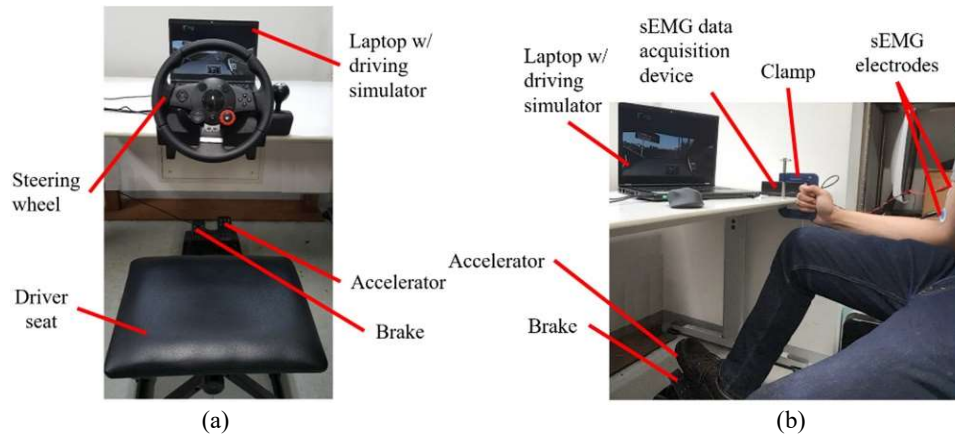


Figure 3.2.6 Driving simulator setups for (a) game steering wheel and (b) steering assistance interface.

3.2.3 Methodology

Section 3.2.3.1 begins with scenarios that were completed with the setup described in Section 3.2.2.1. Lateral vehicle dynamics involved in the scenarios are explained in Section 3.2.3.2, whereas the procedure for evaluating path following accuracy in the context of the scenarios is provided in Section 3.2.3.3.

3.2.3.1 Driving scenarios

The game steering wheel and steering assistance interface were used to perform two types of U-turns. U-turn 1 had a radius of curvature of 3.6 m, which is equal to the minimum turning radius of the simulated automobile (Figure 3.2.7a), whereas the radius of U-turn 2 was twice as long (Figure 3.2.7b). For each U-turn, participants were instructed to accelerate the simulated car from

a full stop at the starting line. A right turn was initiated through an isometric contraction of the right arm biceps brachii or by rotating the game steering wheel rightward with both hands, in accordance with the majority of studies associating rapid steering wheel rotation with high shoulder joint forces [53], [172]. Rotation of the game steering wheel in the opposite direction of the turn, or a subsequent isometric contraction, caused the simulated car to exit the turn. The brake pedal was applied after the simulated car crossed the finish line.

The change in SWA from 0° to a maximum of 65° throughout U-turn 1 (Figure 3.2.7a) is associated with high shoulder joint forces when holding a steering wheel [4]. Given that the steering assistance interface was developed to enable turns without holding the steering wheel, U-turn 1 was completed with steering assistance to test the path following accuracy as shoulder joint forces resulting from manual steering wheel rotation are avoided. Furthermore, since the turn is performed at the maximum SWA, reduced steering portability at high SWAs would be also avoided, if the interface were used in an actual car.

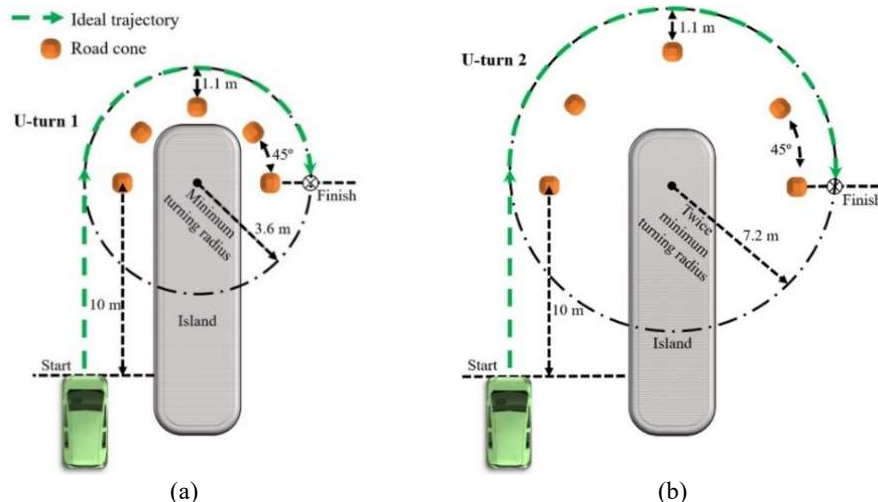


Figure 3.2.7 Driving simulator scenarios consisting of U-turns with radii of curvature equal to (a) 3.6 m and (b) 7.2 m. Note: figures not to scale.

Turning the game steering wheel to the maximum SWA to execute U-turn 1 (Figure 3.2.8a) precludes steering correction involving rightward steering wheel rotation. In contrast, U-turn 2 (Figure 3.2.8b) requires the car to steer at twice the minimum turning radius so that the SWA is below the maximum SWA. Thus, steering correction may be performed by turning the steering wheel rightward when the car understeers, i.e., steers wider than the ideal trajectory. U-turn 2 was therefore designed to test path following accuracy in a scenario that allows for the correction of understeer.

3.2.3.2 Lateral vehicle dynamics

Oversteer and understeer are vehicle characteristics that occur during steady-state cornering along a circular path [82], [83]. After a vehicle undergoes a transient phase to transition from a

longitudinal trajectory into a circular path, the lateral position of the vehicle enters steady-state and remains constant. Understeer or oversteer occur when the lateral position of the vehicle changes along the circular path. On the other hand, if steady-state cornering is maintained at the lowest possible speed along the circular path, the front road wheels are at the Ackermann steer angle for that path. For example, if the simulated vehicle follows the ideal trajectory of U-turn 1 with a constant lateral position and the lowest constant speed, the front road wheels are at the Ackermann steer angle for U-turn 1 (Figure 3.2.7a).

“Ideal trajectory” refers to the path that is followed by an ideal vehicle that can instantaneously transition from a longitudinal trajectory to a steady-state circular trajectory. However, since automobiles always require time to transition, a transient phase necessarily occurs before reaching steady-state. A longer transient phase extends the time to reach steady-state, resulting in higher lateral error. In order to minimize the transient phase, the steering wheel could be rotated by the driver as quickly as possible. In the case of the steering assistance interface, the shortest possible transient phase available in the driving simulator is 0.1 s. Since the maximum SWA of the simulated vehicle is 65° and the SWR of 720 deg/s is attainable through commercially available steering actuators, dividing the maximum SWA by the SWR of the actuator yields an approximate transient phase of 0.1 s [79]. Thus, the minimum transient phase of the driving simulator was set to 0.1 s as a feasible value.

In contrast to U-turn 1, a smaller steady-state SWA applies to U-turn 2 (Figure 3.2.7). Since the steering ratio of the driving simulator is 1:1, the SWA is equal to the front steer angle, δ_H , of the front wheels. Based on the radius of curvature, R , of U-turn 2 and the wheelbase length, l , the front steer angle could be approximated as follows [82], [96]:

$$\delta_H = l/R \quad (3.2)$$

Since R is 7.2 m and l is 4.1 m, dividing l by R and converting to degrees yields an approximate value of 33° for δ_F and the SWA. Thus, in order to perform U-turn 2, the interface is programmed so that $+\delta_{Hset}$ is 33° to the right for the driving simulator.

Although it is possible to correct for understeer and oversteer in the driving simulator through longitudinal deceleration or acceleration, respectively, there is also an option to adjust the SWA in the case of the game steering wheel. Driving simulator trials with U-turn 2 (Figure 3.2.7b) are used to determine if the adjustment of the SWA with the game steering wheel, as oppose to no SWA adjustment with the sEMG interface, would increase path following accuracy. One type of trial is completed by operating the game steering wheel to perform U-turn 2, whereas the other type of trial would consist of the completion of U-turn 2 with the sEMG interface in place of the game steering wheel. If the game steering wheel is significantly more accurate than the sEMG interface, as a result of SWA adjustment, then the ability of manual SWA adjustment to increase accuracy would be confirmed. On the other hand, if the game steering wheel has comparable or significantly less accuracy than the sEMG interface, then this ability is not confirmed. In order to explain the outcome of the interface comparison, vehicle speed and acceleration were also measured with respect to time, t , where $t = 0$ corresponds to the beginning of a turn at the first road cone, and the final time is when the vehicle passes the last road cone.

If the transient phase of the sEMG interface were different than that of the game steering wheel, any difference in accuracy between the two interfaces in the case of U-turn 2 (Figure 3.2.7b) could be attributed to a set of conditions that includes the difference in transient phases and the availability of manual SWA correction with the game steering wheel. Since the experimental trials with U-turn 2 are only intended to assess the effect of manual SWA correction on path following accuracy, the effect of different transient phases must be minimized. Therefore, the transient phase of the sEMG interface was adjusted to be similar in duration to that of the game steering wheel. A survey of data collected from driving simulator trials and field testing indicates that the average time to perform a steering correction ranges from 0.38 s to 0.57 s with an average of approximately 0.5 s [173]. Hence, the transient phase for the sEMG interface was set to 0.5 s to approximate the transient phase associated with manual steering wheel control. Data from driving simulator trials would determine if the difference between the approximated and actual transient phases produces a significant difference in path following accuracy between the two interfaces.

3.2.3.3 Experimental trials

In order to facilitate experimental replicability, driving simulator trials were completed by 16 nondisabled human participants with intact limbs, since amputated limbs have scar tissue or other confounding variables that may affect sEMG measurement and, consequently, experimental results [20]. All test subjects provided their informed written consent before participating in the trials. The study was approved by the Ethics Committee of the Interfaculty Initiative in Information Studies, Graduate School of Interdisciplinary Information Studies, The University of Tokyo (No. 14 in 2017). Four of the test subjects had prior driving simulator experience, while all test subjects had an average of 0.7 standard deviation (SD) 0.9 years of actual driving experience. All participants had standard automobile driver's licenses issued by the Japanese government. The participants were between 20 and 24 years of age, with an average age of 21 years.

All participants were right-handed, except for two people. Given that previous research has found no significant intra-subject difference in sEMG between the biceps brachii muscles of the dominant and non-dominant arms during isometric contraction, it was expected that handedness of the participants would not significantly influence experimental results [174].

Although one out of the 16 test subjects was female, and the sEMG amplitude of the biceps brachii has been previously observed during isometric contraction to be significantly lower in females than in males, the sEMG input threshold of the steering assistance interface was calibrated for each participant to mitigate the effect of inter-subject amplitude variability on the ability of the interface to detect input (Section 3.2.2.3) [175].

U-turns illustrated in Figure 3.2.7 were performed by the participants to test the following hypotheses:

- (H1) For the U-turn with a radius of curvature equal to 3.6 m, the steering assistance interface is comparable or greater in path following accuracy to the game steering wheel.

- (H2) For the U-turn with a radius of curvature equal to 7.2 m, the steering assistance interface is comparable or greater in path following accuracy to the game steering wheel, even if the sEMG interface is used without steering wheel correction.

As indicated in Table 3.3, four experimental conditions were performed to test the hypotheses. Data from conditions 1 and 2 were used to test the first hypothesis, whereas data from conditions 3 and 4 test the second hypothesis. Each of the 16 participants were trained to complete all conditions. Training began with a slide presentation containing written instructions on the performance of each U-turn in Figure 3.2.7 and videos of an expert user demonstrating the operation of game steering wheel, pedal assembly, and the steering assistance interface. Then the participants practiced with the driving simulator by successfully completing each U-turn twice with each interface. After training was finished, the participants completed the experimental conditions. The participants were divided into groups of 4 so that a 4×4 balanced Latin square could be used to randomize the order in which each participant completed the conditions [136]. Each participant attempted each condition five times. An attempt was successful if the simulated car passed the first and last road cones without running over the island. In order to prevent brake pedal depression from interrupting the constant speed of steady-state cornering, drivers were instructed to refrain from pressing the brake pedal during the turn. If correction for oversteer or understeer was necessary, only the game steering wheel, if available, or the accelerator could be used.

Table 3.3 Experimental conditions.

Conditions	sEMG-based interface type	Radius of Curvature of U-turn (m)
1	sEMG setup for U-turn 1	3.6
2	Game steering wheel	3.6
3	sEMG setup for U-turn 2	7.2
4	Game steering wheel	7.2

Trajectories from the first three successful attempts of each condition were used for data analysis to ensure that enough data would be available for processing. Median trajectories across trials were plotted on two-dimensional coordinate planes to compare the trajectories of the interfaces with respect to the ideal trajectories. Note that 1.1 m is the shortest distance between the edge of any road cone and the ideal trajectories (Figure 3.2.7). The lateral error of the simulated automobile was determined by the absolute value of the difference between 1.1 m and the shortest distance between the actual trajectory and the edge of a given road cone. The lateral error was found for each of the five road cones in each scenario. For each condition in Table 3.3, the intertrial median lateral error across all participants was calculated as the path following accuracy. The interquartile range (IQR) was calculated as the extent to which data are spread about the intertrial median lateral error [137].

Comparisons between interfaces were made with statistical analyses conducted in MATLAB. The Shapiro–Wilk test was performed, where $p < 0.05$, i.e., the hypothesis that the population of the data is normally distributed is rejected, if p is less than 0.05. Since $p < 0.05$ for the data from conditions 1 to 4 in Table 3.3, the data were determined to not be normally distributed [138]. Hence, the non-parametric Wilcoxon signed-rank test was selected to determine whether there is any statistical difference in path following accuracy between the game steering and the sEMG interface. The significance level for the Wilcoxon signed-rank test was $p < 0.05$, i.e., if $p < 0.05$ for one of the tested U-turn types, there is a significant difference between the two interfaces, and one rejects the hypothesis that the median intertrial difference in lateral error is zero between the interfaces [139]. For hypothesis (1), data from conditions (1) and (2), were analyzed to determine if there was a statistically significant difference in path following accuracy between the sEMG interface and the game steering wheel. As for hypothesis (2), data from conditions (3) and (4) were analyzed to determine if there was a significant difference in path following accuracy between the two interfaces.

As a means of confirming the steady-state steering for the turning maneuvers, vehicle velocity and translational acceleration were measured and plotted on two-dimensional x-y planes. If the acceleration was within a margin of $\pm 1 \text{ m/s}^2$, then steady-state steering would be considered to be approximated.

3.2.4 Results and discussion

Based on intertrial lateral error data across all participants, the sEMG interface was compared to the game steering wheel with respect to path following accuracy (Figure 3.2.8). For U-turn 1 (Figure 3.2.7a), with a radius of curvature equal to 3.6 m, the sEMG interface with the SWA, $+\delta_{Hset}$, set to 65° was more accurate than the game steering wheel. The difference between the sEMG interface and the game steering wheel, with respect to the intertrial median lateral error, was statistically significant with $p < 0.01$. In the case of U-turn 2 (Figure 3.2.7b), with a radius of curvature equal to 7.2 m, the sEMG interface, with $+\delta_{Hset}$ equal to 33° , was comparable in accuracy to the game steering wheel, since there was no statistically significant difference in path following accuracy.

Median trajectories for each interface are shown in Figure 3.2.8. Throughout the U-turn with a radius of curvature of 3.6 m, the median trajectory of the sEMG interface is closer to the ideal trajectory than the median trajectory of the game steering wheel (Figure 3.2.8c). During the first half of the U-turn with a radius of curvature equal to 7.2 m, the sEMG interface has a median trajectory that tends to be closest to the ideal trajectory, whereas the median trajectory of the game steering wheel tends to be closest in the second half of the turn (Figure 3.2.8d).

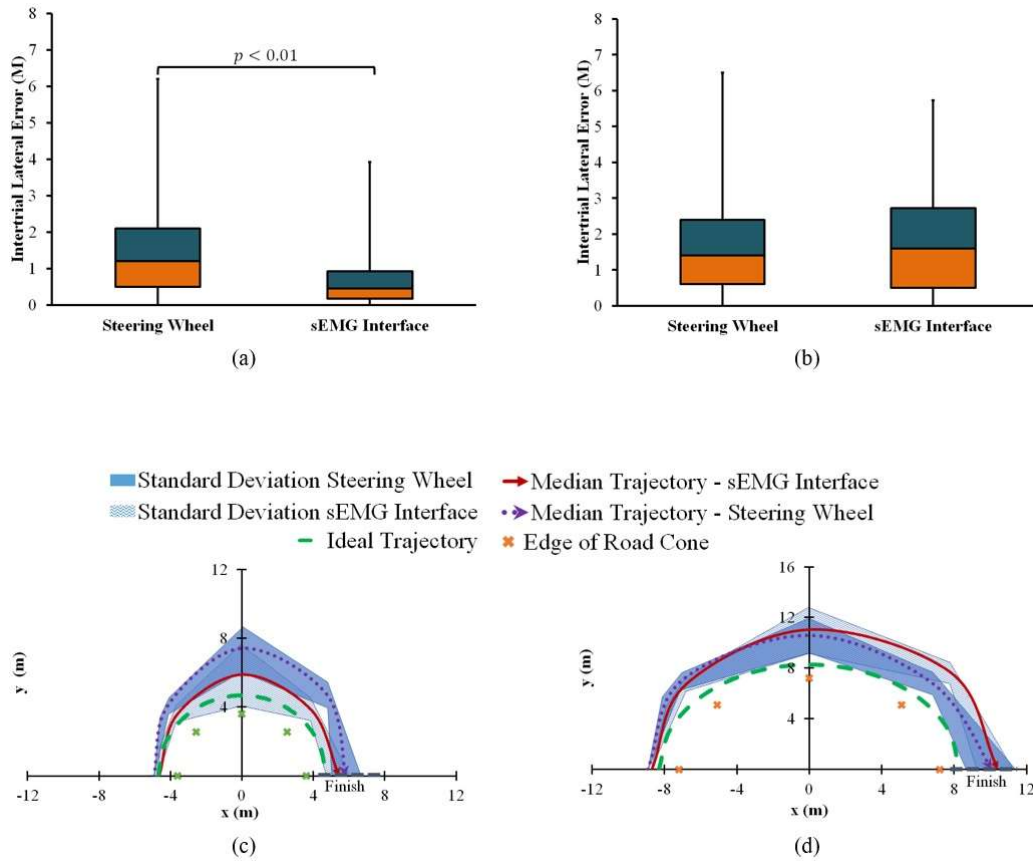


Figure 3.2.8 Path following accuracy of sEMG interface and game steering wheel for U-turns with radii of curvature equal to (a) 3.6 m and (b) 7.2 m. Corresponding steering trajectories are shown for U-turns with radii of curvature equal to (c) 3.6 m and (d) 7.2 m.

Based on calculations from experimental data, intertrial median errors and IQRs are summarized in Table 3.4. For the U-turn with a radius of curvature equal to 3.6 m (Figure 3.2.7a), the sEMG interface had a lower intertrial median error and IQR than the game steering wheel. However, for a radius of curvature equal to 7.2 m (Figure 3.2.8b), the sEMG interface had a higher intertrial median error and IQR than the game steering wheel.

Table 3.4 Summary of results from driving simulator trials.

Conditions	Interface Type	Radius of Curvature of U-Turn (m)	Intertrial Median Error (m)	Interquartile Range (IQR) (m)
1	sEMG setup for U-turn 1	3.6	0.5	0.8
2	Game steering wheel	3.6	1.2	1.6
3	sEMG setup for U-turn 2	7.2	1.6	2.2
4	Game steering wheel	7.2	1.4	1.8

According to the intertrial median lateral errors in Figure 3.2.8, the sEMG interface is at least comparable to the game steering wheel for all the tested U-turns. Therefore, hypotheses (1) and (2) are confirmed (Section 3.2.3.3). The median trajectories in Figure 3.2.8 support potential explanations for the confirmed hypotheses. In the case of the U-turn where the radius of curvature is 3.6 m, the median trajectory of the sEMG interface is closest to the ideal trajectory (Figure 3.2.8c). Since the game steering wheel must be held at the maximum SWA throughout the turn in order to follow the ideal trajectory, it is not expected that any understeer was corrected by steering further rightward. The inability to correct for understeer during the turn could explain why the trajectory of the simulated automobile appears to deviate away from the ideal trajectory during the turn. Notice that the trajectory of the sEMG interface exhibits less deviation than the game steering wheel with respect to the ideal trajectory. This lower deviation may result from a briefer transient phase. Recall that the transient phase of the sEMG interface was set to 0.1 s, in contrast to the previously measured transient phase of 0.268 SD 0.065 s for steering wheel interfaces [53]. As expected from the discussion on transient phases in Section 3.2.3.2, the sEMG interface is associated with steady-state cornering that occurs sooner during the turn than for the game steering wheel, thus resulting in a more accurate trajectory.

The transient phase of the sEMG interface in the case of U-turn 2 (Figure 3.2.8b) was set to approximate the transient phase of the game steering wheel. As expected, the interfaces have similar trajectories in the first half of the turn (Figure 3.2.8d). This result is consistent with the transient phase of sEMG interface being set to 0.5 s to approximate the transient phase of the game steering wheel (Section 3.2.3.2). Since the setting of 0.5 s is an estimate based on empirical data from driving simulations and actual vehicles, the transient phases of the game steering wheel and sEMG interface coincide with some actual automobiles.

Unlike U-turn 1 (Figure 3.2.8a), understeer correction with the game steering wheel is allowed by U-turn 2 (Figure 3.2.8b). This correction may have resulted in the decreased lateral error of the game steering wheel trajectory in the second half of the turn. Conversely, the lack of understeer correction with either the accelerator or the steering wheel may account for the higher lateral error of the sEMG interface at the same part of the turn. Nevertheless, there is no statistically significant difference in intertrial median lateral error between the two interfaces.

The trajectory data from the driving simulator trials suggest that steering assistance could provide path following accuracy that is comparable to a steering wheel interface, even in scenarios where steering wheel correction may be performed. Accuracy in the context of the tested scenarios (Figure 3.2.7) is dependent on steady-state cornering. Although there may be undesired forces within actual steering systems, i.e., steering compliances, that may hinder steady-state cornering by causing deviation from a circular path, modern steering systems can be improved through design optimization in order to mitigate the effects of steering compliances [81], [82]. Therefore, the simulated automobile represents actual automobiles with fully functioning steering systems that have undergone design optimization.

As a means of determining the extent to which steady-state cornering was achieved, vehicle speed and acceleration was averaged across test subjects and plotted with respect to time as shown in Figure 3.2.9. Although there was some variability in acceleration and speed, acceleration only

varied between 1 and -1 m/s^2 . Hence, steady-state cornering, where acceleration is zero, was approximated within a margin of $\pm 1 \text{ m/s}^2$.

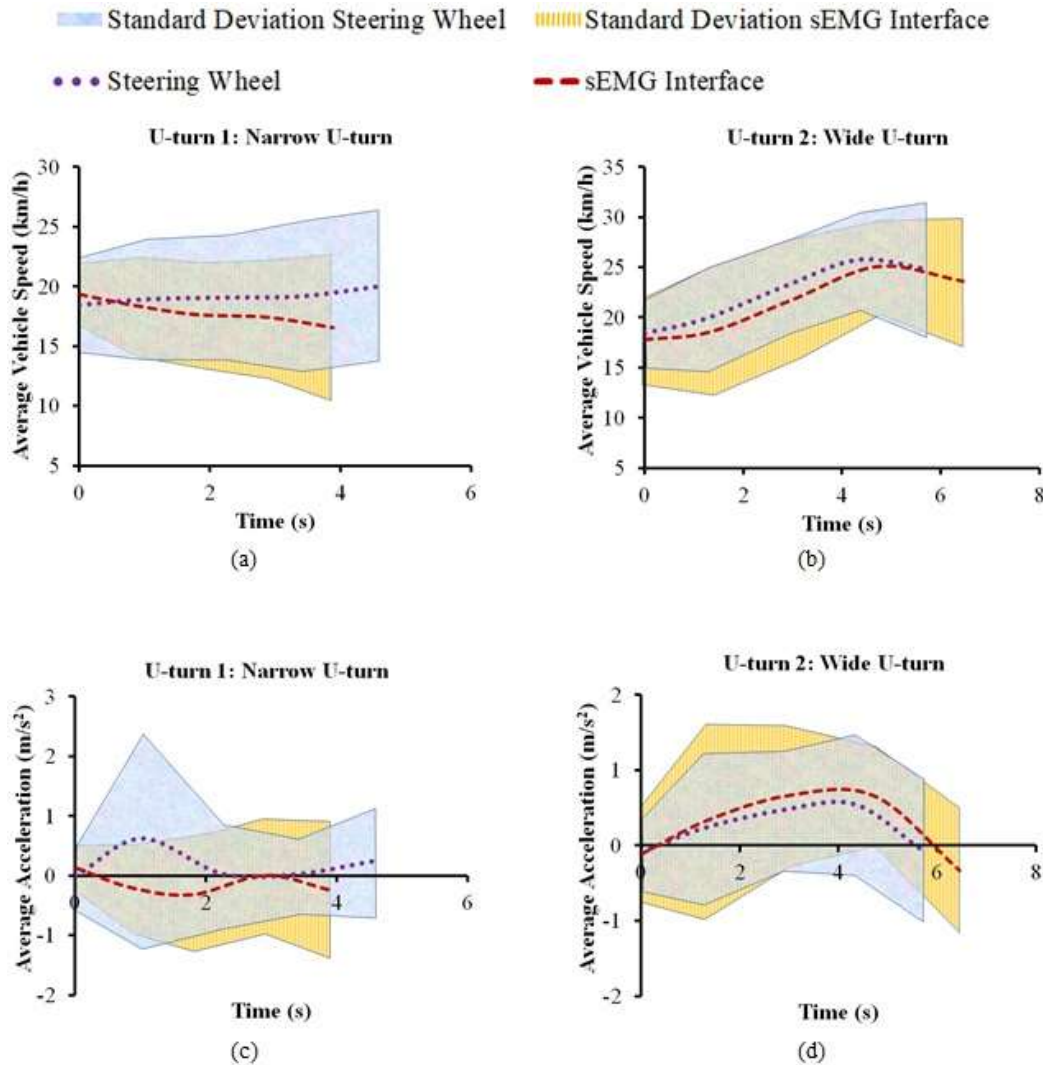


Figure 3.2.9 Average vehicle speed corresponding to sEMG interface and game steering wheel for U-turns with radii of curvature equal to (a) 3.6 m and (b) 7.2 m. Corresponding average vehicle acceleration is shown for U-turns with radii of curvature equal to (c) 3.6 m and (d) 7.2 m.

Since data were collected from 16 participants with Japanese driver's licenses, future studies could recruit a larger sample of test subjects to more accurately represent the population of drivers in Japan. Participants in this study were all persons without disabilities, and thus the results are at least relevant to drivers with one healthy arm. It is expected that a driver who has hemiplegia or upper limb amputation affecting only the left side of the body could use an unaffected right upper limb to operate the sEMG interface with accuracy that is comparable to current experimental results. As for sEMG input from upper limbs with unilateral amputations above the right wrist or

right elbow, comparable operation is possible, if the residual biceps brachii repeatedly provides sEMG signals that are similar in amplitude and activation period to the sEMG signals of intact limbs. Otherwise, future studies including drivers with amputations could be compared to this study to quantify any statistically significant difference in path following accuracy. As the interface continues to be implemented for drivers with disability, the suitability of the interface in relation to specific drivers and automobiles would be assessed by specialists of disability, such as occupational therapists and physiatrists [176].

Based on present and future evaluations of the sEMG interface with respect to path following accuracy, further interface modifications could be realized. One planned modification is the replacement of the disposable wet electrodes with reusable dry electrodes for more efficient mounting and to eliminate the need for drivers to remove conductive gel and electrode adhesive from the skin after using the interface. Additions to the interface handle would include a photoelectric motion sensor to detect the hand of the driver, and a vibrotactile device to provide feedback on the SWA of the steering wheel (Figure 3.2.2d).

3.2.5 Conclusion

A steering assistance interface with sEMG electrodes underwent driving simulator trials to evaluate path following accuracy relative to a game steering wheel. Although further testing was required to confirm the accuracy of the sEMG interface in most cases, trajectory data from the trials indicated that the steering assistance interface was at least comparable to the game steering wheel, with respect to the tested U-turns (Figure 3.2.8). For a U-turn that allows for understeer correction, the steering assistance interface provided comparable accuracy, even in the absence of steering wheel correction. The current study demonstrates how sEMG sensors could be used to address the risk of shoulder overload and reduced steering portability without significantly compromising path following accuracy. Future research could utilize the findings of this study to realize accurate sEMG controlled automobile steering for persons with disability.

3.3 Experimental study III: Pedestrian collision avoidance using steering assistance controlled by Myo armband

3.3.1 Introduction

Whereas other studies discussed in this paper addressed the path following accuracy of sEMG interfaces during non-emergency Ackerman steering at low speeds close to zero, the current study aims to investigate the comparability of a sEMG controlled steering assistance interface to a steering wheel during pedestrian collision avoidance. Since sEMG controlled-steering assistance was intended for speeds at or below 30 km/h in residential and parking areas, test drivers completed pedestrian collision avoidance scenarios that took place in on residential roads at the maximum intended speed. With the maximum speed maintained to simulate cruise control and to ensure experimental repeatability, the sEMG interface was compared to manual steering and to manual takeover during automated driving. Based on this comparison, the current study was relevant to the body of literature concerning mainstream and emerging automotive steering interfaces.

Driving simulations were suitable for this experiment, since the safety of the recruited test drivers was of the utmost importance. Another benefit is the ability to safely and readily repeat driving scenarios to obtain data, if necessary. Steering involving dynamic changes in the trajectory of the simulated vehicle over time, distinguishes the steering of the current study from the steady-state steering, i.e. constant lateral acceleration along a circular path at constant vehicle speed, of the other studies in this paper. By allowing dynamic steering in the driving scenarios, it was possible to evaluate the Myo armband as a steering assistance interface. If the maximum slip angle of the simulated vehicle, when using the Myo armband, was comparable or significantly less than the slip angle corresponding to the other steering interfaces, then the safety of the Myo armband would be validated.

The rest of this paper documents the validation of the Myo armband as follows: Section 3.3.2 details the design of the sEMG interface, followed by a description in Section 3.3.3 regarding the methodology of the driving simulations. Section 3.3.4 presents and discusses the results of the driving simulations, and finally Section 3.3.5 provides concluding remarks about the results.

3.3.2 Design of myo armband steering assistance interface for driving simulator

In order to control the SWA, δ_H , of the driving simulator steering wheel, a control scheme in Figure 3.3.1 was implemented. By extending the wrist of the right arm, resulting sEMG signals was detected by the Myo armband. Based on this detection, a command was sent by the Myo armband to a laptop that translated the command into an ethernet signal that was sent to the driving simulator host computer. Then the host computer sent a command to an electric control unit that provided a voltage signal to a DC motor. Finally, the steering column was rotated by the motor to adjust the SWA.

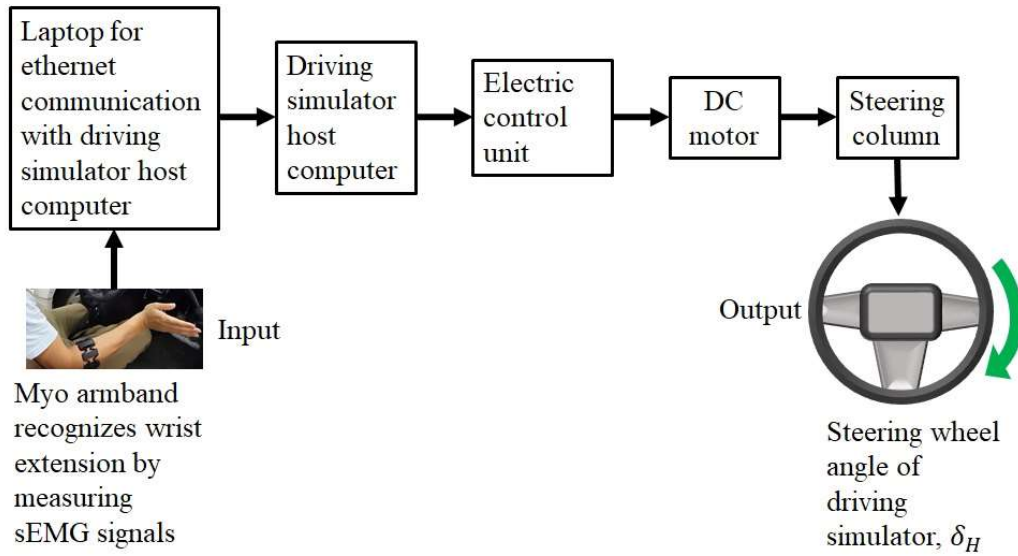


Figure 3.3.1 Overall control scheme of steering assistance interface.

The driving simulator host computer executed a steering wheel control algorithm based on the work of Wang et al. [177]. This algorithm implemented a proportional-integral and proportional-derivative controller as expressed by

$$T_h = K (a_1 e_{y(near)} + a_2 \int e_{y(near)} dt + a_3 e_{\theta(far)} + a_4 \dot{e}_{\theta(far)}) \quad (3.3)$$

The controller incorporates far and near points of the road ahead of the simulated vehicle. The near point centers the vehicle in the lane, whereas the far point enables the controller to adjust to upcoming road curvature. The lateral error, e_y , is defined as the distance between the vehicle and the preprogrammed target trajectory, with respect to the near point. On the other hand, the yaw error, e_θ , is the angle between the longitudinal path of the vehicle and the preprogrammed target trajectory at the far point. Given that the gain, K , is set to 1, the constant values of a_1 through a_4 are decided as 0.19, 0.019, 3.8, and 0.19, respectively, based on trial-and-error driving simulations to confirm the ability of the simulated vehicle to avoid a pedestrian in response to a command from the Myo armband. As described in Figure 1.4, the control method is an instance of Level 2 automation in which the vehicle controls steering, acceleration, and braking, while the driver monitors the vehicle surroundings to intervene by using the armband command, if necessary. The torque applied to the steering wheel, T_h , was limited to 5 N·m so that test drivers could manually correct the SWA at any time [178].

3.3.3 Methodology

Driving scenarios involving the use of either the steering wheel, Myo armband, or manual takeover were designed to replicate some pedestrian collision avoidance circumstances where steering was observed in a previous study to be more effective at avoiding collision than braking

[179]. Since allowing test subjects to brake during the driving scenarios could interfere with the measurement of steering trajectories, programming the simulated vehicle to run on cruise control at 30 km/h, and executing scenarios where steering was more effective than braking, was suited to validating the steering interfaces. The time-to-collision of the simulated vehicle with the pedestrian was set to 0.3 s, which is below the empirically based time-to-collision of 0.4 s, as inferred from [179]. Although the empirically based time-to-collision originated from an experiment without a crosswalk, each steering interface was tested with and without a crosswalk to determine whether or not a crosswalk would affect collision avoidance.

With the test drivers navigating the vehicle on the left lane, as shown in Figure 3.3.2, each driving scenario was programmed to have a pedestrian run perpendicularly across the road from behind a parked vehicle on the left-hand side at 8.34 m/s, after the driver was allowed at least 5 min to adjust to the driving task [180], [181]. The pedestrian came to a full stop upon reaching the center of the left lane. Then the drivers followed instructions to steer the vehicle to the right without pressing the brake.

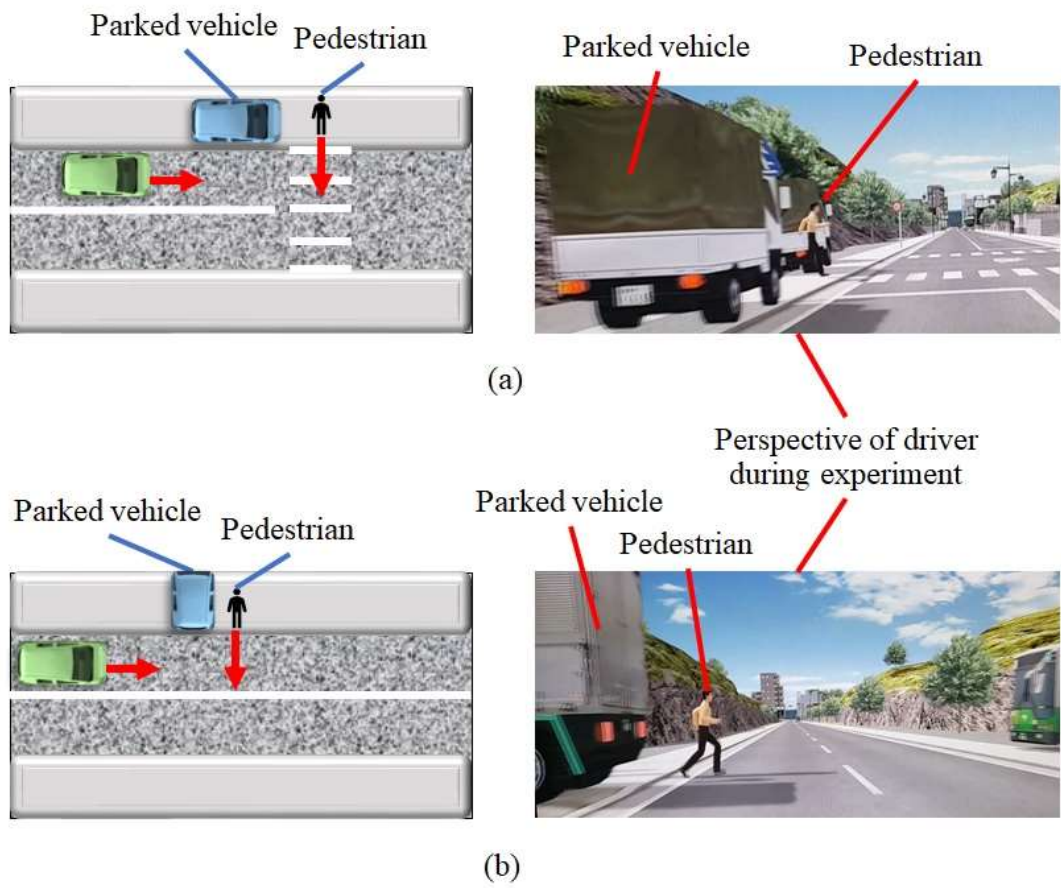


Figure 3.3.2 Driving scenarios with collision avoidance of pedestrian at crosswalk (a) and without crosswalk (b).

With permission from the Ethics Committee of the Interfaculty Initiative in Information Studies, Graduate School of Interdisciplinary Information Studies, The University of Tokyo (No. 14 in 2017), 10 test subjects with an average age of 23.2, an average of 2.8 years of actual driving experience were recruited as test drivers. All subjects gave informed consent prior to participating in the experiment. Only test subjects ages 25 and under were recruited, since it has been reported that drivers at or below 25 years of age are more likely to be involved in pedestrian collision accidents [181]. Hence, there recruitment of drivers within this age bracket would more accurately approximate actual pedestrian collision avoidance scenarios.

As shown in Table 3.5, all test subjects performed seven experimental conditions. Within-subject randomization of conditions was performed to address learning effects resulting from the order in which the conditions were performed. In addition to the six conditions involving pedestrian avoidance, another condition only involving driving without collision avoidance was performed as the fourth condition across all test subjects, in order to reduce the influence on the test results from the expectation among the test subjects that every driving scenario included collision avoidance.

Table 3.5 Conditions for testing steering interfaces during pedestrian collision avoidance. Except for fourth condition without pedestrian collision avoidance, within-subject randomization of conditions performed for each test subject.

Condition Number	Interface Type	Drivers performed pedestrian collision avoidance?	Pedestrian used crosswalk?
1	Myo armband	Yes	Yes
2	Myo armband	Yes	No
3	Steering wheel	Yes	Yes
4	Steering wheel	No	Not applicable
5	Steering wheel	Yes	No
6	Manual takeover	Yes	Yes
7	Manual takeover	Yes	No

Training of all test subjects also included, as the first scenario, use of steering wheel without any collision avoidance. Subsequent training scenarios all involved pedestrian collision avoidance at the same crosswalk, while the driver used one of three steering interfaces in the following order: steering wheel, Myo armband, manual takeover. In the case of manual takeover, drivers began the training scenario with acceleration and steering on autopilot. When the pedestrian began running across the road, the steering was switched to manual mode so that the driver could manually resume control of the steering wheel. The training scenarios for the Myo armband, as well as the experimental scenarios for the Myo armband and manual takeover, began in autopilot mode.

Since there were three interfaces, there were three training scenarios with collision avoidance, although there was also a manual steering wheel operation scenario without collision avoidance, for a total of four training scenarios. For the sake of efficiency, all training scenarios lasted up to

2.5 min.

As a basis for comparing the steering interfaces with respect to vehicle stability, the vehicle slip angle, β , as graphically defined in Figure 2.2, was measured at 120 Hz [182]. In order to observe the change in vehicle stability over time, the derivative of β was also measured. Increasing vehicle stability was associated with the derivative approaching zero, whereas decreasing vehicle stability would have resulted in divergence from zero. However, if the derivative of the vehicle slip angle was relatively small, in contrast to the simultaneous vehicle slip angle, it was possible that the derivative may not be responsive enough to represent the change in the physical rotation of the vehicle. In order to address this issue, the yaw rate of the vehicle was also measured to directly represent the change in physical rotation of the vehicle during vehicle slip. The yaw rate was therefore a secondary measure of the change in vehicle stability over time.

In order to eliminate the possibility that recorded vehicle slip angles at or close to zero could skew the average vehicle slip angle towards zero, especially in instances where the vehicle travels along a longitudinal trajectory before steering to avoid the simulated pedestrian, data points less than 0.1° or greater than -0.1° , were excluded from analysis. Since the vehicle slip angle could either positive or negative, yet the control design of the Myo armband interface was to reduce the absolute value of the vehicle slip angle, the absolute value of the measured vehicle slip angle was calculated. If the Myo armband was, at minimum, comparable to the other interfaces with respect to the absolute average vehicle slip angle across all test subjects, then the Myo armband would be validated. Before comparing the steering interfaces, the interaction between the presence and absence of a crosswalk in each of the driving scenarios in Figure 3.3.2 was assessed. Since the Shapiro–Wilk test in MATLAB, indicated that the vehicle slip data were not normally distributed, where the $p < 0.05$ [138], the nonparametric Friedman test was used in MATLAB to determine interaction between the driving scenarios [183], [184]. Given the Friedman test only compares datasets of equal size, after the absolute average vehicle slip angle data were equalized by excluding a minimal number of data points toward the end of the datasets.

Since the Friedman test indicated with $p < 0.05$ that the presence of a crosswalk significantly affected the magnitude of the vehicle slip angle, for each driving scenario, the interfaces were compared with respect to the absolute average vehicle slip angle. Based on the Shapiro-Wilks test and the unequal number of data points across the vehicle slip angle datasets for each interface, the comparison was performed in Excel with the nonparametric t -Test for unequal variances, where the two-tailed $p < 0.05$ for statistical significance. As means of graphically explaining the outcome of the interface comparison, steering trajectories, lateral acceleration over time as illustrated in Figure 2.2, vehicle slip over time, and box plots of the absolute vehicle slip angle were plotted on two-dimensional planes. For the time-dependent plots, $t = 0$ is when the pedestrian begins to cross the road in front of the car, where the final time is the moment before the car passes the location of the pedestrian along the road.

3.3.4 Results and discussion

A comparison of the steering interfaces with regard to pedestrian collision avoidance scenarios

is shown in Figure 3.3.3. Regardless of whether or not the pedestrian was using a crosswalk, the Myo armband was associated with significantly lower average vehicle slip than the other steering interfaces. Therefore, the Myo armband was validated with respect to vehicle stability.

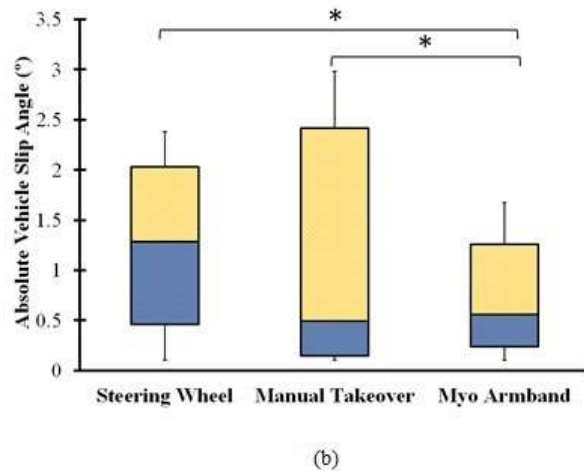
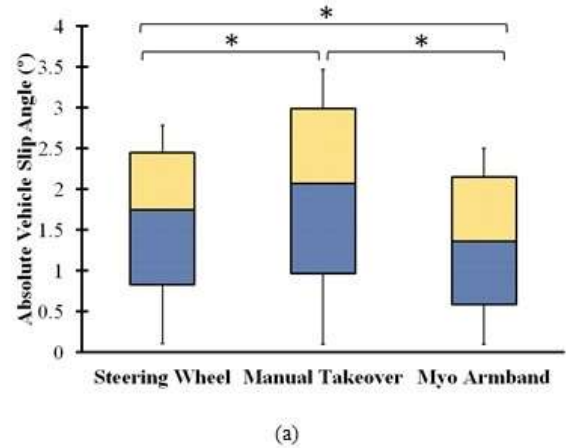


Figure 3.3.3 Comparison of steering interfaces with regard to absolute vehicle slip angle in pedestrian collision avoidance scenarios with a crosswalk (a) and without a crosswalk (b). “*” indicates statistically significant difference, with respect to absolute average vehicle slip angle, between two interfaces.

Based on the comparison of the steering interfaces with respect to absolute average vehicle slip, there are expected observable differences among the interfaces, if measured vehicle slip and its derivative are plotted over time, as shown in Figure 3.3.4. Regardless of whether or not a crosswalk was present, the Myo armband had significantly lower maximum and minimum vehicle slip due to the path following steering control algorithm developed for the Myo armband. The change in vehicle slip over time is correspondingly lowest for the Myo armband in both scenarios. In contrast, direct steering wheel operation and manual takeover were executed by human test drivers, thus resulting larger vehicle slip and change in vehicle slip over time. The derivative of

vehicle slip for the accordingly deviates less from zero for the Myo armband than for the other two interfaces.

Whereas vehicle slip was well below 4° for manual takeover, when the pedestrian used a crosswalk, vehicle slip came close to 4° for the same interface, when the pedestrian did not use a crosswalk. This result suggests that the absence of a crosswalk could lead to increased vehicle slip. However, this suggestion is not generalizable across all interfaces.

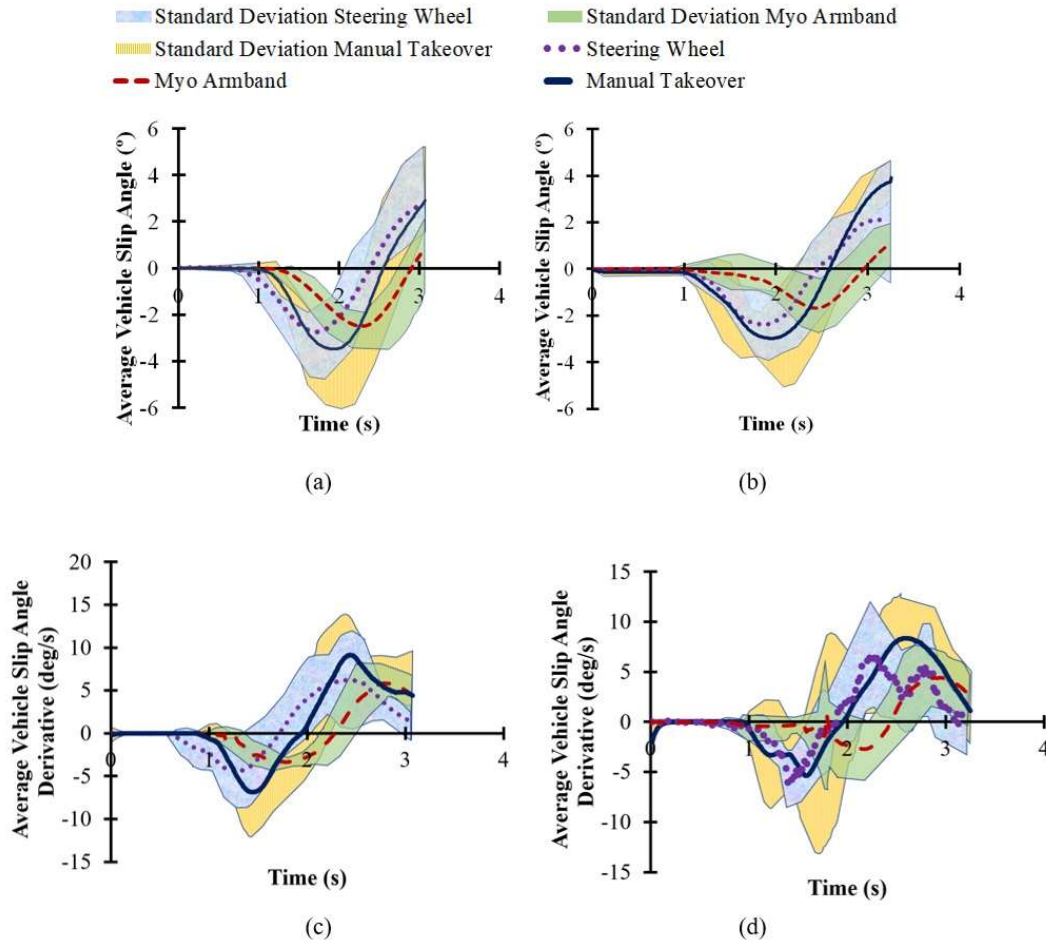
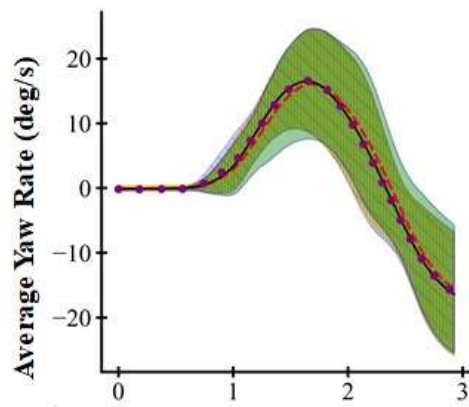
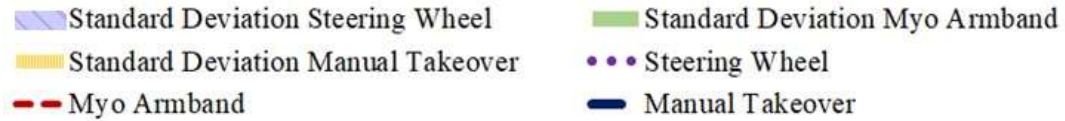


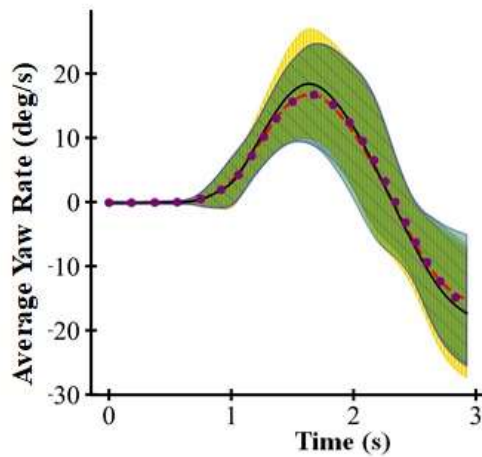
Figure 3.3.4 Comparison of steering interfaces with regard to average vehicle slip angle and derivative of average vehicle slip angle in pedestrian collision avoidance scenarios with a crosswalk (a), (c) and without a crosswalk (b), (d).

The average yaw rate of the vehicle over time across all trials agrees with the derivative of the average vehicle slip angle. Figure 3.3.5 indicates with a positive average yaw rate that the vehicle rotates rightward as it swerves right to avoid the pedestrian. Upon entering the opposing lane, the vehicle steers in the opposite direction, resulting in a negative average yaw rate. In accordance with the derivative of the average vehicle slip angle for the scenario with a crosswalk, the steering wheel and Myo armband have similar yaw rates. However, the difference between manual

takeover and the other two interfaces, with respect to averages and standard deviations, is not as pronounced. However, there is a more distinct difference between manual takeover and the other interfaces when there is no crosswalk, as expected from the derivatives of the average vehicle slip angles and standard deviations in Figure 3.3.4d. Overall, the average yaw rate indicates that the Myo armband has the lowest change in vehicle stability, in contrast to manual takeover and the steering wheel, whereas manual takeover was associated with the largest overall change.



(a)

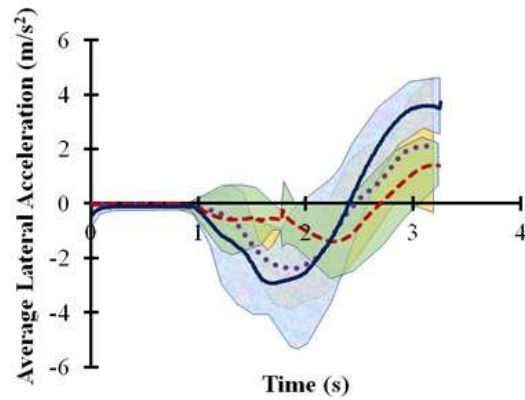
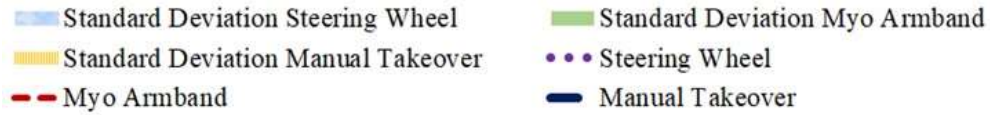


(b)

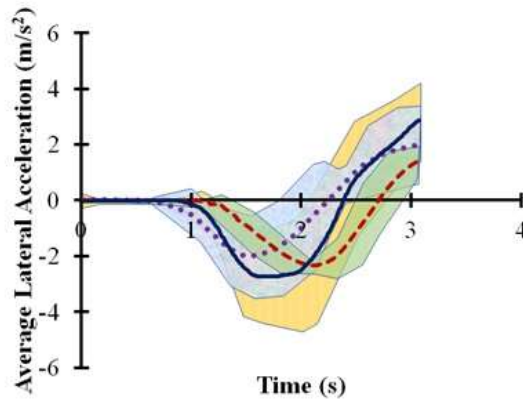
Figure 3.3.5 Comparison of steering interfaces with regard to average yaw rate over time in pedestrian collision avoidance scenarios with a crosswalk (a) and without a crosswalk (b).

Since lateral acceleration can contribute to the loss in tire traction, and consequently, vehicle

stability, during pedestrian collision avoidance, the steering interfaces were compared with respect to lateral acceleration, as shown in Figure 3.3.6 [182]. The period during collision avoidance between 1 s and 3 s, corresponds to dynamic changes in lateral acceleration that, in turn, could have resulted in dynamic changes in vehicle stability, as expected in Figure 3.3.4.



(a)



(b)

Figure 3.3.6 Comparison of steering interfaces with regard to average lateral acceleration over time in pedestrian collision avoidance scenarios with a crosswalk (a) and without a crosswalk (b).

One method for explaining the change in lateral acceleration on the simulated vehicle during pedestrian collision avoidance is to observe changes in the collision avoidance trajectories, as shown in Figure 3.3.7. Noting that the position of the vehicle was measured relative to the absolute x-y origin in the driving simulation, the vehicle runs parallel to the x-axis at the beginning of each driving scenario. In order to avoid the pedestrian, drivers were instructed to steering the vehicle rightward from the left lane, thereby causing the vehicle to change into the

right lane. In the case of the steering wheel and manual takeover from automated driving, this lane change was executed, on average, at a farther distance from the pedestrian, than the distance observed in the case of the Myo armband. This indicates a faster response time for conventional steering and manual takeover with regard to steering initiation. However, the less gradual lane change with the steering wheel or during manual takeover can be attributed to the turning of the steering of wheel by human drivers, as opposed to the automatic steering control algorithm in the case of the Myo armband. Consequently, the lateral acceleration on the simulated vehicle was higher, when human drivers steered, as expected in Figure 3.3.4. This higher lateral acceleration could have led to the higher degree of vehicle slip associated with the steering wheel and manual takeover, as evidenced by Figure 3.3.3. Therefore, the driving simulator data suggests that the Myo armband could be used to execute more gradual pedestrian collision avoidance trajectories that lead to higher vehicle stability.

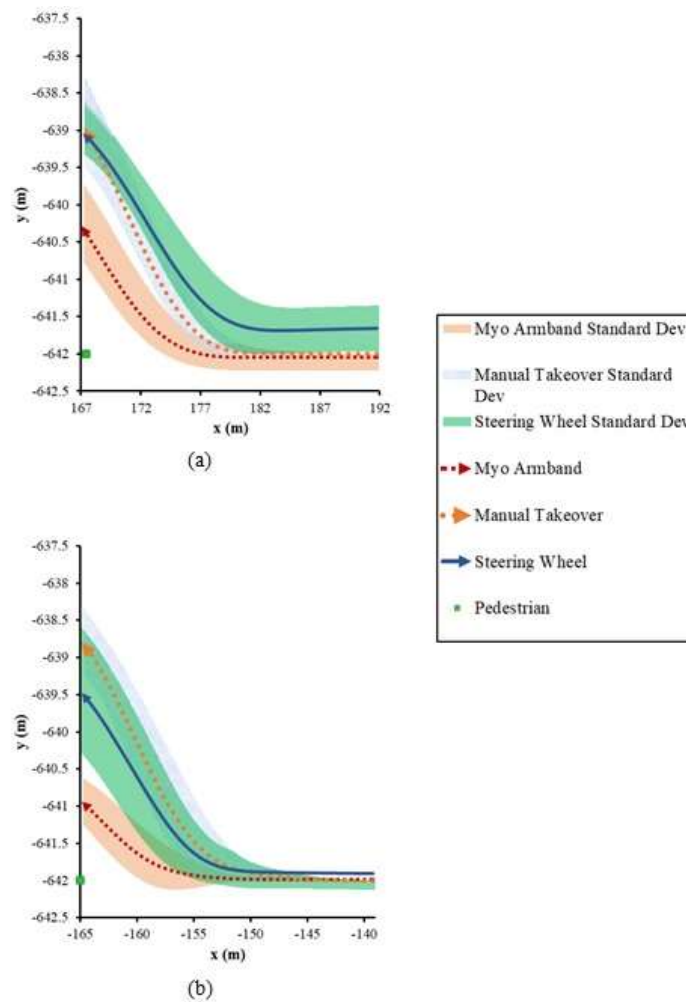


Figure 3.3.7 Comparison of average pedestrian collision avoidance trajectories over time in driving scenarios with a crosswalk (a) and without a crosswalk (b).

Notice that the initial lateral positions of the simulated vehicle in Figure 3.3.7 vary with respect to the type of steering interface. This variability was caused by the inability of drivers to maintain the same lateral position during manual operation of the steering wheel. However, the variability in lateral position between the interfaces of 0.5 m or less is negligible relative to the maximum change in lateral position of the vehicle for each driving scenario.

There is also a difference between the steering interfaces with respect to the steering wheel angle response over time, as observed in Figure 3.3.8. Conventional steering wheel operation and manual takeover from automated driving both had lower maximum and minimum steering wheel angles than the Myo armband interface regardless of whether or not the pedestrian was at a crosswalk. As expected, the larger maximum and minimum steering wheel angles for the steering wheel-based interfaces correspond to larger maximum changes in lateral vehicle position shown in Figure 3.3.7, and consequently, the respective absolute vehicle slip angles and larger absolute lateral accelerations in Figures 3.3.4 and 3.3.6, respectively.

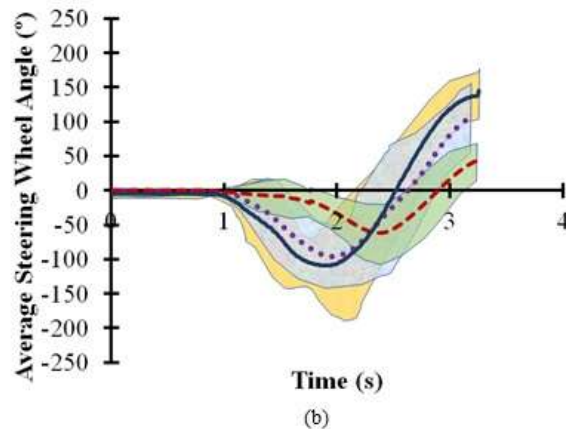
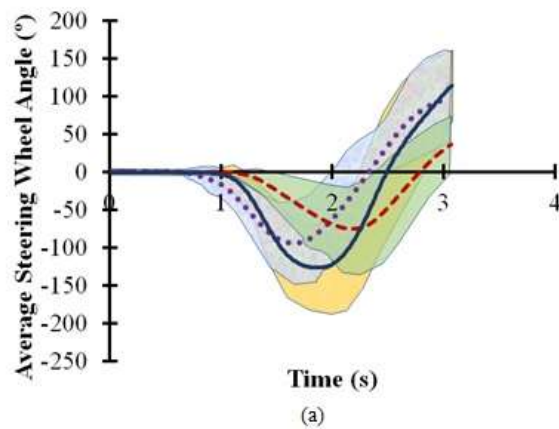
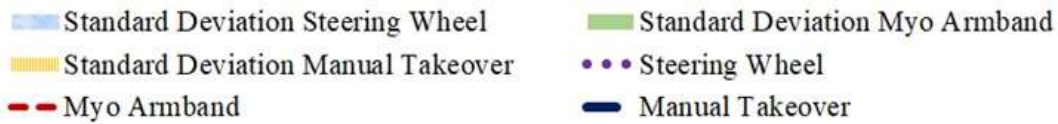


Figure 3.3.7 Comparison of average steering wheel angles over time in driving scenarios with a crosswalk (a) and without a crosswalk (b).

The difference in maximum and minimum steering angles between manual takeover and conventional steering wheel operation, when the pedestrian was not at a crosswalk, was less than when the pedestrian was at a crosswalk. Furthermore, the reaction time for these two steering wheel-based interfaces was less when the pedestrian was at the crosswalk, as opposed to not being at crosswalk. These results suggest that the drivers were more responsive when the pedestrian was at the crosswalk because the crosswalk allowed the drivers to anticipate the presence of the pedestrian. The same explanation may also apply to the lower reaction time of the Myo armband interface, when the pedestrian was at the crosswalk, as opposed to not using the crosswalk.

Using the Myo armband also produced a noticeable difference in response time, in contrast to the other steering interfaces, as indicated by Figure 3.3.8. Nevertheless, the lower response time was associated with lower maximum and minimum steering wheel angles that resulted in lower lateral acceleration and yaw rate, along with higher vehicle stability as shown in Figures 3.3.4, 3.3.5 and 3.3.6. Therefore, the results indicate that response time is a tradeoff for higher vehicle stability. Given that the objective of the current study was to validate the vehicle stability of the Myo armband interface, such as tradeoff is acceptable, since the Myo armband had higher vehicle stability, and was therefore safer than the other tested interfaces.

3.3.5 Conclusion

The Myo armband was validated through its comparison with manual takeover from automated driving and with manual steering wheel operation. By having a higher degree of vehicle stability during simulated pedestrian collision avoidance scenarios, use of the Myo armband resulted in more gradual collision avoidance trajectories that were observed to translate into higher vehicle stability. Although the response time of the Myo armband, with respect to the change in steering angle over time, was longer than the steering wheel-based interfaces, such a tradeoff was acceptable, since the Myo armband interface had higher vehicle stability, and was therefore safer than the other tested interfaces. In contrast to other studies in this paper that only tested sEMG-controlled interfaces during non-emergency Ackermann steering with negligible vehicle slip, the current driving simulator study demonstrates the superiority of the Myo armband over the other steering interfaces in scenarios involving observable vehicle slip. Although future work could consider other dynamic steering scenarios involving vehicle slip, the current study supports the implementation of the Myo armband for steering assistance in some emergency scenarios.

3.4 Improvement of response times of the sEMG interfaces

With regard to the experiment involving low-speed turns with an actual vehicle, it was observed that the SWR could be increased in order to improve path following accuracy in the case of 90° turns. This observation was supported by two prior driving simulator studies with the prototype sEMG-based interfaces, where the fast-turning sEMG-based interface response time of 0.1 s, from a straight trajectory to a steering trajectory at the minimum turning radius of the vehicle, had a significantly higher path following accuracy than response times of 1 s and 0.268 s for the slow-steering sEMG-based interface and manual steering, respectively. However, empirical observations during preparation for the actual vehicle experiments indicated that sudden rapid steering wheel rotation by a DC motor resulted in a jerking steering wheel motion that may startle and reduce the safety of the driver. Further research could thus optimize SWR response time without compromising the safety and comfort of the driver. For example, optimization by increasing the magnitude of the voltage command to the DC motor for the steering column could reduce the SWR response time.

A further optimization concerns the response time of the detection algorithm for the sEMG-interface. One way to implement the fast-turning sEMG-interface in an actual automobile is to adapt the detection algorithm from the first two driving simulator experiments. Since an increased sEMG signal detection response time affects the ability of the driver to avoid collision with obstacles in the vehicle environment, the response time should be reduced as much as possible to optimize the safety of the driver, any passengers, or persons outside the vehicle. For example, preliminary tests with the prototype sEMG-based interface indicated that the original number of data points for the moving average window could be reduced from 70 data points to lower value such as 10 data points. Thus, if the fast-turning sEMG-based interface were to be implemented in an actual automobile, it is possible to achieve a detection response time less than or equal to 0.1 s, as specified in Figure 2.5. However, decreasing the window size would also increase the sensitivity of the algorithm to low frequency noise resulting from the movement of sEMG electrode wires, relative movement between the electrodes and the skin surface, etc. Therefore, the window size could be adjusted to optimize between the sEMG SNR and detection response time.

On the other hand, one solution to preventing low frequency noise is to substitute the prototype sEMG equipment with the Myo armband. Although the Myo armband relies on a proprietary gesture recognition algorithm, previous research has modified the Myo armband so that it can only be used to wirelessly transmit raw sEMG data as input for custom sEMG processing algorithms, such as the moving average algorithm from the first two driving simulator studies [88]. In addition to avoiding electrode wire movement noise through a Bluetooth connection, the Myo armband can acquire raw sEMG at 200 Hz, as an improvement over the original 81 Hz from the first two driving simulator experiments. Hence, the moving average algorithm could receive newly acquired data points at a higher frequency.

Although the Myo armband is conventionally used to measure forearm muscle activity, a previous study modified the Myo armband to obtain signals from the upper arm to control a powered prosthetic arm [14]. Similarly, the Myo armband could be modified to measure biceps

brachii sEMG signals resulting from isometric contractions or forearm rotation, as achieved in the first two driving simulator experiments.

As a preliminary estimation of the potential of the fast-turning sEMG-based interface to improve path following accuracy, trajectories were generated as shown in Figure 5.1. The trajectories account for the 0.1 s delay in steering initiation introduced by the fast-turning sEMG-based interface, in addition to the empirically observed delay based on the operation of the interface by the driver. Since the both of these delays also apply to the Myo armband, trajectories for both interfaces begin at the same vehicle location coordinates for each driving scenario. However, unlike the Myo armband, the fast-turning sEMG-based interface turns the steering wheel to the maximum SWA in 0.1 s. Thus, the trajectories for the fast-turning sEMG-based interface have a radius of curvature equal to the minimum turning radius of the vehicle. Based on this curvature, the estimated fast-turning sEMG-based interface could respectively reduce average lateral error by 46%, 9%, 69%, and 41% for the 45° turn, 90° turn, narrow U-turn, and wide U-turn.

The improvement for the 90° turn is lowest because experiments with an actual automobile demonstrated that drivers delayed steering initiation more for the 90° turn than the other steering maneuvers. Such a delay may have resulted from a lack of confidence or experience with the Myo armband interface. Thus, other than increasing the magnitude of the voltage command from the motor control circuit to the DC motor for the steering column or implementing the faster sEMG signal detection response time from the first two driving simulator experiments, drivers could increase path following accuracy by learning to steer sooner through training and experience.

It is expected that a lower response time would enhance path following accuracy, although the significance of this enhancement relative to the current results would be empirically confirmed. Given that the Myo armband interface was operated mostly at steady-state speeds below 2 km/h in the actual vehicle experiments, it is not likely that understeer and oversteer would affect path following accuracy, if the fast-turning sEMG-based interface is used under similar conditions to approximate Ackermann steering.

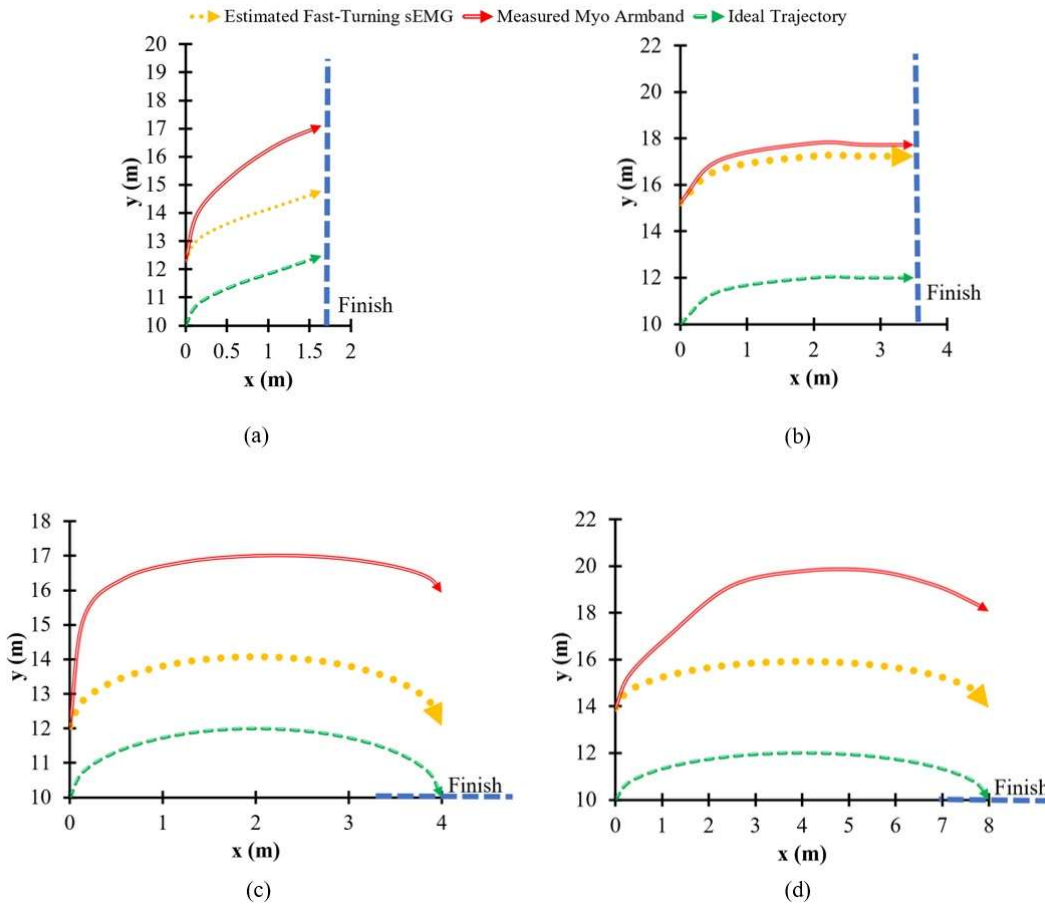


Figure 5.1 Estimated average turning trajectories of fast turning sEMG interface with response time of 0.1s from linear forward trajectory to steering trajectory for: (a) 45° turn, (b) 90° turn, (c) narrow U-turn, and (d) wide U-turn. Comparison made with measured trajectory of previously tested Myo armband interface for COMS vehicle from previous field test experiment.

Whereas reduced response time would improve path following accuracy during low-speed routine turns, vehicle stability could be compromised during pedestrian collision avoidance. If the Myo armband were to be converted into a fast-turning sEMG interface, it could take 0.1 s to rotate the steering wheel rightward from 0° to the maximum average angle of 75° that was observed from the results of the pedestrian collision avoidance driving simulator study. In order to observe the effect of this response time in a safe setting environment, preliminary driving simulator testing without human test subjects was conducted by automatically steering a simulated vehicle. As indicated in Figure 5.2, the fast-turning sEMG interface would distinguishably increase the distance to the pedestrian, in contrast to the previously tested Myo armband interface with a response time of 1 s. Notice that the trajectories in Figure 5.2a have been plotted to demonstrate collision avoidance from the time that the pedestrian begins running perpendicular to the path of the vehicle until the moment when the vehicle passes the center of the adjacent lane. As mentioned in Chapter 3, there is no significant difference between

trajectories with respect to the presence or absence of a crosswalk. However, the presence of a crosswalk is associated with an observably lower response time, as oppose to scenario without the crosswalk. Nevertheless, the fast-turning sEMG-based interface would have an advantage over the previous Myo armband interface, even if there were a crosswalk.

On the other hand, a lower response time of 0.1 s could markedly increase the vehicle slip angle as shown in Figure 5.2b. Unlike the gradual change in vehicle slip angle associated with the previously tested Myo armband interface, changing the Myo armband into a fast-turning interface could make the vehicle unable to move in the same direction as its heading because the vehicle could lose traction with the road. Therefore, despite having a more effective collision avoidance trajectory than the previously tested Myo armband interface, the response time of the fast-turning interface could put the driver, passengers, and other people in the vehicle environment in danger of collision through lose of steering control. A safer alternative would be to adjust the output of the steering column motor control circuit to determine an intermediate response time between 0.1 s and 1 s that would optimize the distance to the pedestrian without compromising vehicle stability.

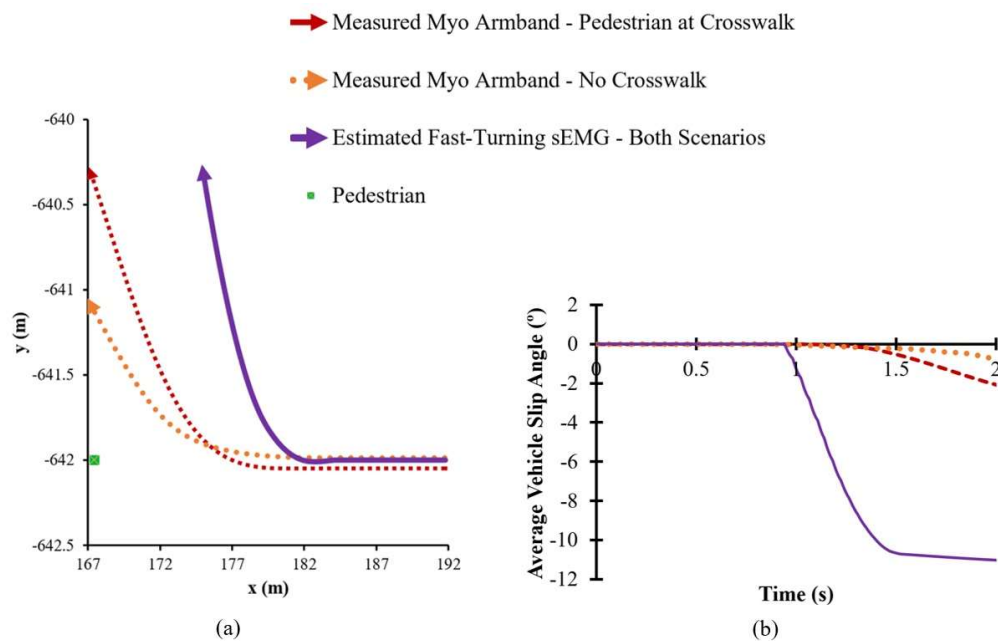


Figure 5.2 Estimated average trajectory (a) and average vehicle slip angle (b) of fast-turning sEMG interface with a response time of 0.1s from a linear forward trajectory to a pedestrian collision avoidance trajectory with steering wheel angle of 75°. Comparison made with measured average trajectory and average vehicle slip angle of Myo armband interface from driving simulator experiment.

Chapter 4

Experiments with an Actual Automobile

4 Experiments with an Actual Automobile

In order to implement sEMG-controlled steering assistance, as a practical feature in an actual automobile, the Myo armband was used to receive sEMG input from drivers. Unlike the previous prototype sEMG interfaces developed for the studies in Chapter 3, the Myo armband had dry electrodes that did not require mounting adhesive or electrode gel. The first study in Section 4.1, validates the Myo armband during dynamic steering scenarios that were previously included in the studies described in Chapter 3. On the other hand, static steering during parking is covered by the study in Section 4.2. Both experiments demonstrate the safety of sEMG-controlled steering assistance by validating the path following accuracy of the Myo armband during static and dynamic steering.

4.1 Experimental study I: Steering assistance of an actual automobile during different low speed turns

4.1.1 Introduction

In order to determine the extent to which the laptop-based driving simulation results involving circular, steady-state steering trajectories are applicable to an actual automobile, the trajectories were performed with the COMS B•COM vehicle, which is henceforth referred to as the “COMS.” This automobile is a small-scale electric vehicle by Toyota Auto Body Co., as shown in Figure 4.1.1a [185].

Previous sEMG-controlled steering interfaces employed prototype sEMG data acquisition equipment, whereas the current study uses the mass-marketed Myo armband, as depicted in Figure 4.1.1b, to facilitate experimental replicability [32], [88]. Since the eventual application of the armband interface is to assist numerous automobile drivers with only one healthy arm, the successful validation of a mass-produced sEMG-based interface device with respect to path following accuracy, would provide evidence to support the safe operation of the interface for these drivers. In order to validate the interface, the lateral error of the COMS was measured for several maneuvers: 45° turn, 90° turn, a narrow U-turn with a radius equal to the minimum turning radius of the COMS, and a wide U-turn with turning radius twice as large as the minimum turning radius. If the Myo armband was at least comparable overall to the steering wheel of the COMS, with respect to path following accuracy, then the Myo armband would be validated.

The rest of this chapter is organized as follows. Section 4.1.2 describes the experimental equipment, followed by details in Section 4.1.3 on the optimization of the SWA controller as well as the validation of the controller and the lateral error of the vehicle. Validation results are presented and discussed in Section 4.1.4. Based on the results and discussion, conclusions are provided in Section 4.1.5.



(a)



(b)

Figure 4.1.1 Steering of COMS electric vehicle (a) controlled by Myo Armband (b).

4.1.2 Materials

The proposed steering assistance employs the Myo armband to measure sEMG signals from the forearm [88]. The armband enables the user to wirelessly transmit steering commands to the COMS electric vehicle through a limited set of hand gestures that are preprogrammed by the manufacturer of the armband. Since the COMS or some of its features have been employed in other studies to develop steering systems, the COMS is a suitable platform for developing an sEMG-controlled interface [145], [186], [187].

In order to measure the position of the COMS during turning maneuvers, a GPS data acquisition unit (Racelogic RLVB2SX) was mounted in the cabin of the COMS. GPS satellite signal transmission with the unit was achieved by mounting and wiring two metal ground plane antennas on top of the vehicle as shown in Figure 4.1.2. Since the roof of the COMS was not

made of metal, aluminum foil sheets were placed between the top of the vehicle and the antennas. The position, speed, and lateral acceleration of the vehicle were recorded at 20 Hz. Position accuracy was ± 20 cm during optimal satellite communication.

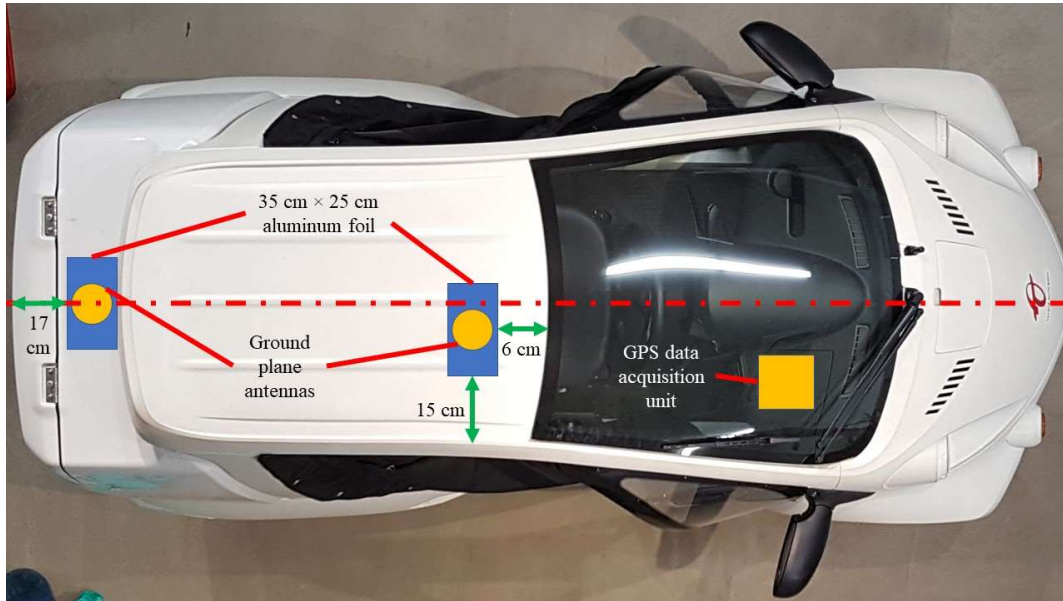


Figure 4.1.2 Setup of wired ground plane antennas for GPS data logging system mounted in cabin of COMS vehicle.

The ground plane antenna closest to the rear of the COMS was the primary antenna through which all vehicle motion parameters were calculated. Since vehicle position, speed, and lateral acceleration were the only parameters examined, it was not necessary to measure pitch and roll by aligning the primary and secondary ground plane antennas along the longitudinal axis of the vehicle, i.e. the dashed red line in Figure 4.1.2.

4.1.2.1 Steering assistance control system

The overall static steering assistance control system is shown in Figure 4.1.3. A Myo armband is mounted onto the left or right forearm to recognize sEMG signals from four hand gestures: wrist extension, wrist flexion, spread fingers, and tapping together of the middle finger and thumb. In order to prevent the accidental detection of sEMG signals due to unintentional hand gestures, deactivation of the armband is performed by rapidly tapping the middle finger and thumb together twice. Subsequently performing the same gesture activates the armband. If the armband is worn on the right arm, wrist extension turns the steering wheel to the right, whereas wrist flexion turns the steering wheel to the left. For the left hand, the direction of steering wheel rotation is reversed for wrist extension and wrist flexion. Spreading of the fingers stops the steering wheel rotation. If the driver does not stop steering wheel rotation, then depending on the initial SWA, the steering wheel will automatically rotate from 0° toward either the maximum leftward or rightward SWA

or away from either of the maximum SWAs toward 0°.

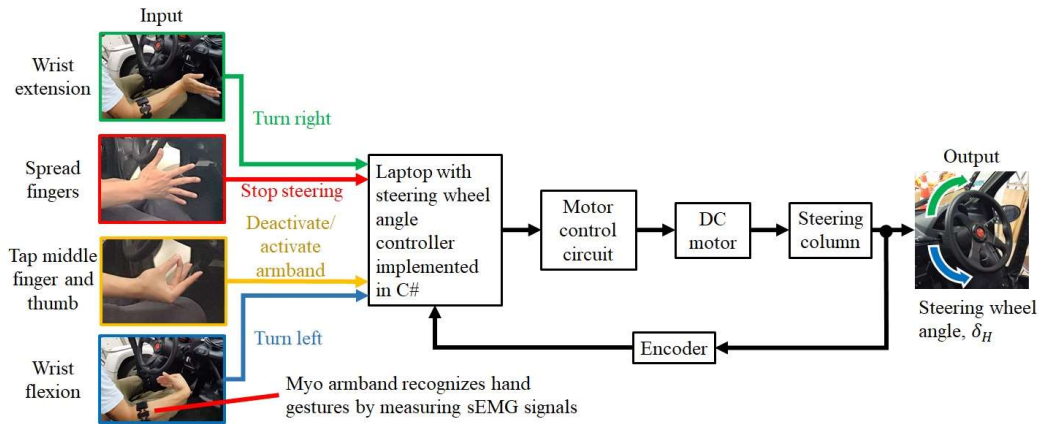


Figure 4.1.3 Setup of static steering assistance for steering wheel angle controller in production electric vehicle.

The armband wirelessly transmits detection signals for the hand gestures to a PC platform laptop (Acer, Inc., N17C1) that implements a steering wheel angle controller through a custom C# program. Based on the type of hand gesture, the steering wheel angle controller sends DC motor commands to a motor control circuit (Oriental Motor Co., Ltd, Controller BLV620K200S-3). A voltage signal is sent from the motor control circuit to a brushless DC motor (Oriental Motor Co., Ltd, Motor BLV620K200S-3). The DC motor is connected to the steering column of the COMS automobile by a pair of gears with a ratio of 1:1. These gears allow the steering column to be rotated by the DC motor to adjust the SWA. Based on the measured SWA at 100 Hz from an encoder (SICK AG, SKM36S-HVA0-K02) that is driven by the steering column, the steering wheel angle controller determines the difference between the measured SWA and the target SWA. The steering wheel angle controller alters the command to the motor control circuit according to this difference, thereby achieving closed-loop SWA control.

The steering system was defined as an assembly consisting of the motor control circuit, DC motor, and steering column (Figure 4.1.4). In accordance with a voltage setting command from the steering wheel angle controller, the motor control circuit provided voltage to the DC motor that rotates the steering column. The output of the steering system was the steering wheel angle, δ_H .

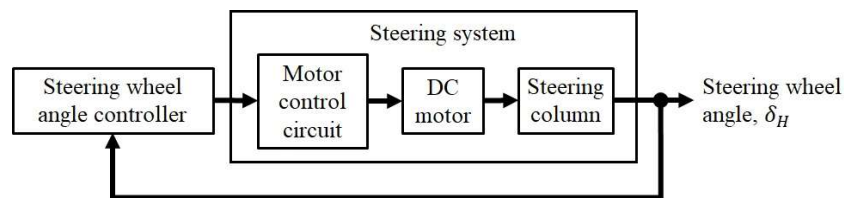


Figure 4.1.4 Static steering assistance control system model with steering wheel angle controller and steering system.

Figure 4.1.5 illustrates the algorithm for controlling the steering wheel angle of the COMS. The algorithm was only developed to address steering wheel rotation between 0° and the maximum rightward SWA of 625° , since the COMS only executed right turns in the driving scenarios. When the driver performs wrist extension with the wheel at 0° , the Myo armband recognizes this gesture and sends a command to the steering wheel angle controller to initiate rightward steering wheel rotation. The voltage command sent from the controller to the DC motor control circuit is increased in increments of 0.01 V from an initial value of 0 V . With the exception of the wide U-turn with a radius of curvature equal to twice the minimum turning radius of the COMS, all driving scenarios were designed to be performed with the target SWA being equal to the maximum SWA. In the case of the wide U-turn, trial and error testing determined the target SWA to be equal to 405° .

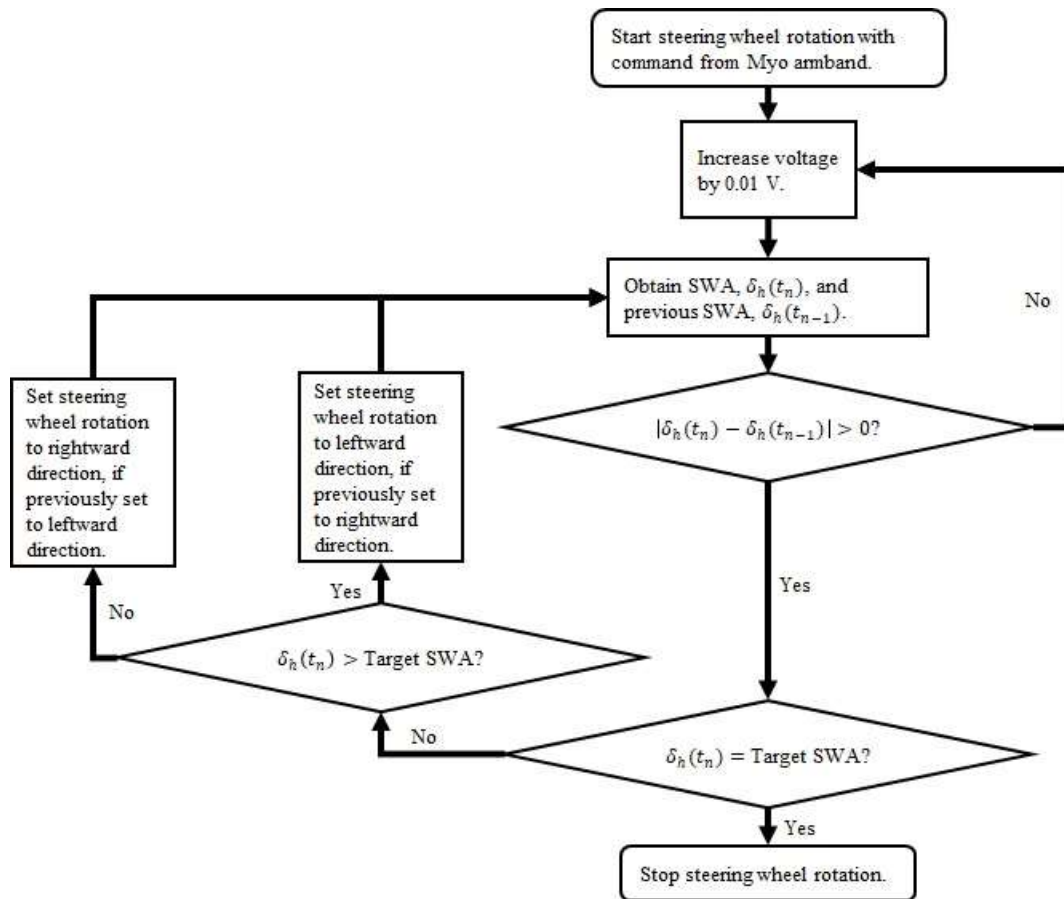


Figure 4.1.5 Steering wheel angle control algorithm for rightward steering wheel rotation.

As opposed to the commonly applied proportional derivative control, the method shown in Figure 4.1.5 gradually increased the rotation speed of the steering wheel to reduce wear on the steering system caused by jerk on the steering column from the DC motor. This jerk was observed by the sudden rotation of steering wheel when testing proportional control. A more important benefit is the reduced risk of injury to the driver from accidentally holding the steering wheel

during rotation, since the steering wheel is rotated gradually. Further details on the procedure for evaluating the performance of this algorithm with respect to the steering wheel angle, are described in the methodology section of this study. Data from the performance evaluation are contained in the results and discussion section of this study.

4.1.3 Methodology

With permission from the Ethics Committee of the Interfaculty Initiative in Information Studies, Graduate School of Interdisciplinary Information Studies, The University of Tokyo (No. 15 in 2018), five test subjects with an average age of 36 and an average of 15.4 years of driving experience were recruited as test drivers. Since permission from the ethics committee was restricted to the recruitment of staff at The University of Tokyo, the number of eligible participants of the study was limited to a few test subjects relative to the driving simulator studies. All subjects provided informed consent prior to participating in the experiment.

As illustrated in Figure 4.1.6, the test drivers performed several driving scenarios: a 45° turn, 90° turn, narrow U-turn with a radius of curvature equal to the minimum turning radius of 2 m for the COMS, and a wide U-turn with a radius of curvature equal to the twice the minimum turning radius. Since the objective of the experiment was to determine the extent which the results of previously conducted driving simulations were applicable to an actual automobile, with the exception of the radii of curvatures of the turns, the driving scenarios replicated the driving simulator scenarios shown in Figures 3.4 and 3.2.8. Using within subject randomization to determine the order in which the scenarios were performed, each scenario was performed once by each driver.

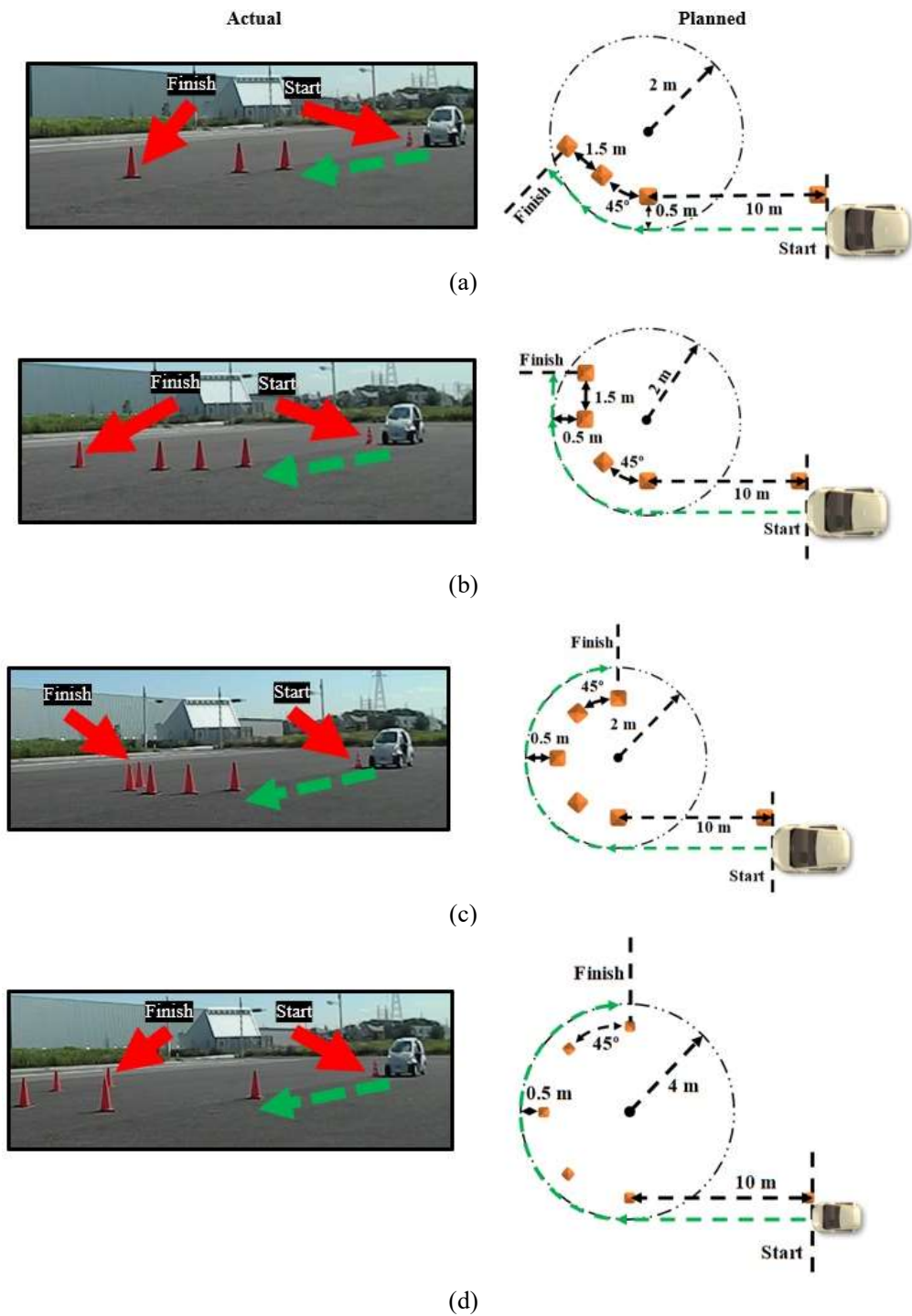


Figure 4.1.6 All drivers tested path following accuracy of steering wheel and Myo armband by performing: (a) 45° turn, (b) 90° turn, (c) narrow U-turn, and (d) wide U-turn. Excluding radii of curvature of each turn, all turning maneuvers replicated maneuvers from previously conducted driving simulator experiments.

VBOX File Processor software was used to convert the GPS data, including position, speed, and lateral acceleration, into two-dimensional cartesian coordinates that were read by Microsoft Excel. Then the position data was rotated in Excel to be plotted on two-dimensional coordinate planes to provide a graphical representation of the turning trajectories. Graphs for speed and lateral acceleration were also generated. All of the graphical data would be used to understand the turning trajectory results.

Since there was inter-subject variability in the steering trajectories, the number of available datapoints for the trajectories varied across subjects. Consequently, the average trajectories for each steering interface differed with respect to the number of datapoints. In order to determine whether or not there was any significant difference in average lateral error between the Myo armband and the COMS steering wheel, Welch's *t*-test for unequal variances was used because the test does not require compared datasets to have equal numbers of datapoints. Welch's *t*-test was performed for each driving scenario shown in Figure 4.1.6. In order for the Myo armband to be validated, it would have to be at least comparable overall to the steering wheel.

Based on the average trajectory data, the SWA throughout each driving scenario was calculated by multiplying Equation 3.2 by the COMS steering ratio of 14.2:1. The SWA was plotted as function of time to determine the performance of the steering wheel controller for the Myo armband. A comparison was made between the SWR for the Myo armband and the steering wheel. As described in the previously performed driving simulations of the same driving scenarios, in order to minimize oversteer or understeer that reduce path following accuracy, it was critical to maximize the SWR to attain Ackermann steering during turning maneuvers so that speed and SWA are at steady-state, and lateral acceleration is at or close to zero. Therefore, between the steering wheel and Myo armband, the steering interface that provided the highest maximum SWR during the initiation of a particular driving scenario would be considered superior with respect to steering system response for scenario. Superior system response would be used along with average steering trajectory, average speed, and average lateral acceleration to explain the outcome of comparing the steering interfaces with respect to path following accuracy.

4.1.4 Results and discussion

Comparison between the steering wheel of the COMS vehicle and the Myo armband was conducted by analyzing measured turning trajectory data from the experimental sessions with the test drivers. With respect to path following accuracy, Figure 4.1.7 indicates that the Myo armband was more accurate than the steering wheel for the 45° turn and the narrow U-turn, whereas the two interfaces were comparable to each other in the case of the wide U-turn. On the other hand, the steering wheel was more accurate in the case of the 90° turn. Overall, the Myo armband was validated because it was at comparable or superior to the steering wheel in most cases.

As predicted by the previous studies involving driving simulations of the driving scenarios from the current study, the Myo armband was more accurate in the case of the narrow U-turn, and comparably accurate in the case of the wide U-turn. However, with regard to the 90° turn, the Myo armband was unexpectedly less accurate than the steering wheel. In order to explain these results, the following discussion will consider turning trajectories of the COMS in relation to

average vehicle speed, average lateral acceleration on the vehicle throughout each turn, and the average SWR.

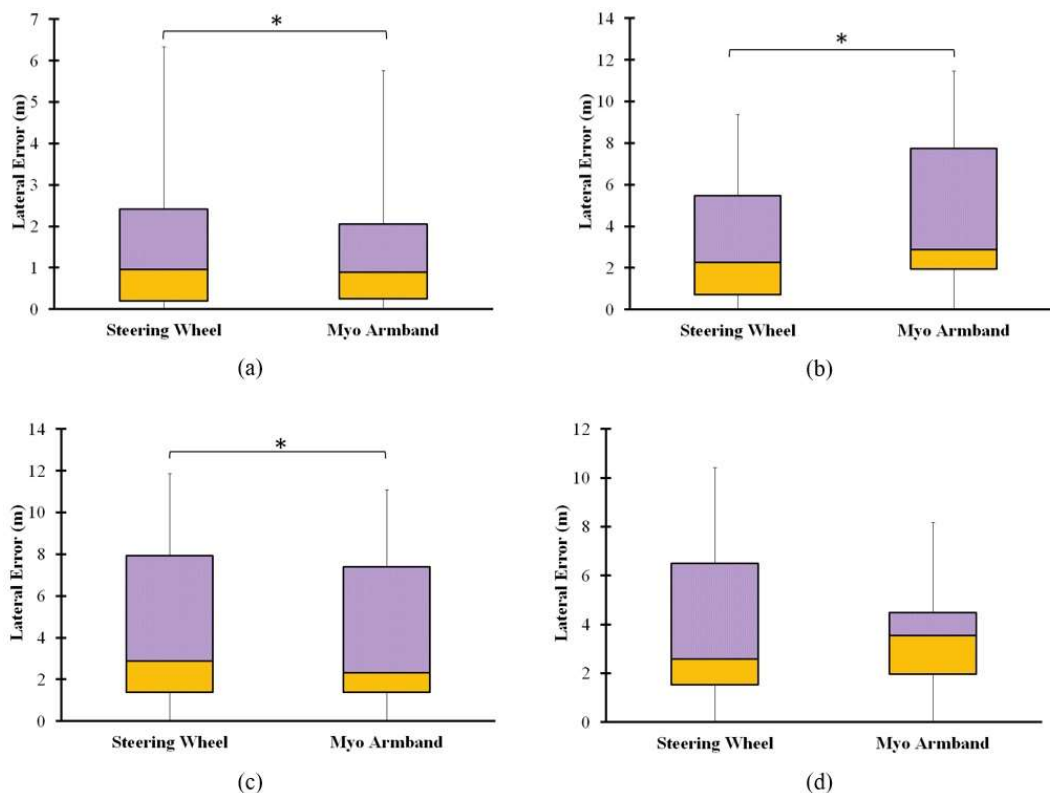


Figure 4.1.7 Median lateral errors used to evaluate path following accuracy of steering wheel and Myo armband in the case of four driving scenarios: (a) 45° turn, (b) 90° turn, (c) narrow U-turn, and (d) wide U-turn. With the exception of the wide turn, “*” indicates significant difference between averages of lateral error distributions. For the 45° turn and narrow U-turn, Myo armband was significantly more accurate than steering wheel, whereas steering wheel was significantly more accurate than Myo armband in case of 90° turn.

According to the turning trajectories in Figure 4.1.8 that were measured after the COMS vehicle passed the second road cone along the ideal path of each driving scenario, drivers tend to initiate turning later into the 90° turn, when using the Myo armband as opposed to the steering wheel. Hence, the turning trajectory associated with the Myo armband tends to follow the ideal trajectory less accurately than the trajectory associated with the steering wheel. This observation supports the lower path following accuracy of the Myo armband in the case of the 90° turn, as shown in Figure 4.1.7.

Contrastingly, in the case of the 45° turn and the narrow U-turn, the trajectories of the Myo armband tend to follow the ideal trajectories more accurately than the trajectories of the steering wheel. Thus, the Myo armband has higher path following accuracy, as indicated by Figure 4.1.7. The previous driving simulator study involving the wide U-turn predicted that steering wheel, and

an sEMG-based interface with a fixed SWR throughout the U-turn, would have comparable path following accuracy despite the steering correction provide by the steering wheel in the direction of the turn. This steering correction is evident in the steering wheel turning trajectory in Figure 4.1.8d, and as expected, the Myo armband with a fixed SWR throughout the wide U-turn, and the steering wheel have comparable path following accuracy, despite the steering correction of the steering wheel.

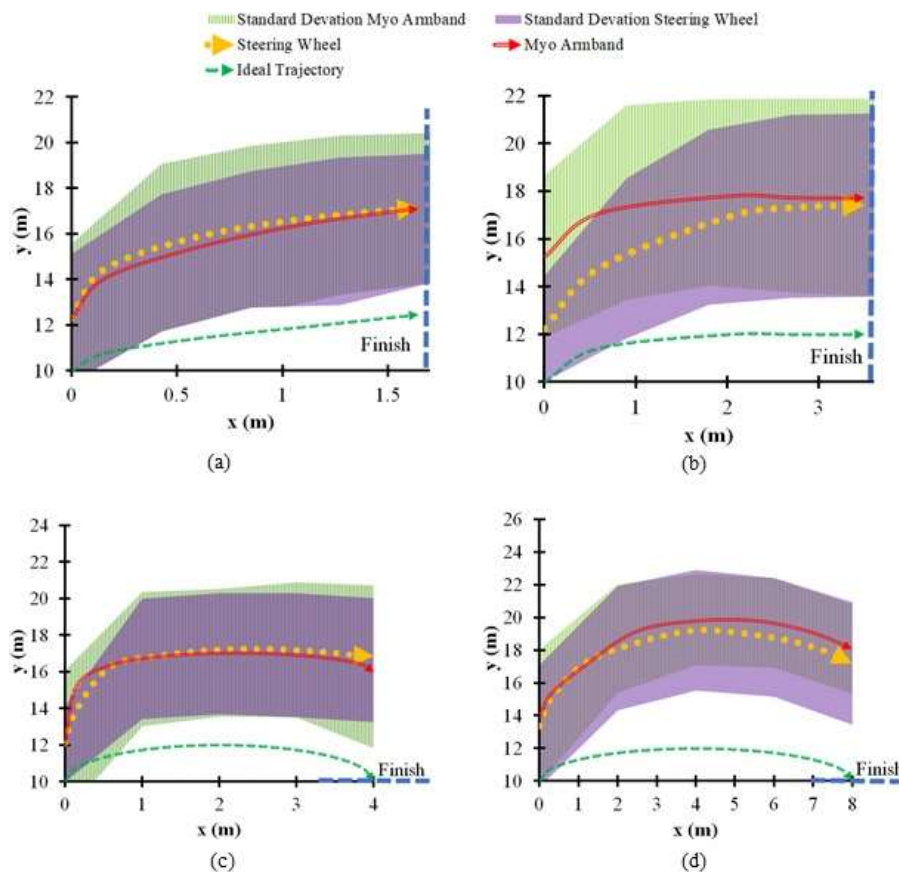


Figure 4.1.8 Average turning trajectories of steering wheel and Myo armband resulting from five test drivers performing: (a) 45° turn, (b) 90° turn, (c) narrow U-turn, and (d) wide U-turn. With the exception of the 90° turn, steering interfaces have graphically similar turning trajectories, although Myo armband tends to have better path following accuracy relative to the 45° turn and narrow U-turn.

The difference in vehicle speed between the steering interfaces is associated with path following accuracy. As shown in Figure 4.1.9, the average speeds for the interfaces, in the case of the 45° turn and narrow U-turn, are within 0.5 km/h of each other. For these turning maneuvers, the Myo armband was more accurate than the steering wheel. One possible steering characteristic that explains this greater accuracy concerns the fixed SWA of the Myo armband. By maintaining a constant SWA with the Myo armband, the COMS could have been able to follow the circular

path of the narrow U-turn and 45° turn more accurately at a vehicle speed that was comparable that of the steering wheel. On the other hand, the maximum difference in speed between the steering interfaces is larger in the cases of the wide U-turn and the 90° turn. For these maneuvers, the Myo armband was comparable in path following accuracy to the steering wheel in the case of the U-turn, whereas the Myo armband was less accurate with respect to the 90° turn .

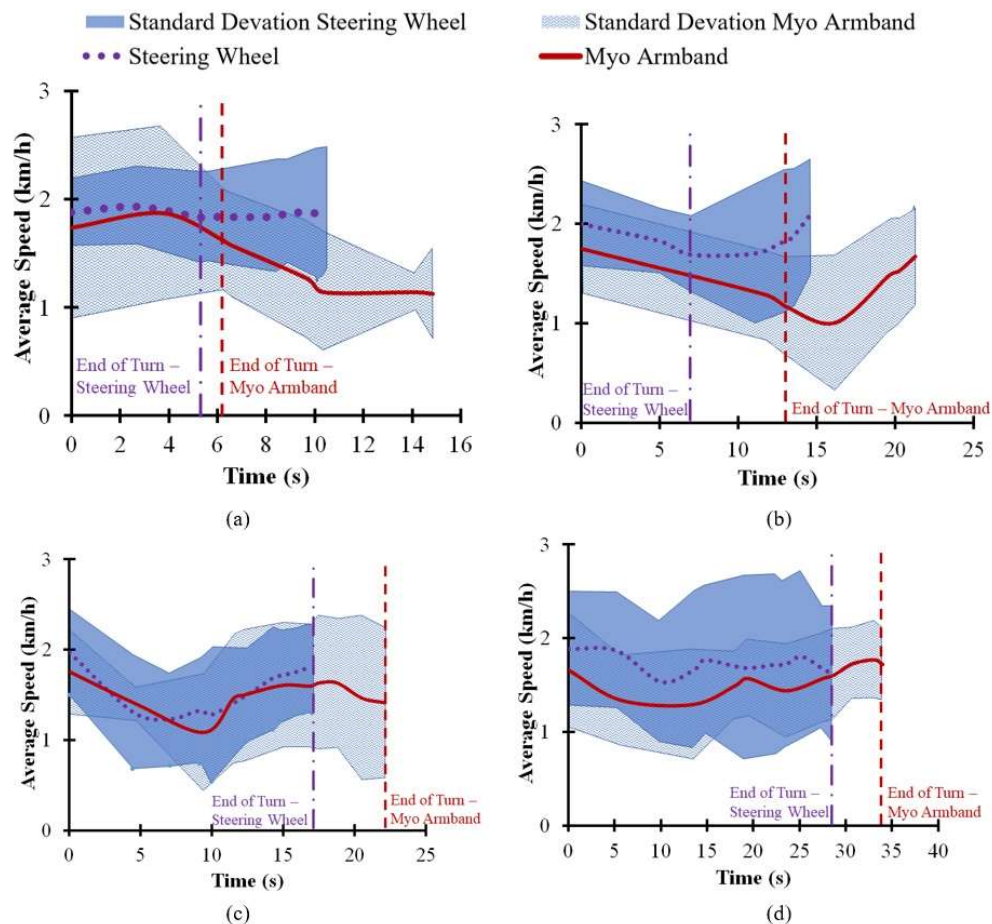


Figure 4.1.9 Average vehicle speed associated with steering wheel and Myo armband for: (a) 45° turn, (b) 90° turn, (c) narrow U-turn, and (d) wide U-turn. For the 45° turn and narrow U-turn, the speeds of the interfaces were within 0.5 km/h of each other, whereas the difference in speed was greater for the 90° turn and wide U-turn. Vertical dashed lines indicate average times when drivers exited turns by reverting from circular trajectory to longitudinal trajectory.

The tendency of the speed corresponding to the Myo armband to be slower for the wide U-turn and the 90° turn could indicate a tendency of the drivers to avoid understeer by decelerating the vehicle. Support for this tendency, in the case of the 90° turn, is shown by the trajectories in Figure 4.1.8b. Relative to the turning trajectory steering wheel, drivers used the Myo armband to initiate the turn at a further distance from the start of the driving scenario. Hence, the drivers may have decelerated the vehicle to reduce understeer as suggested by the decreasing speed indicated

by Figure 4.1.9b. Drivers may have also decelerated the vehicle, in the case of the wide U-turn, to reduce understeer as indicated by Figure 4.1.9d. Although the Myo armband was statistically comparable to the steering wheel with respect to path following accuracy for the wide U-turn, the trajectories in Figure 4.1.8d suggest that using the Myo armband instead of the steering wheel may have made the COMS more susceptible to understeer, thus motivating the drivers to decelerate.

For the steering wheel and the Myo armband, as shown in Figure 4.1.10a, lateral acceleration on the COMS vehicle was at or close to zero in the case of the 45° turn. Furthermore, since the average speed for both in interfaces was relatively constant, i.e. within 0.5 km/h of 2 km/h, Ackermann steering is considered to be attained. In contrast, significant lateral acceleration between -0.5 m/s^2 and -2 m/s^2 towards the center of the turn, i.e. centripetal acceleration is observed for the wide U-turn and the narrow U-turn in Figure 4.1.10. This transient change in lateral acceleration could have resulted from decelerating the vehicle in order to follow the beginning of the turns. Nevertheless, Ackermann steering is considered to be attained towards the end of each turn.

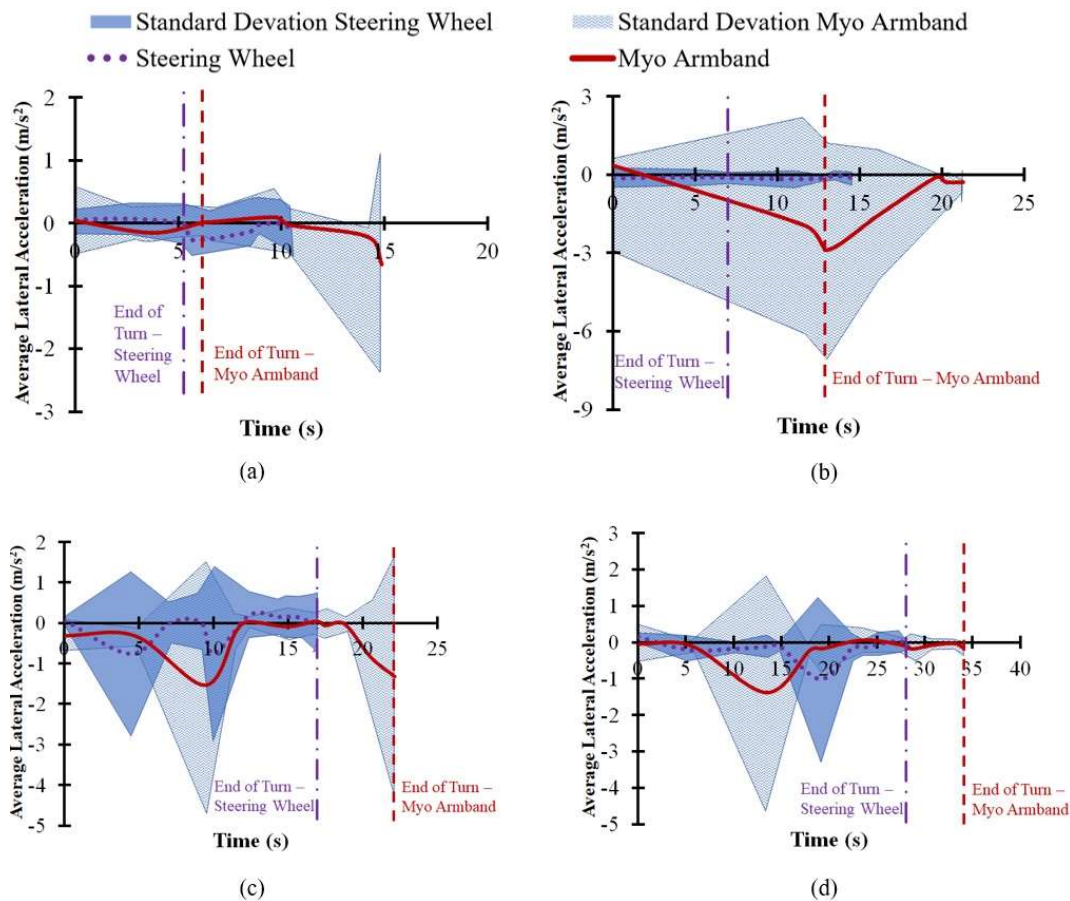


Figure 4.1.10 Average lateral acceleration on COMS vehicle for: (a) 45° turn, (b) 90° turn, (c) narrow U-turn, and (d) wide U-turn. Vertical dashed lines indicate average times when drivers exited turns by reverting from circular trajectory to longitudinal trajectory.

However, for the 90° turn, the Myo armband was associated with increasing lateral acceleration approaching -3 m/s towards from the center of the inside of the turn. This observable lateral acceleration is explained by the initiation of the turn with the Myo armband at distance between 5 to 6 m away from the ideal path as shown by Figure 4.1.8b. Drivers had to decelerate the vehicle in order to prevent understeer, although this was not sufficient to provide path following accuracy comparable to manual steering wheel operation.

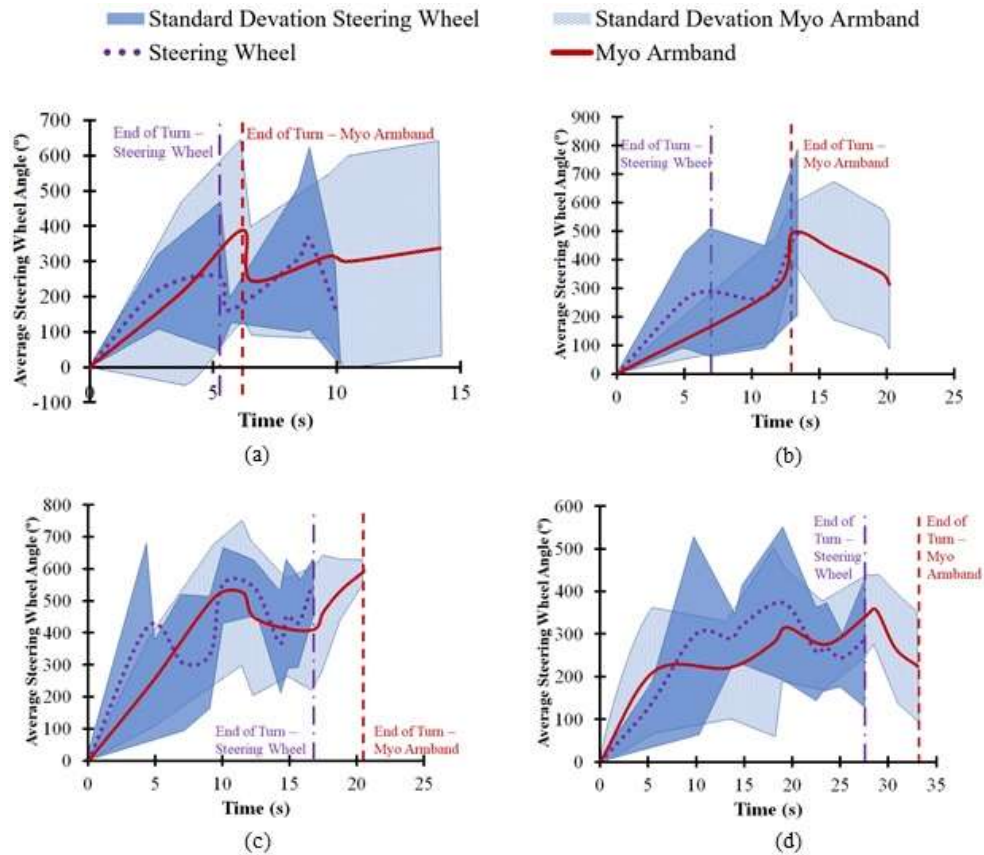


Figure 4.1.11 Average steering wheel angle of COMS vehicle for: (a) 45° turn, (b) 90° turn, (c) narrow U-turn, and (d) wide U-turn. Vertical dashed lines indicate average times when drivers exited turns by reverting from circular trajectory to longitudinal trajectory.

By considering the changing SWA through each turn with respect to time, i.e. SWR, it is possible to determine the effect of vehicle deceleration on steering ability of the steering system for the Myo armband. Another consequence of decreasing speed is increasing ground reaction force at the front steering tires of the COMS vehicle [123], [124]. For conventional steering wheels, more torque input from the driver is required to turn the steering wheel. Similarly, the steering control system for the armband has to provide more power to the DC motor that applies torque the steering column. As suggested by Figures 4.1.9b and Table 4.1, the lower vehicle speed associated with using the Myo armband resulted in higher torque input from the DC motor that

translated into higher average and maximum SWRs for the Myo armband, as opposed to the steering wheel. Increased SWR for the Myo armband is especially noticeable at the end of the 90° turn (Figure 4.1.11b). In contrast, Figure 4.1.11b indicates that the SWR for the Myo armband was lower at the beginning of the turn. As suggested by Figure 4.1.9b, the higher vehicle speed at the beginning of the turn resulted in lower ground reaction forces at the front steering tires, and thus less torque was applied by the DC motor to produce a lower SWR.

Table 4.1 Performance of steering interfaces based on steering wheel rate.

Interface	Driving scenario	Average steering wheel rate (°/s)	Standard Deviation of Steering Wheel Rate (°/s)	Maximum Steering Wheel Rate (°/s)
Steering wheel	45° turn	152.82	185.18	499.11
	90° turn	47.08	37.61	96.94
	Narrow U-turn	87.73	79.93	247.31
	Wide U-turn	18.32	9.44	34.04
Myo armband	45° turn	89.98	136.60	364.05
	90° turn	57.35	55.61	149.84
	Narrow U-turn	42.86	34.87	95.11
	Wide U-turn	20.13	13.80	44.62

When manually operating the steering wheel to perform the 45° turn, drivers applied the highest maximum and average SWRs (Table 4.1). Although the controller for the Myo armband had lower SWRs, it had higher path following accuracy than the steering wheel. Since the SWR increases as more torque is inputted into the steering column, the lower SWRs of the Myo armband suggest that the steering wheel angle controller of the Myo armband uses less energy than manual steering wheel operation to achieve path following accuracy during the 45° turn. This difference in energy usage could be due to driver behavior that produces excessive SWR.

Although the Myo armband is superior overall to the steering wheel with regard to steering system response, as quantified by average SWR, increased lateral acceleration from the higher maximum SWR of the Myo armband during the 90° turn, supports the possibility of understeer lowering path following accuracy, as shown by the trajectories of the 90° turn in Figure 4.1.8b. Similarly, although higher maximum SWRs are provided by the steering wheel for the other driving scenarios, as shown in Table 4.1, the Myo armband was comparable or superior to the steering with respect to path following accuracy, as indicated by Figure 4.1.7. Therefore, given that increasing SWR could result in higher lateral acceleration, and consequently lower path following accuracy, higher SWR does not necessarily correspond to higher path following accuracy.

It is evident from Figure 4.1.11d that drivers applied a larger SWR to steer the vehicle closer to the ideal path at the beginning of the wide U-turn, as shown in Figure 4.1.8d. In contrast, using

the Myo armband enabled drivers to steer to a fixed maximum steering wheel angle. Consequently, the maximum steering wheel angle for the Myo armband is lower than that of the steering wheel. The lower maximum steering wheel angle of the Myo armband explains how the trajectory of the Myo armband deviates further than the trajectory of the steering wheel from the ideal trajectory, towards the end of the wide U-turn (Figure 4.1.8d). Given that lateral acceleration for the two interfaces is at or close to zero towards the end of the wide U-turn, as shown in Figure 4.1.10d, the experimental data indicates that a lower maximum steering wheel angle, rather than understeer, contributed to the decreased path following accuracy of the Myo armband. Nevertheless, there is no significant difference in path following accuracy, as indicated in Figure 4.1.7d.

The steering trajectories in Figure 4.1.7b suggest that drivers using the Myo armband could be trained, through formal instruction or experience, to initiate steering earlier into the 90° turn, in order to improve path following accuracy. Further testing with driving simulations or an actual automobile would confirm the effect of earlier steering on the trajectory of the vehicle. With regard to the current results, the Myo armband has higher accuracy than the steering wheel, in the case of the 45° turn and narrow U-turn, whereas the interfaces are comparable for the wide U-turn. If it is possible in future experiments for users of the Myo armband to obtain accuracy that is equal or superior to the accuracy of a steering wheel, then the Myo armband would be advantageous over the steering wheel in most of the test cases. Future experiments could also involve persons with disability affecting one arm, in order to test the usability of the Myo armband or similar sEMG interfaces.

4.1.5 Conclusions

Based on the performance of four turning maneuvers with an actual automobile, the path following accuracy of the Myo armband was validated with respect to the steering wheel of the automobile. Overall, the Myo armband was comparable with regard to the wide U-turn, and superior in the case of the 45° turn and narrow U-turn. However, only with regard to the 90° turn was the steering wheel more accurate.

As predicted by previously conducted driving simulator studies described elsewhere in this paper, an sEMG interface, e.g. the Myo armband, can be used to perform the narrow U-turn more accurately than the steering wheel, while enabling comparable steering, relative to the wide U-turn. Whereas driving simulations predicted that an sEMG interface can enable comparable steering during the 45° turn, the Myo armband was more accurate than the steering wheel for the same scenario in the current study. On the other hand, unlike the comparability of an sEMG interface in the 90° turn of a previous driving simulator study, experiments with an actual automobile demonstrated that the steering wheel was more accurate.

One recommendation to improve the path following accuracy of the Myo armband, based on observations of the measured turning trajectories, was for steering to be initiated earlier into the 90° turn. Despite this possibility for improvement in accuracy, the results of the current study are significant, since the results validate, for the first time with an actual automobile, the path following accuracy of an sEMG interface in multiple scenarios. Based on the promising results of this study, further development and testing of the Myo armband with actual automobiles is

recommended to enable drivers with disability to perform maneuvers involving Ackermann steering.

4.2 Experimental study II: Steering assistance during parking of an actual automobile

4.2.1 Introduction

The other studies previously detailed in this paper considered the application of sEMG-based interfaces to dynamic turning maneuvers involving a moving car at low speeds. In order to provide a more comprehensive investigation with regard to the variety of driving scenarios, the current study concerns the use of the Myo armband to perform static steering during the parking of an actual vehicle.

The Myo armband remotely commanded a DC motor to change the steering wheel angle (SWA). A steering wheel angle controller employing a model reference adaptive control scheme was implemented as a C# program on a PC platform laptop to enable the DC motor to provide sufficient torque. Validation of the steady-state error of the steering wheel angle controller was performed with the COMS vehicle. In order to evaluate path following accuracy, the lateral error of the vehicle relative to the measured lateral errors in previous studies for perpendicular parking was also validated.

The rest of this chapter is organized as follows. Section 4.2.2 describes the experimental equipment, followed by details in Section 4.2.3 on the optimization of the SWA controller as well as the validation of the controller and the lateral error of the vehicle. Validation results are presented and discussed in Section 4.2.4. Based on the results and discussion, conclusions are provided in Section 4.2.5.

4.2.2 Materials

As described for the experiment involving the performance of multiple types of circular turning maneuvers with the COMS, the Myo armband measured sEMG signals from the forearm to control steering [88]. Although the Myo armband could command a DC motor to rotate the steering column, increased loads on the COMS require the motor to apply more torque to the steering column. In order to enable the motor to apply sufficient torque, a model reference adaptive controller (MRAC) was developed. In contrast to multiple system response tuning parameters for controller configurations such as proportional-derivative, proportional-integral, and proportional-integral-derivative controllers, the MRAC only has one tuning parameter [188], [189]. The MRAC can thus be more efficiently optimized with respect to different vehicle loading conditions. In order to explain the MRAC as means of controlling the SWA, the control system incorporating the MRAC is discussed in Section 3.3.2.1, while the design of the MRAC is discussed in Section 3.3.2.2.

4.2.2.1 Steering assistance control system

The overall static steering assistance control system is shown in Figure 4.1.3. A Myo armband is mounted onto the left or right forearm to recognize sEMG signals from four hand gestures:

wrist extension, wrist flexion, spread fingers, and tapping together of the middle finger and thumb. In order to prevent the accidental detection of sEMG signals due to unintentional hand gestures, deactivation of the armband is performed by rapidly tapping the middle finger and thumb together twice. Subsequently performing the same gesture activates the armband. If the armband is worn on the right arm, wrist extension turns the steering wheel to the right, whereas wrist flexion turns the steering wheel to the left. For the left hand, the direction of steering wheel rotation is reversed. Spreading of the fingers stops the steering wheel rotation. If the driver does not stop steering wheel rotation, then depending on the initial SWA, the steering wheel will automatically rotate from 0° toward either the maximum leftward or rightward SWA or away from either of the maximum SWAs toward 0° .

The armband wirelessly transmits detection signals for the hand gestures to a PC platform laptop (Acer, Inc., N17C1) that implements a steering wheel angle controller through a custom C# program. Based on the type of hand gesture, the steering wheel angle controller sends DC motor commands to a motor control circuit (Oriental Motor Co., Ltd, Controller BLV620K200S-3). A voltage signal is sent from the motor control circuit to a brushless DC motor (Oriental Motor Co., Ltd, Motor BLV620K200S-3). The DC motor is connected to the steering column of the COMS automobile by a pair of gears with a ratio of 1:1. These gears allow the steering column to be rotated by the DC motor to adjust the SWA. Based on the measured SWA at 100 Hz from an encoder (SICK AG, SKM36S-HVA0-K02) that is driven by the steering column, the steering wheel angle controller calculates the error between the measured SWA and the steering system model SWA. The steering wheel angle controller alters the command to the motor control circuit according to the error, thereby achieving closed-loop SWA control. As the steering wheel is rotated, all four tires (Yokohama Tire Corp., Ecos ES300 145/70R12) have an air pressure of 200 kps as recommended by the vehicle manufacturer. Once the steering wheel automatically rotates to the final SWA, steering assistance will shut down so that the driver can resume manual control of the steering wheel. Whereas static steering can be addressed by the steering assistance control system, the driver is responsible for manually performing dynamic steering corrections when the vehicle speed is greater than 0 km/h.

The steering system was defined as an assembly consisting of the motor control circuit, DC motor, and steering column (Figure 4.1.4). In accordance with a voltage setting command from the steering wheel angle controller, the motor control circuit provided voltage to the DC motor that rotates the steering column. The output of the steering system was the steering wheel angle, δ_H . Open loop control rotated the steering wheel from 0° to the maximum leftward and rightward SWAs with a step input voltage setting of 6 V to the motor control circuit (Figure 4.1.3). This voltage setting was sufficient for steering wheel rotation with the test driver in the vehicle. The use of open loop control relied on the mechanically limited SWA range of the steering system to prevent the SWA output from overshooting the maximum leftward and rightward angles. In cases where the steering wheel rotated away from a maximum SWA towards 0° , closed loop control shown in Figure 4.1.3 was applied to minimize the steady-state error in the SWA output.

4.2.2.2 Design of steering wheel angle controller

The steering system was modeled by a time domain function with SWA as the dependent variable. This function is the average response across 30 trials to a step input with a voltage setting amplitude of 2.2 V. The resulting change in the SWA is from -625° towards 0° (Figure 4.2.4), as measured by the encoder (Figure 4.1.3). A step input amplitude of 2.2 V was chosen because it was the minimum observed amplitude associated with a steady-state SWA that approaches 0° . Since the weight of the driver is not defined as part of the steering system, no driver was seated in the vehicle when the data for the steering system model was acquired. If the weight of a seated driver increased the load on the COMS, the steering wheel angle controller would have to raise the voltage setting above 2.2 V to cause the DC motor to provide sufficient torque to the steering column [124].

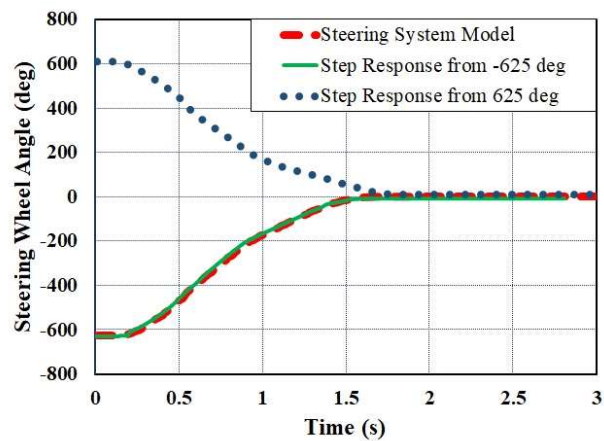


Figure 4.2.1 Step responses of steering system measured by encoder at a vehicle speed of zero with initial steering wheel angles of 625° and -625° (dotted and solid curves). Steering system model function also shown with initial steering wheel angle of -625° (dashed curve).

In order to adjust SWAs greater than or equal to 0° , the controller could rely on a steering system model based on the step response beginning from a rightward SWA and ending at 0° . Alternatively, the steering system model in Figure 4.2.1 for SWAs equal to or less than 0° could be used because of the similarity of system behavior for angles greater than or less than 0° . As a result of a step input at 0 s and an amplitude of 2.2 V, approximately symmetrical step responses were measured with initial SWAs at the extreme values of 625° and -625° (Figure 4.2.1). As in the case of data acquisition for the steering system model, no driver was seated in the COMS when the step responses were recorded. The settling times of 2.5 s for rotation from -625° and 2.6 s for rotation from 625° had a negligible percent difference of 8%. Furthermore, the steady-state values were -8° for the response with an initial SWA of -625° and 8° for the other response. Therefore, finding the absolute value of the SWA output of the steering system model for angles less than or equal to 0° would enable the steering wheel angle controller to adjust angles greater than or equal to 0° . The current study was thus conducted more efficiently by only optimizing and validating system behavior for SWAs less than or equal to 0° , since the results could be converted to apply to SWAs greater than or equal to 0° .

The amount of torque required to turn the steering wheel with the DC motor increases exponentially by a power of 1.5 with an increase in the total weight of the vehicle, including the driver and cargo [124], [186]. In order to adapt to changes in vehicle loading conditions, the steering wheel angle controller shown in Figure 4.1.4 employed a model reference adaptive control scheme (Figure 4.2.2). The adaptive mechanism in the control scheme uses the steering system model as a reference for the steering wheel angle. As expressed in Equation 4.1, the steering system model, $g_{model}(t)$, approximates the actual steering system, $g_{actual}(t)$, as follows:

$$g_{model}(t) \approx g_{actual}(t) = Kg(t) \quad (4.1)$$

where an unknown parameter, K , is multiplied by an unknown function, $g(t)$, to obtain the SWA output of the actual steering system output.

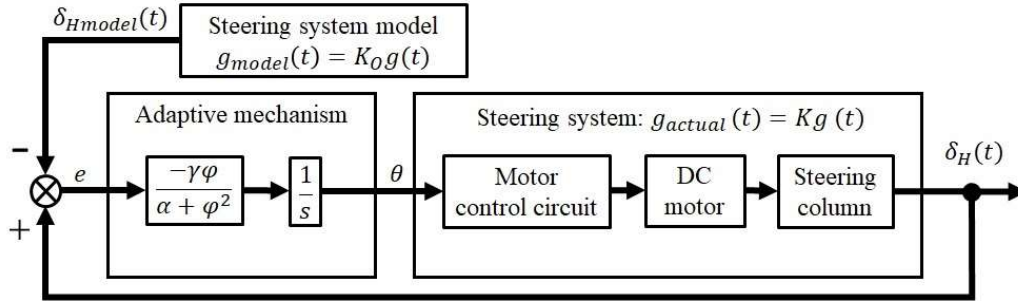


Figure 4.2.2 Model reference adaptive control scheme used in C# program to control steering wheel angle. Steering wheel angle controller consists of adaptive mechanism and steering system model. Note: Direction of steering wheel rotation selected based on hand gesture of driver before execution of control scheme.

Figure 4.2.2 shows that the input of the adaptive mechanism is the error, e , between the SWA output of the steering system model and the SWA output of the actual steering system. The adaptive mechanism outputs the voltage setting, θ , which is partly determined by e to adjust the voltage setting output of the steering wheel angle controller. θ originates from an adaptive control technique referred to as the MIT (Massachusetts Institute of Technology) rule. It has been demonstrated that the MIT rule is comparable to or superior to PID control for disturbances to or changes in DC motors [190].

In order to minimize the error, e , the MIT rule adjusts θ to minimize the cost function [189]:

$$J(\theta) = e^2/2 \quad (4.2)$$

The adjustment of θ is expressed as

$$d\theta/dt = -\gamma\partial J/\partial\theta \quad (4.3)$$

In order to adapt to changes in the response of the steering system, γ is selected to adjust the gain of the voltage setting from the adaptive mechanism. According to the function of J in Equation 4.2 the MIT rule is entailed by Equation 4.3 as

$$d\theta/dt = -\gamma e \partial e / \partial \theta \quad (4.4)$$

Since the MIT rule is sensitive to large changes in the reference input, the normalization of the MIT rule has been proposed. θ is calculated by integrating its derivative as expressed by a modified version of the MIT rule [189]:

$$d\theta/dt = -\gamma e \varphi / (\alpha + \varphi^2) \quad (4.5)$$

where φ is defined as

$$\varphi = \partial e / \partial \theta = K / K_o \delta_{Hmodel}(t) \quad (4.6)$$

The parameter, α , is set to a small value such as 0.01 to address cases in which φ^2 is equal to zero. Although K is unknown, K_o is a chosen parameter, and thus it is possible to let K_o be some number equal to K . This is accomplished by merely setting φ equal to $\delta_{Hmodel}(t)$. Equations 4.5 and 4.6 are therefore applied as shown by the block diagram in Figure 4.2.2. Since it is possible for θ to exceed the maximum voltage setting of 7 V or fall below the minimum voltage setting of 0 V, the C# program was configured to only transmit θ -values greater than 0 V or less than or equal to 7 V to the motor control circuit.

4.2.3 Methodology

This section details the optimization and validation procedures related to the steering assistance system. Methods for validating and optimizing the controller, as proposed in Section 3.3.3.1, were implemented along with the validation of the lateral error of the vehicle, as described in Section 3.3.3.2.

4.2.3.1 Validation of steering wheel angle controller

Optimization and validation of the steering wheel angle controller were conducted with the COMS at zero vehicle speed on the concrete floor in an indoor laboratory, as opposed to an outdoor track. This ensured SWA output repeatability by reducing the influence of fluctuating environmental temperature on tire pressure [191]. A test driver weighing 62.2 kg, including clothes, was recruited to sit in the COMS, while operating the steering assistance interface (Figure 4.2.3). Since the COMS was commercially available in Japan, typical loading due to the weight of the center of gravity of the driver, W_{driver} , was provided by choosing a male driver with a mass that was close to the average weight of 61.9 kg for males in Japan [192]. Permission to

recruit the driver was obtained from the Ethics Committee of the Interfaculty Initiative in Information Studies, Graduate School of Interdisciplinary Information Studies, The University of Tokyo (No. 15 in 2018).

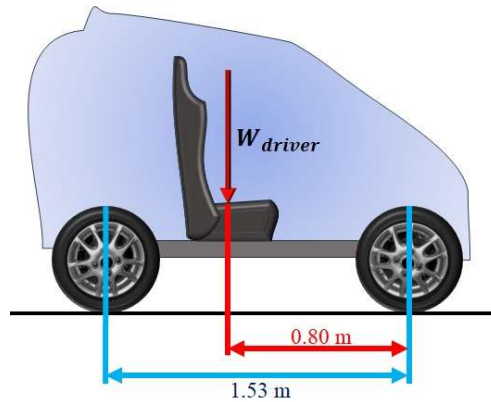


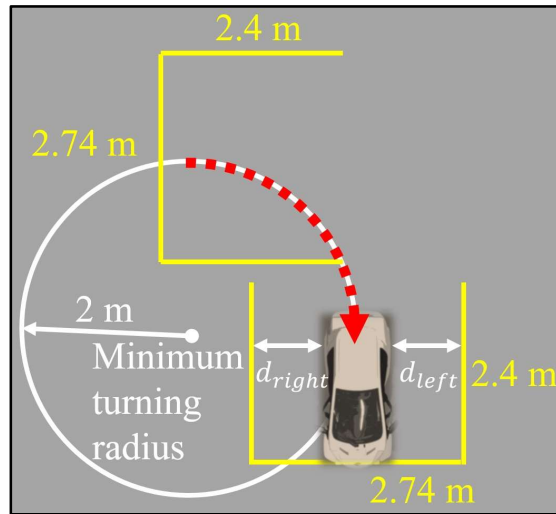
Figure 4.2.3 Loading configuration of COMS vehicle for experiment. W_{driver} represents weight from the center of gravity of driver.

The adaptive control scheme in Figure 4.2.2 was implemented as a custom C# program on a PC laptop. With the Myo armband mounted on the right forearm of the driver, γ was adjusted before the driver gestured to rotate the steering wheel from -625° to 0° , as indicated by the encoder (Figure 4.1.3). This sequence was repeated with different values of γ until the steady state error was minimized. Consequently, the steering wheel angle controller was optimized with a γ -value of 143.

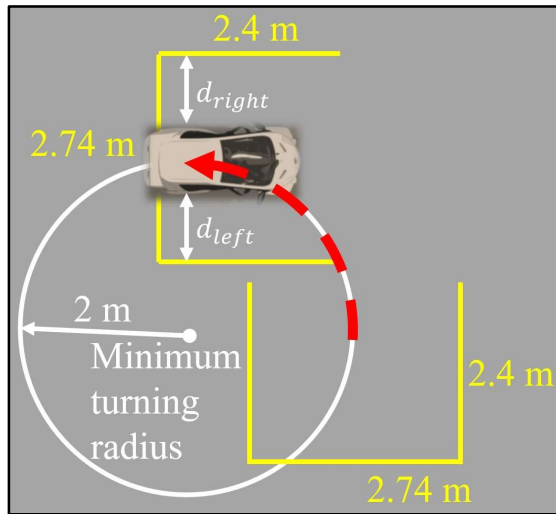
The objective of validation was to confirm that the error in the SWA output the controller relative to the SWA output of the steering system model was within $\pm 20^\circ$ of 0° . This error margin was chosen because, after using the steering assistance interface, the driver would only have to make a relatively minor SWA adjustment relative to the initial SWA of -625° . During the validation session, the driver used the Myo armband to rotate the steering wheel 15 times from -625° to 0° . The average SWA output over time was calculated so that the average steady-state value could be subtracted from 0° to obtain the average steady-state error. In order to explain the SWA output settling time and steady-state SWA, the voltage setting for the DC motor control circuit was recorded as the input for the steering system (Figure 4.1.4).

4.2.3.2 Validation of lateral error of vehicle during parking

Validation of lateral error was based on previous field studies on parking [193], [194]. A study involving 102 vehicles in the United States in the city of Ann Arbor, Michigan found that 2/3 of all parking spaces were perpendicular as opposed to angle or parallel [193]. The average width of the parking spaces was 108 in or approximately 2.74 m. Thus, the current study only validates for perpendicular parking with parking space widths being set to 2.74 m (Figure 4.2.4).



(a)



(b)

Figure 4.2.4 Validation of path following accuracy of steering assistance relative to lateral error of vehicle in two parking scenarios: (a) Forward perpendicular parking and (b) reverse perpendicular parking. Path following accuracy in each scenario is lateral error obtained by subtracting d_{right} from d_{left} .

Since one of the aims of this study was to validate the lateral error of the vehicle rather than human factors, the same test driver who validated the steering wheel angle controller adjusted the longitudinal position of the vehicle in accordance with verbal guidance from one of the

investigators rather than personal preference. In order to mitigate the influence of the driver on parking trajectory, the driver was also instructed to only adjust the SWA when the car was at a full stop and to keep the speed of the vehicle at a constant value close to zero throughout the turn.

On a closed outdoor test track at The University of Tokyo campus in Kashiwa, the path following accuracy associated with the steering assistance interface was validated with respect to the average lateral error of the COMS in each of the two parking scenarios (Figure 4.2.4). The parking spaces in each scenario were demarcated by yellow masking tape. For the first parking scenario shown in Figure 4.2.4a, the initial position of the car with an SWA of 0° was laterally centered in one of the parking spaces. In order to perform Ackermann steering, the driver was instructed to use the Myo armband on the right forearm to rotate the steering wheel rightward to maximum SWA. The driver would then resume manual control by deactivating the steering assistance before holding the steering wheel throughout the turn. Without changing the SWA, the driver turned rightward at the minimum turning radius of the car by pressing the accelerator to sufficiently move the car at close to 0 km/h. The resulting circular trajectory led to the other parking space. Since the longitudinal error of the vehicle was not being validated, the driver was verbally guided by one of the investigators so that the front tires reached the parking space guideline perpendicular to the direction of the vehicle. In order to calculate the lateral error of the car relative to the parallel parking space guidelines, the final lateral position of the center of the car was measured. The two minimum lateral distances, d_{left} and d_{right} , between the parallel guidelines and the tire walls closest to the lines were obtained with measuring tape (Figure 4.2.4). If the distances were equal, the car would be centered in the parking space with a lateral error of 0 cm. Otherwise, the lateral error of the uncentered car would be obtained by subtracting d_{right} from d_{left} . A negative difference between the two distances indicated a leftward bias in the alignment of the car with the parking space, whereas a positive difference indicated a rightward bias. Since the average yaw angles of vehicles during perpendicular parking were observed to be negligibly small at 0.02° in [194] and 0.1° in [193], the yaw angle of the COMS was not taken into account when measuring lateral distances. After the lateral distances were measured, the driver would center the car in the parking space with the help of one of the investigators before the SWA was set to 0° . Then the driver performed the perpendicular parking scenario in Figure 4.2.4b by using the Myo armband to rotate the steering wheel to the maximum SWA, resuming manual control, and reversing into the other parking space without changing the SWA. The lateral error of the vehicle was also measured through the same procedure for forward perpendicular parking. This cycle of forward perpendicular parking followed by reverse perpendicular parking was repeated until each driving scenario was performed five times. More attempts could have been performed, although the number of attempts was limited to reduce any effect of muscle fatigue on the operation of the armband.

The mean and standard deviation of the lateral error for each parking scenario was calculated along with the intertrial mean and standard deviation across both scenarios (Figure 4.2.4). Based on the Shapiro-Wilk test, where the significance criterion of $p < 0.05$ would reject the null hypothesis that the lateral error data were normally distributed, the lateral error data between and across scenarios were determined to be normally distributed [138]. Since the variances between the scenarios were unequal, the lateral errors of the scenarios were compared with an unequal

variances *t*-test, i.e. Welch's *t*-test, where $p < 0.05$ to reject the null hypothesis that there is no significant difference between the scenarios [195]. Comparing the scenarios would determine if the direction of vehicle movement affected lateral error. Welch's *t*-test was also used to compare the intertrial mean to the previously reported mean in [193] for 102 parked vehicles, since these means also had unequal variances. If there was no significant difference between the intertrial mean and the previously reported mean, then the steering assistance system would be validated.

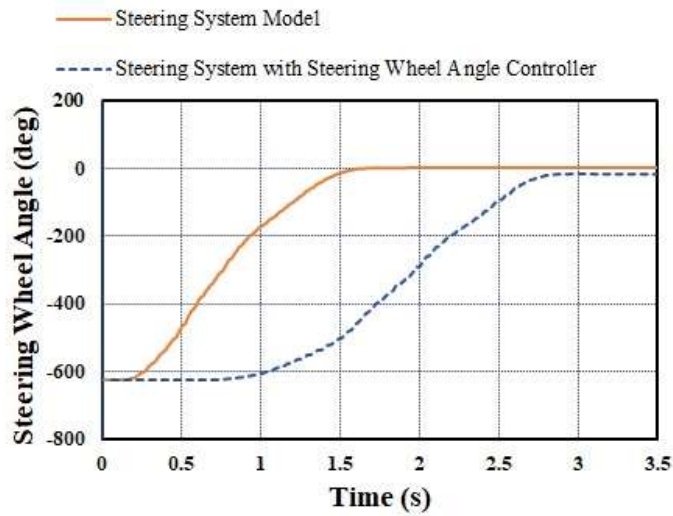
4.2.4 Results and discussion

This section is divided into two parts. The validation of the steering wheel angle controller is addressed in subsection 4.2.4.1 whereas subsection 4.2.4.2 concerns the validation of the lateral error of the test vehicle.

4.2.4.1 Validation of steering wheel angle controller

Based on the measured SWA output of the steering system with the steering wheel angle controller, the average steady-state error across all 15 trials was -15° with an SD (standard deviation) of 5° (Figure 4.2.5a). The controller was validated since the average steady-state error was within the targeted margin of $0 \pm 20^\circ$. According to step response analysis performed in MATLAB, the steering system model had a settling time of 1.5 s, whereas the measured SWA output had a longer settling time of 2.7 s because of a gradual increase in the voltage setting by the controller (Figure 4.2.5b). It is possible to simply increase the voltage setting to 6.9 V with a step function, but since the steering system behaves linearly, the steady-state SWA could overshoot the targeted SWA of 0° , since a step function of 2.2 V produced a steady-state SWA close to 0° . Although the average steering wheel rate of 327 deg/s for the steering system model was faster than the average rate of 206 deg/s associated with the steering wheel angle controller, both rates are more efficient than 180 deg/s for manual steering [196].

The SWA output resulting from the use of the steering wheel angle controller resulted from the voltage setting of the DC motor, as determined by the controller parameter, γ . Since γ was optimized with respect to the weight of the driver, it is possible that different γ -values would correspond to different driver weights. This change in the configuration of the controller is determined by the positive association between the load on the COMS and the amount of steering wheel torque applied by the DC motor. In order to measure the outcome of this association resulting from a minor change in load relative to the weight of the vehicle, the driver was substituted with a commercially available 5 kg kettlebell weight that was centered on the top surface of the driver seat, where the center of gravity of the driver was approximately located (Fig. 6) (Harrison et al, 1999). The steering wheel angle controller was able to change the SWA from -625° to an acceptable -7° , given the targeted angle of $0 \pm 20^\circ$. It is therefore expected that minor changes in the weight of the driver up to 5 kg would not require the adjustment of γ . On the other hand, it is recommended that significant changes in vehicle loading, including the addition of cargo over 5 kg, would require the adjustment of γ .



(a)



(b)

Figure 4.2.5 (a) Steering wheel angle (SWA) output of steering system model compared to average measured SWA output of steering system with steering wheel angle controller. Steering system model was used as reference for steering wheel angle controller to rotate steering wheel from leftward SWA of -625° toward 0° . (b) DC motor voltage setting without SWA controller (solid curve) compared to average voltage setting with SWA controller (dashed curve).

Since the steering assistance control system was developed to assist persons with disability, the controller could be optimized to for the weight of specific individuals. However, if the controller is to be applied in cases were the loading of the vehicle could vary significantly, a torque sensor at the steering wheel or a load cell in the driver seat could be used as feedback for

the automatic adjustment of γ . The realization of automatic adjustment could be accomplished in future studies. Consideration would also be given to the possibility of developing the controller for dynamic steering scenarios where the reaction torques at the interface between the road and tires vary, and consequently, the torque required for the DC motor to rotate the steering column would change as well [197].

This experiment focuses partly on the validation of the steering wheel angle controller, whereas the validation of the gesture recognition accuracy of the Myo armband is not performed. Nevertheless, previous work has confirmed the reliable accuracy of the Myo armband in comparison to conventional sEMG acquisition equipment [88], [109].

4.2.4.2 Validation of path following accuracy

Later errors of the COMS vehicle were measured relative to the parallel guidelines of the parking spaces during perpendicular parking. A comparison of mean lateral errors was made between forward and reverse perpendicular parking. Based on the data in Table 4.2, an unequal variances *t*-test indicated that the means were significantly different. This difference is partly due to the understeer, as evidenced by the leftward bias, i.e. the negative mean, relative to the center of the parking space in the case of forward parking. Another cause for the difference between the means is oversteer during reverse parking, as indicated by the corresponding negative mean. Since Ackermann steering was performed for both parking directions, it is expected that changes in SWA, longitudinal speed, or turning radius had a minor effect on lateral error. However, it is possible that changes in longitudinal speed caused by minor changes in the depression of the accelerator or undesired kinematic and elastic characteristics of the steering and suspension system contributed to understeer and oversteer during forward and reverse parking, respectively [82], [83].

Table 4.2 Lateral error of vehicle during perpendicular parking.

Driving direction	Mean lateral error (cm)	Standard deviation (cm)	Mean intertrial lateral error (cm)	Intertrial standard deviation (cm)
Forward	-27	13	-16	16
Reverse	-4	8		

Although there was a statistically significant difference in mean lateral error between forward and reverse parking, the combined, the unequal variances *t*-test indicated that the mean intertrial lateral error was statistically comparable to the previously reported mean of -10 SD 23 cm obtained from a sample of 102 vehicles [193]. Therefore, the path following accuracy of the steering assistance system was validated.

Even though other parking scenarios could have also been tested, including angle and parallel parking, the current study is directly supported by previous studies in which the majority of parking spaces were perpendicular [193], [194]. Future studies could include other parking

scenarios and more test drivers in order to measure other variables such as human factors. Further iterations of the interface utilizing other sEMG measurement devices and configurations could be compared to the currently employed Myo armband with respect to human factors or vehicle dynamics.

4.2.5 Conclusions

A steering assistance system was developed to facilitate steering wheel operation. The wheel angle controller for the system was designed and validated for a sEMG-controlled static steering assistance control system. Validation resulted in an average steady-state error of $-15 \text{ SD } 5^\circ$, which was acceptably close to the targeted angle of $0 \pm 20^\circ$.

Path following accuracy with respect to the lateral error of the steering assistance system was validated for perpendicular parking. Despite a significant difference in median lateral error between forward and reverse parking, the intertrial median lateral error across both directions was statistically comparable to previously published data.

As a link between previously conducted driving simulations and future field testing, this study has realized and validated sEMG-controlled steering assistance. The content presented in this paper could be used to advance human-centered automation for persons with disability.

Chapter 5

General Conclusions

5 General Discussion

Based on the results of all the experiments described in this thesis, the sEMG-based interfaces were validated as safe implementations of steering assistance. Further development of the proposed human-centered steering assistance, in the context of advancing vehicle automation, is described in Section 5.1. Further details on future work and limitations are explained in Section 5.2.

5.1 Role of the human driver in the human-centered steering assistance system

In order to realize the vehicle dynamics of the proposed sEMG-based steering assistance, it is necessary for future research to implement vehicle automation that is capable assisting humans by dynamically adjusting the steering wheel angle in order to navigate various turns. For example, the pedestrian collision avoidance experiment considered a simulated vehicle that could change lanes in order to steer around an unexpected crossing pedestrian. As a means of achieving lane keeping prior to and after collision avoidance, ADAS technology could rely on convolutional neural networks to detect lanes from RGB camera sensor images [159]. Furthermore, since recent production vehicles, such as the 2016 Tesla Model S, have already achieved Level 1 and Level 2 automation that is necessary to implement automatic steering, the automation of the sEMG-controlled steering assistance is technologically feasible [198].

The main difference between these two levels is the extent to which the driver delegates control to the vehicle. In the case of the routine low-speed scenarios for the first two driving simulator experiments and the final experiment with the actual vehicle, Level 1 automation enables the driver to only assign the steering task to the vehicle. On the other hand, the driver relies on Level 2 automation during pedestrian collision avoidance to allow the vehicle to control speed and steering, while allowing the driver to decide when to initiate steering based on the vehicle environment. At both levels of automation, the driver is able to intervene through the sEMG-based commands during emergency scenarios such as unexpected road obstacles or traffic.

An ideal human-centered steering assistance system would be able to transition between Levels 1 and 2 depending on the driving scenario and, ultimately, the judgement of the driver. The driver would be responsible for determining whether or not some or all of the driving tasks could be delegated to the vehicle. For example, the driver could decide to directly control vehicle steering through sEMG input during parking that requires large, repetitive changes in the steering wheel angle. If the vehicle speed approaches 30 km/h as the driver exits the parking area onto residential roads, the driver could assign steering, braking and acceleration to the vehicle in order to perform another task that is not related to driving, such as navigating an entertainment console. However, the driver would be responsible for monitoring the vehicle surroundings in case there is a need to intervene with an sEMG steering command.

As vehicle automation advances to Level 3, it would be possible for the vehicle to monitor the environment, while performing the other aforementioned driving tasks. Since this automation completely removes the human from the control loop during normal operation, it is not applicable

to the proposed steering assistance interface. Nevertheless, it would be possible to integrate sEMG-based interfaces to enable persons with disabilities to operate in-vehicle controls for tasks such as entertainment or to convey locations to which the vehicle would navigate. Furthermore, if there is a problem with the vehicle automation equipment, e.g. a malfunction prohibiting the safe navigation to a desired location, a driver with a disability could be notified by the vehicle to resume control of the driving tasks without having to rely on conventional steering wheels. One advantage the proposed sEMG-based steering assistance over a steering wheel is the ability to achieve safer vehicle motion by transitioning less abruptly from a straight trajectory to a steering trajectory. Furthermore, in cases where an abrupt trajectory is necessary to avoid a collision, sEMG-based steering assistance can be adjusted automatically by the vehicle automation system to transition more rapidly.

Given the above examples, it is expected that human drivers would have increasingly supportive roles as vehicle automation reaches Level 3.

5.2 Limitations and future studies

The objective of the present work was to determine the feasibility of safe human-centered sEMG-controlled steering assistance for drivers restricted by disabilities to one-handed steering wheel rotation. Based on concepts utilized in prosthetics control and vehicle dynamics, the design and implementation of the sEMG interfaces was detailed in Chapter 2, along with equations relating SWR to path following accuracy. These equations were the theoretical foundation for interpreting the results of driving simulator trials and field testing that were conducted in the past couple of years. Future studies could rely on this foundation to interpret results concerning path following accuracy and other related vehicle dynamics.

Although these studies provide a theoretical and empirical foundation that confirms the safety of the sEMG-based interfaces, the effect of sEMG-controlled steering assistance on human factors has yet to be investigated. A link between path following accuracy and efficiency in the execution of Ackermann steering was established by the driving simulator study involving sEMG interface signals resulting from forearm supination. Therefore, future studies could evaluate the user performance of sEMG-controlled steering with respect to path following accuracy, i.e. effectiveness, and the duration of turning maneuvers, i.e. efficiency. It is also possible to evaluate the other factors such as cognitive workload with respect to pupil dilation, and perceived workload through questionnaires [178], [199]. For example, a future study could determine if steering with the Myo armband increases cognitive workload during perpendicular parking in comparison to manual steering wheel operation. If sEMG-controlled steering assistance is to be implemented as an assistive technology, test subjects with upper limb disabilities could be recruited for future studies, and input from experts in fields such as medicine and psychology could evaluate human factors for specific individuals with disabilities. Implementing this steering assistance for production vehicles would require extensive evaluation of human factors on statistically significant populations of drivers to identify and prevent negative interactions between vehicle automation and humans that could lead to automotive accidents.

As an opportunity for technological innovation, the proposed interfaces could be further

developed with respect to sEMG measurement accuracy and precision. For the driving simulator studies, disposable wet electrodes were used as substitutes for dry electrode armbands that have yet to be developed for automobiles. Other potential sensors that could be integrated into the armbands include capacitive sEMG sensors and force sensors [200], [201]. Although the mass-produced Myo armband was used during field testing, new sEMG devices could be developed specifically for automotive applications. Examples of potential applications include: the operation of non-driving related devices, steering control during collision avoidance and parking, and longitudinal acceleration and braking. Since sEMG-controlled vehicles emerged around a decade ago, and the current research is a preliminary advancement of these vehicles, there still exists a variety of possibilities for innovation.

6 General Conclusions

As stated at the beginning of this thesis, the objective of the current research is to determine the feasibility of inclusive sEMG-controlled steering assistance as a form of safe human-centered automation. This feasibility was validated by comparing the sEMG-based interfaces with steering wheels in terms of vehicle stability and path following accuracy during static and dynamic steering. Based on this validation, the objective of the current research was satisfied as follows:

- a) In order to prevent collision accidents during turning maneuvers, driving simulator studies and testing with an actual automobile demonstrated that sEMG-controlled steering assistance provides path following accuracy and safer vehicle motion that were comparable, and in some cases superior, to steering wheel-based interfaces.
 - Driving simulator studies and testing with an actual automobile validated the path following accuracy of sEMG-based interfaces for static steering during parking and low-speed dynamic steering on residential roads. With respect to 45° turns, 90° turns, and wide U-turns at twice the minimum turning radius of tested vehicles, sEMG-based interfaces were generally comparable to steering wheel-based interfaces, whereas the sEMG-based interfaces were significantly superior to the steering wheel-based interfaces during narrow U-turns at the minimum turning radius of the tested vehicles.
 - One of the driving simulator studies found that sEMG-controlled steering assistance provided significantly higher vehicle stability, during pedestrian collision avoidance, in contrast to conventional steering wheel operation and manual takeover from automated driving.
- b) The results of the experiments indicate that sEMG-controlled steering assistance is applicable to static and dynamic steering at vehicle speeds less than or equal to the speed limit of 30 km/h for residential roads in Japan.
- c) The sEMG-based interfaces enabled drivers at least 20 years of age to remotely rotate steering wheel-based interfaces with one healthy arm. Therefore, inclusive sEMG-controlled steering assistance could enable drivers without disability as well as drivers with disability who are restricted to steering with one-healthy arm by the following health conditions:
 - Hemiplegia
 - Transradial or more severe amputation affecting one arm, i.e. unilateral amputation

Given that each of the above items corresponds to the specifications for the thesis objective, as stated in Chapter 1, the experiments of the current research provide an empirical basis for the application of inclusive sEMG-controlled steering assistance as a safe method for persons, with and without the above disabilities.

References

- [1] N. V Iqbal, K. Subramaniam, and S. A. P., “A Review on Upper-Limb Myoelectric Prosthetic Control,” *IETE J. Res.*, vol. 64, no. 6, pp. 740–752, Nov. 2018.
- [2] M. Hakonen, H. Piitulainen, and A. Visala, “Current state of digital signal processing in myoelectric interfaces and related applications,” *Biomed. Signal Process. Control*, vol. 18, pp. 334–359, 2015.
- [3] N. Akhlaghi *et al.*, “Real-Time Classification of Hand Motions Using Ultrasound Imaging of Forearm Muscles,” *IEEE Trans. Biomed. Eng.*, vol. 63, no. 8, p. w, Aug. 2016.
- [4] M. Asghari Oskoei and H. Hu, “Myoelectric control systems-A survey,” *Biomedical Signal Processing and Control*. 2007.
- [5] S. N. Pierrie, R. G. Gaston, and B. J. Loeffler, “Current Concepts in Upper-Extremity Amputation,” *J. Hand Surg. Am.*, vol. 43, no. 7, pp. 657–667, Jul. 2018.
- [6] A. Fougner, Ø. Stavadahl, P. J. Kyberd, Y. G. Losier, and P. A. Parker, “Control of Upper Limb Prostheses: Terminology and Proportional Myoelectric Control—A Review,” *IEEE Trans. Neural Syst. Rehabil. Eng.*, vol. 20, no. 5, pp. 663–677, 2012.
- [7] V. Surakka, M. Illi, and P. Isokoski, “Gazing and Frowning As a New Human--computer Interaction Technique,” *ACM Trans. Appl. Percept.*, vol. 1, no. 1, pp. 40–56, Jul. 2004.
- [8] A. B. Barreto, S. D. Scargle, and M. Adjouadi, “A practical EMG-based human-computer interface for users with motor disabilities.,” *J. Rehabil. Res. Dev.*, vol. 37, no. 1, pp. 53–63.
- [9] N. Wang, K. Lao, and X. Zhang, “Design and Myoelectric Control of an Anthropomorphic Prosthetic Hand,” *J. Bionic Eng.*, 2017.
- [10] S. Viteckova, P. Kutilek, and M. Jirina, “Wearable lower limb robotics: A review,” *Biocybern. Biomed. Eng.*, vol. 33, no. 2, pp. 96–105, Jan. 2013.
- [11] J. M. Hahne, M. A. Schweisfurth, M. Koppe, and D. Farina, “Simultaneous control of multiple functions of bionic hand prostheses: Performance and robustness in end users,” *Sci. Robot.*, vol. 3, no. 19, p. eaat3630, Jun. 2018.
- [12] S. Lawoyin, X. Liu, D. Y. Fei, and O. Bai, “Detection methods for a low-cost accelerometer-based approach for driver drowsiness detection,” in *Conference Proceedings - IEEE International Conference on Systems, Man and Cybernetics*, 2014.
- [13] J. E. Cheesborough, L. H. Smith, T. A. Kuiken, and G. A. Dumanian, “Targeted muscle reinnervation and advanced prosthetic arms,” *Semin. Plast. Surg.*, vol. 29, no. 1, pp. 62–72, 2015.
- [14] M. S. Johannes, J. D. Bigelow, J. M. Burck, S. D. Harshbarger, M. V. Kozlowski, and T. Van Doren, “An overview of the developmental process for the modular prosthetic limb,” *Johns Hopkins APL Technical Digest (Applied Physics Laboratory)*. 2011.
- [15] M. Atzori and H. Müller, “Control Capabilities of Myoelectric Robotic Prostheses by Hand Amputees: A Scientific Research and Market Overview,” *Front. Syst. Neurosci.*, vol. 9, 2015.
- [16] T. A. Kuiken *et al.*, “Targeted Muscle Reinnervation for Real-time Myoelectric Control of

- Multifunction Artificial Arms,” *JAMA*, vol. 301, no. 6, pp. 619–628, Feb. 2009.
- [17] S. Benatti, B. Milosevic, E. Farella, E. Gruppioni, and L. Benini, “A Prosthetic Hand Body Area Controller Based on Efficient Pattern Recognition Control Strategies,” *Sensors*, vol. 17, no. 4, 2017.
- [18] B. Hudgins, P. Parker, and R. N. Scott, “A new strategy for multifunction myoelectric control,” *IEEE Trans. Biomed. Eng.*, vol. 40, no. 1, pp. 82–94, Jan. 1993.
- [19] C. L. Pulliam, J. M. Lambrecht, and R. F. Kirsch, “Electromyogram-based neural network control of transhumeral prostheses,” *J. Rehabil. Res. Dev.*, vol. 48, no. 6, pp. 739–754, 2011.
- [20] E. J. Scheme and K. B. Englehart, “Electromyogram pattern recognition for control of powered upper-limb prostheses: state of the art and challenges for clinical use.,” *J. Rehabil. Res. Dev.*, vol. 48, no. 6, pp. 643–659, 2011.
- [21] N. A. Alshammary, S. A. Dalley, and M. Goldfarb, “Assessment of a multigrasp myoelectric control approach for use by transhumeral amputees,” *2012 Annu. Int. Conf. IEEE Eng. Med. Biol. Soc.*, vol. 2012, pp. 968–971, 2012.
- [22] M. Merad, É. De Montalivet, A. Touillet, N. Martinet, A. Roby-Brami, and N. Jarrassé, “Can we achieve intuitive prosthetic elbow control based on healthy upper limb motor strategies?,” *Front. Neurobot.*, vol. 12, no. 1, 2018.
- [23] R. A. M. Abayasiri, D. G. K. Madusanka, N. M. P. Arachchige, A. T. S. Silva, and R. A. R. C. Gopura, “MoBio: A 5 DOF trans-humeral robotic prosthesis,” in *2017 International Conference on Rehabilitation Robotics (ICORR)*, 2017, pp. 1627–1632.
- [24] A. L. Ciancio *et al.*, “Control of prosthetic hands via the peripheral nervous system,” *Front. Neurosci.*, 2016.
- [25] S. Christina, B. Malte, and K. Marc, “Designs and performance of three new microprocessor-controlled knee joints,” *Biomedical Engineering / Biomedizinische Technik*, vol. 64, p. 119, 2019.
- [26] T. Roland, S. Amsüss, M. F. Russold, C. Wolf, and W. Baumgartner, “Capacitive Sensing of Surface EMG for Upper Limb Prostheses Control,” *Procedia Eng.*, vol. 168, pp. 155–158, Jan. 2016.
- [27] Y. Yabuki *et al.*, “Development of new cosmetic gloves for myoelectric prosthetic hand using superelastic rubber,” *Rob. Auton. Syst.*, vol. 111, pp. 31–43, Jan. 2019.
- [28] Y. Yabuki *et al.*, “Development of New Cosmetic Gloves for Myoelectric Prosthetic Hand by Using Thermoplastic Styrene Elastomer,” in *Intelligent Autonomous Systems 14*, 2017, pp. 269–282.
- [29] I.-J. Ding, R.-Z. Lin, and Z.-Y. Lin, “Service robot system with integration of wearable Myo armband for specialized hand gesture human–computer interfaces for people with disabilities with mobility problems,” *Comput. Electr. Eng.*, vol. 69, pp. 815–827, Jul. 2018.
- [30] K. Nagata, K. Ando, K. Magatani, and M. Yamada, “Development of the hand motion recognition system based on surface EMG using suitable measurement channels for pattern recognition,” in *2007 29th Annual International Conference of the IEEE Engineering in Medicine and Biology Society*, 2007, pp. 5214–5217.
- [31] T. Felzer and B. Freisleben, “HaWCoS: The ‘Hands-free’ Wheelchair Control System,” in

- ASSETS '02 The 5th ACM SIGCAPH Conference on Assistive Technologies*, 2002, pp. 127–134.
- [32] J. Kwak, T. W. Jeon, H. Park, S. Kim, and K. An, “Development of an EMG-Based Car Interface Using Artificial Neural Networks for the Physically Handicapped,” *Korea IT Serv. J.*, vol. 7, no. 2, pp. 149–164, 2008.
- [33] P. Ju, L. P. Kaelbling, and Y. Singer, “State-based classification of finger gestures from electromyographic signals,” in *ICML '00 Proceedings of the Seventeenth International Conference on Machine Learning*, 2000, pp. 439–446.
- [34] B. K. Sovacool, “Early modes of transport in the United States: Lessons for modern energy policymakers,” *Policy Soc.*, 2009.
- [35] A. Markovich, “Look, Ma--No Wheel!,” *Popular Mechanics*, New York, pp. 91–93, 1965.
- [36] A. Meschtscherjakov, “The Steering Wheel: A Design Space Exploration BT - Automotive User Interfaces: Creating Interactive Experiences in the Car,” G. Meixner and C. Müller, Eds. Cham: Springer International Publishing, 2017, pp. 349–373.
- [37] F. Baronti, F. Lenzi, R. Roncella, and R. Saletti, “Distributed sensor for steering wheel rip force measurement in driver fatigue detection,” in *2009 Design, Automation & Test in Europe Conference & Exhibition*, 2009, pp. 894–897.
- [38] L. Diwischek and J. Lisseman, “Tactile feedback for virtual automotive steering wheel switches,” in *Proceedings of the 7th International Conference on Automotive User Interfaces and Interactive Vehicular Applications - AutomotiveUI '15*, 2015, pp. 31–38.
- [39] A. Kirli and M. S. Arslan, “Steering Feel Design: The Effect of Mass Variation,” *IFAC-PapersOnLine*, vol. 49, no. 21, pp. 617–622, Jan. 2016.
- [40] X. Tao, B. Cheng, B. Wang, F. Zhang, G. Li, and C. Chen, “SEMG Based Recognition for Lumbar Muscle Fatigue During Prolonged Driving,” in *Proceedings of the FISITA 2012 World Automotive Congress*, 2013, pp. 773–783.
- [41] A. J. Pick and D. J. Cole, “Measurement of Driver Steering Torque Using Electromyography,” *J. Dyn. Syst. Meas. Control*, vol. 128, no. 4, pp. 960–968, Apr. 2006.
- [42] A. J. Pick and D. J. Cole, “Neuromuscular dynamics in the driver-vehicle system,” *Veh. Syst. Dyn.*, 2006.
- [43] L. Angelini *et al.*, “WheelSense: Enabling tangible gestures on the steering wheel for in-car natural interaction,” in *Lecture Notes in Computer Science (including subseries Lecture Notes in Artificial Intelligence and Lecture Notes in Bioinformatics)*, 2013.
- [44] D. Otte, T. Facius, and S. Brand, “Injury Mechanisms of Aortic Ruptures to Vehicle Occupants and Vulnerable Road Users – An In-Depth-Investigation over Time,” *J. Forensic Biomech.*, vol. 08, no. 01, pp. 1–12, Mar. 2017.
- [45] R. Chen and H. C. Gabler, “Risk of thoracic injury from direct steering wheel impact in frontal crashes,” *J. Trauma Acute Care Surg.*, vol. 76, no. 6, pp. 1441–1446, Jun. 2014.
- [46] J. J. Gil, I. Díaz, P. Ciáurriz, and M. Echeverría, “New driving control system with haptic feedback: Design and preliminary validation tests,” *Transp. Res. Part C Emerg. Technol.*, vol. 33, pp. 22–36, 2013.
- [47] M. Wada and F. Kameda, “A joystick car drive system with seating in a wheelchair,” in *2009 35th Annual Conference of IEEE Industrial Electronics*, 2009, pp. 2163–2168.

- [48] J. Östlund, “Joystick-controlled cars for drivers with severe disabilities,” Swedish National Road Administration, the Vehicle Standards Division, 1999.
- [49] WHO (World Health Organization), “World report on disability 2011,” *Am. J. Phys. Med. Rehabil. Assoc. Acad. Physiatr.*, 2011.
- [50] F. Cordella *et al.*, “Literature review on needs of upper limb prosthesis users,” *Frontiers in Neuroscience*. 2016.
- [51] T. Verrall and J. R. Kulkarni, “Driving appliances for upper limb amputees,” *Prosthet. Orthot. Int.*, vol. 19, pp. 124–127, 1995.
- [52] A. Yamamoto *et al.*, “Prevalence and risk factors of a rotator cuff tear in the general population,” *J. Shoulder Elb. Surg.*, 2010.
- [53] P. Pandis, J. A. I. Prinold, and A. M. J. Bull, “Shoulder muscle forces during driving: Sudden steering can load the rotator cuff beyond its repair limit,” *Clin. Biomech.*, vol. 30, no. 8, pp. 839–846, 2015.
- [54] N. I. O. A. A. M. A. S. D. (NIAMS), “The human shoulder joint,” 2006. [Online]. Available: http://www.pueblo.gsa.gov/cic_text/health/sports/shoulder.gif. [Accessed: 06-Sep-2006].
- [55] N. Jung, H. Kim, and M. Chang, “Muscle activation of drivers with hemiplegia caused by stroke while driving using a steering wheel or knob,” *J. Phys. Ther. Sci.*, vol. 27, no. 4, pp. 1009–1011, 2015.
- [56] M. Hitosugi, I. Takehara, S. Watanabe, Y. Hayashi, and S. Tokudome, “Support for stroke patients in resumption of driving: Patient survey and driving simulator trial,” *Int. J. Gen. Med.*, 2011.
- [57] J. Davidson, “A survey of the satisfaction of upper limb amputees with their prostheses, their lifestyles, and their abilities,” *J. Hand Ther.*, vol. 15, pp. 62–70, 2002.
- [58] S. Darcy and P. F. Burke, “On the road again: The barriers and benefits of automobility for people with disability,” *Transp. Res. Part A Policy Pract.*, vol. 107, pp. 229–245, Jan. 2018.
- [59] Y. Murata, K. Yoshida, K. Suzuki, and D. Takahashi, “Proposal of an Automobile Driving Interface Using Gesture Operation for Disabled People,” in *ACHI 2013, The Sixth International Conference on Advances in Computer-Human Interactions*, 2013, pp. 472–478.
- [60] T. Minato, Y. Murata, and A. Suzuki, “Proposal of Automobile Driving Interface Using Strain Sensor for the Disabled People,” in *2015 Tohoku-Section Joint Convention of Institutes of Electrical and Information Engineers*, 2015.
- [61] F. Pradko and R. A. Lee, “Theory of Human Vibration Response and its Application to Vehicle Design,” in *Biomechanics*, 1969, pp. 105–118.
- [62] A. Kar and P. Corcoran, “A review and analysis of eye-gaze estimation systems, algorithms and performance evaluation methods in consumer platforms,” *IEEE Access*, vol. 5, pp. 16495–16519, 2017.
- [63] O. Tuisku, V. Rantanen, O. Špakov, V. Surakka, and J. Lekkala, “Pointing and Selecting with Facial Activity,” *Interact. Comput.*, vol. 28, no. 1, pp. 1–12, 2016.
- [64] N. Jiang, S. Muceli, B. Graimann, and D. Farina, “Effect of arm position on the prediction

- of kinematics from EMG in amputees,” *Med. Biol. Eng. Comput.*, vol. 51, no. 1–2, pp. 143–151, Feb. 2013.
- [65] D. S. Childress, “Upper-Limb Prosthetics: Control of Limb Prostheses,” in *Atlas of Limb Prosthetics: Surgical, Prosthetic, and Rehabilitation Principles*, 2nd ed., H. K. Bowker and J. W. Michael, Eds. Rosemont: American Academy of Orthopedic Surgeons, 2002.
- [66] M. B. I. Raez, M. S. Hussain, and F. Mohd-Yasin, “Techniques of EMG signal analysis: detection, processing, classification and applications,” *Biol. Proced. Online*, vol. 8, pp. 11–35, Mar. 2006.
- [67] Y. Fukuoka *et al.*, “Development of a Compact Wireless Laplacian Electrode Module for Electromyograms and Its Human Interface Applications,” *Sensors*, vol. 13, no. 2. 2013.
- [68] A. T. Vehkaoja, J. A. Verho, M. M. Puurtinen, N. M. Nojd, J. O. Leikkala, and J. A. Hyttinen, “Wireless Head Cap for EOG and Facial EMG Measurements,” in *2005 IEEE Engineering in Medicine and Biology 27th Annual Conference*, 2005, pp. 5865–5868.
- [69] “J3016,” SAE International, 2014.
- [70] R. Umeno, M. Itoh, and S. Kitazaki, “Influence of automated driving on driver’s own localization: a driving simulator study,” *J. Intell. Connect. Veh.*, vol. 1, no. 3, pp. 99–106, Oct. 2018.
- [71] D. A. Norman, “The ‘Problem’ with Automation: Inappropriate Feedback and Interaction, not ‘Over-Automation,’” *Philos. Trans. R. Soc. B Biol. Sci.*, vol. 327, no. 1241, pp. 585–593, Apr. 1990.
- [72] H. Muslim and M. Itoh, “A theoretical framework for designing human-centered automotive automation systems,” *Cogn. Technol. Work*, Jul. 2018.
- [73] M. Mulder, D. A. Abbink, E. R. Boer, and M. M. van Paassen, “Human-centered Steer-by-Wire design: Steering wheel dynamics should be task dependent,” in *2012 IEEE International Conference on Systems, Man, and Cybernetics (SMC)*, 2012, pp. 3015–3019.
- [74] W. Wang, J. Xi, C. Liu, and X. Li, “Human-Centered Feed-Forward Control of a Vehicle Steering System Based on a Driver’s Path-Following Characteristics,” *IEEE Trans. Intell. Transp. Syst.*, pp. 1–14, 2016.
- [75] D. W. J. van der Wiel, M. M. van Paassen, M. Mulder, M. Mulder, and D. A. Abbink, “Driver Adaptation to Driving Speed and Road Width: Exploring Parameters for Designing Adaptive Haptic Shared Control,” in *2015 IEEE International Conference on Systems, Man, and Cybernetics*, 2015, pp. 3060–3065.
- [76] R. Zheng, S. Yamabe, K. Nakano, and Y. Suda, “Biosignal analysis to assess mental stress in automatic driving of trucks: Palmar perspiration and masseter electromyography,” *Sensors (Switzerland)*, 2015.
- [77] Y. Liu, Q. Liu, C. Lv, M. Zheng, and X. Ji, “A study on objective evaluation of vehicle steering comfort based on driver’s electromyogram and movement trajectory,” *IEEE Trans. Human-Machine Syst.*, vol. 48, no. 1, pp. 41–49, 2018.
- [78] W. Wen *et al.*, “Continuous Estimation of Stress Using Physiological Signals during a Car Race,” *Psychology*, vol. 08, no. 07, pp. 978–986, May 2017.
- [79] D. Forkenbrock and D. Elsasser, “An Assessment of Human Driver Steering Capability,” National Highway Traffic Safety Administration, Liberty, 2005.

- [80] D. D. Dinh and H. Kubota, "Profile-speed data-based models to estimate operating speeds for urban residential streets with a 30km/h speed limit," *IATSS Res.*, vol. 36, pp. 115–122, 2013.
- [81] J. P. Pauwelussen, *Essentials of vehicle dynamics*. Oxford: Elsevier, Ltd., 2015.
- [82] "ISO 4138:2012(E)," International Standards Office, Geneva, 2012.
- [83] D. F. Tandy, J. Colborn, J. C. Bae, C. Coleman, and R. Pascarella, "The True Definition and Measurement of Oversteer and Understeer," *SAE Int. J. Commer. Veh.*, vol. 8, pp. 160–181, 2015.
- [84] Y. Yi, Z. Lu, Q. Xin, L. Jinzhou, L. Yijin, and W. Jianhang, "Smooth path planning for autonomous parking system," in *2017 IEEE Intelligent Vehicles Symposium (IV)*, 2017, pp. 167–173.
- [85] A. Gupta, R. Divekar, and M. Agrawal, "Autonomous parallel parking system for Ackerman steering four wheelers," in *2010 IEEE International Conference on Computational Intelligence and Computing Research*, 2010, pp. 1–6.
- [86] B. Song, D. Kim, and H. Choi, "Cooperative lateral control for automatic valet parking," in *2011 11th International Conference on Control, Automation and Systems*, 2011, pp. 567–570.
- [87] A. Searle and L. Kirkup, "A direct comparison of wet, dry and insulating bioelectric recording electrodes," *Physiol. Meas.*, vol. 21, no. 2, pp. 271–283, May 2000.
- [88] I. G. Mendez *et al.*, "Evaluation of classifiers performance using the Myo armband," in *Conference Proceedings, Myoelectric Controls and Upper Limb Prosthetics Symposium, MEC17, 15-18 August 2017, Fredericton, New Brunswick, Canada*, 2017, p. No. 98.
- [89] K. Ando, K. Nagata, D. Kitagawa, N. Shibata, M. Yamada, and K. Magatani, "Development of the input equipment for a computer using surface EMG.," *Conf. Proc. IEEE Eng. Med. Biol. Soc.*, 2006.
- [90] P. Geethanjali, "Myoelectric control of prosthetic hands: State-of-the-art review," *Med. Devices Evid. Res.*, vol. 9, pp. 247–255, 2016.
- [91] K. R. Wheeler and C. C. Jorgensen, "Gestures as input: neuroelectric joysticks and keyboards," *IEEE Pervasive Comput.*, vol. 2, no. 2, pp. 56–61, Apr. 2003.
- [92] H. Burger and G. Vidmar, "A survey of overuse problems in patients with acquired or congenital upper limb deficiency," *Prosthet. Orthot. Int.*, vol. 40, no. 4, pp. 497–502, 2016.
- [93] Y. Sato, M. Kaji, T. Tsuru, and K. Oizumi, "Carpal Tunnel Syndrome Involving Unaffected Limbs of Stroke Patients," *Stroke*, vol. 30, no. 2, pp. 414–418, Feb. 1999.
- [94] Y. Chae, C. Choi, J. Kim, and S. Jo, "Noninvasive sEMG-based control for humanoid robot teleoperated navigation," *Int. J. Precis. Eng. Manuf.*, vol. 12, no. 6, pp. 1105–1110, 2011.
- [95] G. Boccia, D. Dardanello, V. Rosso, L. Pizzigalli, and A. Rainoldi, "The Application of sEMG in Aging: A Mini Review," *Gerontology*, vol. 61, no. 5, pp. 477–484, 2015.
- [96] R. Rajamani, "Lateral Vehicle Dynamics BT - Vehicle Dynamics and Control," R. Rajamani, Ed. Boston: Springer US, 2012, pp. 15–46.
- [97] D. Lee and M. Yannakakis, "Principles and methods of testing finite state machines—a survey," *Proc. IEEE*, vol. 84, no. 8, pp. 1090–1123, 1996.

- [98] “J266 - Steady-State Directional Control Test Procedures for Passenger Cars and Light Trucks,” Warrendale, 1996.
- [99] N. Takizawa, Y. Wakita, K. Nagata, and K. Magatani, “A Development of the Equipment Control System Using SEMG,” in *IFMBE Proceedings*, 2009, pp. 923–926.
- [100] H. Hermens and B. Freriks, “The State of the Art on Sensors and Sensor Placement Procedures for Surface ElectroMyoGraphy: A proposal for sensor placement procedures,” SENIAM, Enschede, 1997.
- [101] R. B. Miller, “Response time in man-computer conversational transactions,” in *Proceedings of the December 9-11, 1968, fall joint computer conference, part I on - AFIPS '68 (Fall, part I)*, 1968.
- [102] C. J. De Luca, “Surface electromyography: Detection and recording,” DelSys Inc., 2002.
- [103] “AnalogRead().” [Online]. Available: <https://www.arduino.cc/en/Reference/analogRead>. [Accessed: 20-Apr-2019].
- [104] R. S. Figliola and D. E. Beasley, *Theory and Design for Mechanical Measurements*, Fourth. Hoboken: Wiley, 2006.
- [105] A. Chatham, W. Walmink, and F. Mueller, “UnoJoy!: A Library for Rapid Video Game Prototyping Using Arduino,” in *CHI '13 Extended Abstracts on Human Factors in Computing Systems*, 2013, pp. 2787–2788.
- [106] “JoyToKey Website.” [Online]. Available: <https://joytokey.net/en/>. [Accessed: 20-Dec-2018].
- [107] W. Youn and J. Kim, “Development of a compact-size and wireless surface EMG measurement system,” in *2009 ICCAS-SICE*, 2009, pp. 1625–1628.
- [108] P. Kaczmarek, T. Mańkowski, and J. Tomczyński, “putEMG—A Surface Electromyography Hand Gesture Recognition Dataset,” *Sensors*, vol. 19, no. 16, p. 3548, Aug. 2019.
- [109] S. Pizzolato, L. Tagliapietra, M. Cognolato, M. Reggiani, H. Müller, and M. Atzori, “Comparison of six electromyography acquisition setups on hand movement classification tasks,” *PLoS One*, vol. 12, no. 10, pp. 1–17, 2017.
- [110] S. Masson, F. S Fortuna, F. Moura, and D. Soriano, “INTEGRATING MYO ARMBAND FOR THE CONTROL OF MYOELECTRIC UPPER LIMB PROSTHESIS,” in *XXV Congresso Brasileiro de Engenharia Biomédica – CBEB 2016*, 2016, pp. 17–20.
- [111] A. Boyali, N. Hashimoto, and O. Matsumoto, “Hand posture and gesture recognition using MYO armband and spectral collaborative representation based classification,” in *2015 IEEE 4th Global Conference on Consumer Electronics (GCCE)*, 2015, pp. 200–201.
- [112] N. Nasri, S. Orts-Escolano, F. Gomez-Donoso, and M. Cazorla, “Inferring Static Hand Poses from a Low-Cost Non-Intrusive sEMG Sensor,” *Sensors*, vol. 19, no. 2, 2019.
- [113] M. ur Rehman *et al.*, “Multiday EMG-Based Classification of Hand Motions with Deep Learning Techniques,” *Sensors*, vol. 18, no. 8, 2018.
- [114] G. Li, Y. Li, L. Yu, and Y. Geng, “Conditioning and Sampling Issues of EMG Signals in Motion Recognition of Multifunctional Myoelectric Prostheses,” *Ann. Biomed. Eng.*, vol. 39, no. 6, pp. 1779–1787, Jun. 2011.
- [115] E. N. Kamavuako, J. C. Rosenvang, R. Horup, W. Jensen, D. Farina, and K. B. Englehart,

- “Surface Versus Untargeted Intramuscular EMG Based Classification of Simultaneous and Dynamically Changing Movements,” *IEEE Trans. Neural Syst. Rehabil. Eng.*, vol. 21, no. 6, pp. 992–998, Nov. 2013.
- [116] F. Riillo *et al.*, “Optimization of EMG-based hand gesture recognition: Supervised vs. unsupervised data preprocessing on healthy subjects and transradial amputees,” *Biomed. Signal Process. Control*, vol. 14, pp. 117–125, Nov. 2014.
- [117] X. Chen, A. Ke, X. Ma, and J. He, “SoC-based Architecture for Robotic Prosthetics Control Using Surface Electromyography,” in *2016 8th International Conference on Intelligent Human-Machine Systems and Cybernetics (IHMSC)*, 2016, pp. 134–137.
- [118] Y. Gu, D. Yang, Q. Huang, W. Yang, and H. Liu, “Robust EMG pattern recognition in the presence of confounding factors: features, classifiers and adaptive learning,” *Expert Syst. Appl.*, vol. 96, pp. 208–217, Apr. 2018.
- [119] D. Ramírez-Martínez, M. Alfaro-Ponce, O. Pogrebnyak, M. Aldape-Pérez, and A.-J. Argüelles-Cruz, “Hand Movement Classification Using Burg Reflection Coefficients,” *Sensors*, vol. 19, no. 3, 2019.
- [120] E. J. C. Nacpil, R. Zheng, T. Kaizuka, and K. Nakano, “A surface electromyography controlled steering assistance interface,” *J. Intell. Connect. Veh.*, Apr. 2019.
- [121] E. J. C. Nacpil, Z. Wang, R. Zheng, T. Kaizuka, and K. Nakano, “Design and Evaluation of a Surface Electromyography-Controlled Steering Assistance Interface,” *Sensors*, vol. 19, no. 6, 2019.
- [122] Y. Takada, E. R. Boer, and T. Sawaragi, “Driving assist system: Shared haptic human system interaction,” in *12th IFAC Symposium on Analysis, Design, and Evaluation of Human-Machine Systems*, 2013, pp. 203–210.
- [123] B. Ma, Y. Yang, Y. Liu, X. Ji, and H. Zheng, “Analysis of vehicle static steering torque based on tire-road contact patch sliding model and variable transmission ratio,” *Adv. Mech. Eng.*, vol. 8, no. 9, pp. 1–11, 2016.
- [124] R. S. Sharp and R. Granger, “On car steering torques at parking speeds,” *Proc. Inst. Mech. Eng. Part D J. Automob. Eng.*, vol. 217, no. 2, pp. 87–96, 2003.
- [125] E. J. Nacpil, R. Zheng, T. Kaizuka, and K. Nakano, “Implementation of a sEMG-machine interface for steering a virtual car in a driving simulator,” in *AHFE 2017 International Conference on Human Factors in Simulation and Modeling*, 2018, pp. 274–282.
- [126] J. Bader, M. R. Boland, D. Greybe, A. Nitz, T. Uhl, and D. Pienkowski, “Muscle activity during maximal isometric forearm rotation using a power grip,” *J. Biomech.*, vol. 68, pp. 24–32, 2018.
- [127] P. Yih and J. C. Gerdes, “Modification of vehicle handling characteristics via steer-by-wire,” *IEEE Trans. Control Syst. Technol.*, vol. 13, no. 6, pp. 965–976, 2005.
- [128] M. Land and J. Horwood, “Which parts of the road guide steering?,” *Nature*, vol. 377, pp. 339–340, 1995.
- [129] M. F. Land and D. N. Lee, “Where we look when we steer,” *Nature*, vol. 369, no. 6483, pp. 742–744, Jun. 1994.
- [130] U. E. Manawadu, M. Kamezaki, M. Ishikawa, T. Kawano, and S. Sugano, “A multimodal human-machine interface enabling situation-Adaptive control inputs for highly automated

- vehicles,” in *2017 IEEE Intelligent Vehicles Symposium (IV)*, 2017.
- [131] D. Renfro, P. T. Semones, and A. Roberts, “Quantitative Measure of Transient Oversteer of Road Vehicles,” in *20th International Technical Conference on the Enhanced Safety of Vehicles*, 2007.
- [132] “Nissan ProPILOT Assist technology reduces the hassle of stop-and-go highway driving, ready for U.S. launch,” 2017. [Online]. Available: <http://nissannews.com/en-US/nissan/usa/releases/nissan-propilot-assist-technology-reduces-the-hassle-of-stop-and-go-highway-driving-ready-for-u-s-launch?la=1&la=1>. [Accessed: 27-Aug-2018].
- [133] J. A. Mercer, N. Bezodis, D. DeLion, T. Zachry, and M. D. Rubley, “EMG sensor location: Does it influence the ability to detect differences in muscle contraction conditions?,” *J. Electromyogr. Kinesiol.*, vol. 16, no. 2, pp. 198–204, 2006.
- [134] R. Nakamura and R. Taniguchi, “Dependence of reaction times on movement patterns in patients with Parkinson’s disease and those with cerebellar degeneration,” *Tohoku J. Exp. Med.*, vol. 132, no. 2, pp. 153–158, 1980.
- [135] R. Nakamura and H. Saito, “Preferred Hand and Reaction Time in Different Movement Patterns,” *Percept. Mot. Skills*, vol. 39, no. 3, pp. 1275–1281, 1974.
- [136] M. Shuttleworth, “Counterbalanced Measures Design,” 2009. [Online]. Available: <https://explorable.com/counterbalanced-measures-design>. [Accessed: 12-Oct-2018].
- [137] G. Upton and I. Cook, *Understanding Statistics*. Oxford: Oxford University Press, 1996.
- [138] S. S. Shapiro and M. B. Wilk, “An Analysis of Variance Test for Normality (Complete Samples),” *Biometrika*, vol. 52, no. 3/4, pp. 591–611, 1965.
- [139] E. Whitley and J. Ball, “Statistics review 6: Nonparametric methods,” *Crit. Care*, vol. 6, pp. 509–513, 2002.
- [140] “Driver’s License Statistics.” [Online]. Available: https://www.npa.go.jp/toukei/menkyo/pdf/h26_main.pdf. [Accessed: 25-Jan-2019].
- [141] H. A. Rahman, Y. C. Fai, and E. S. L. Ming, “Analysis of Human Hand Kinematics: Forearm Pronation and Supination,” *J. Med. Imaging Heal. Informatics*, vol. 4, no. 2, pp. 245–249, 2014.
- [142] G. Bergmann, F. Graichen, A. Bender, M. Kääb, A. Rohlmann, and P. Westerhoff, “In vivo glenohumeral contact forces-Measurements in the first patient 7 months postoperatively,” *J. Biomech.*, vol. 40, pp. 2139–2149, 2007.
- [143] C. H. Jang *et al.*, “A survey on activities of daily living and occupations of upper extremity amputees,” *Ann. Rehabil. Med.*, vol. 35, no. 6, pp. 907–921, Dec. 2011.
- [144] J. V. Basmajian and C. J. De Luca, *Muscles Alive: Their Functions Revealed by Electromyography*, 5th ed. Baltimore: Williams and Wilkins, 1985.
- [145] X. Liu *et al.*, “Driving Assist System for Ultra-Compact EVs—Fundamental Consideration of Muscle Burden Owing to Differences in the Drivers’ Physiques,” *Actuators*, vol. 7, no. 3, 2018.
- [146] Y. Liu, Q. Liu, X. Ji, R. Hayama, T. Mizuno, and S. Nakano, “A New Objective Evaluation Method for Vehicle Steering Comfort,” *J. Dyn. Syst. Meas. Control*, vol. 139, no. 9, pp. 91010–91013, Jun. 2017.
- [147] Y. Liu, X. Ji, R. Hayama, T. Mizuno, and S. Nakano, “Method for measuring a driver’s

- steering efficiency using electromyography,” *Proc. Inst. Mech. Eng. Part D J. Automob. Eng.*, vol. 228, no. 10, pp. 1170–1184, Apr. 2014.
- [148] W. Dong, C. Zhu, Y. Wang, L. Xiao, D. Ye, and Y. Huang, “Stretchable sEMG Electrodes Conformally Laminated on Skin for Continuous Electrophysiological Monitoring,” in *Intelligent Robotics and Applications*, 2017, pp. 77–86.
- [149] D. S. Hurwitz *et al.*, “Backing collisions: a study of drivers’ eye and backing behaviour using combined rear-view camera and sensor systems,” *Inj. Prev.*, vol. 16, no. 2, pp. 79–84, Apr. 2010.
- [150] Y. Murata and K. Yoshida, “Automobile Driving Interface Using Gesture Operations for Disabled People,” *Int. J. Adv. Intell. Syst.*, vol. 6, no. 3 & 4, pp. 329–341, 2012.
- [151] M. Wada and Y. Kimura, “Stability analysis of car driving with a joystick interface,” in *2013 IEEE 4th International Conference on Cognitive Infocommunications (CogInfoCom)*, 2013, pp. 493–496.
- [152] J. Ackermann, “Robust control prevents car skidding,” *IEEE Control Syst. Mag.*, vol. 17, no. 3, pp. 23–31, 1997.
- [153] Y. Yamazaki, M. Suzuki, and T. Mano, “Pulse control during rapid isometric contractions of the elbow joint,” *Brain Res. Bull.*, vol. 34, no. 6, pp. 519–531, Jan. 1994.
- [154] S. Juds, *Photoelectric Sensors and Controls: Selection and Application*. New York: Marcel Dekker, Inc., 1988.
- [155] W. Whiting and S. Rugg, *Dynatomy with Web Resource: Dynamic Human Anatomy*. Champaign: Human Kinetics, 2006.
- [156] C. Cipriani, F. Zacccone, S. Micera, and M. C. Carrozza, “On the shared control of an EMG-controlled prosthetic hand: Analysis of user-prosthesis interaction,” *IEEE Trans. Robot.*, vol. 24, no. 1, pp. 170–184, 2008.
- [157] K. A. Kaczmarek, J. G. Webster, P. Bach-y-Rita, and W. J. Tompkins, “Electrotactile and vibrotactile displays for sensory substitution systems,” *IEEE Trans. Biomed. Eng.*, vol. 38, no. 1, pp. 1–16, 1991.
- [158] T. Dang, J. Desens, U. Franke, D. Gavrilu, L. Schäfers, and W. Ziegler, “Steering and Evasion Assist,” in *Handbook of Intelligent Vehicles*, 1st ed., A. Eskandarian, Ed. London: Springer-Verlag, 2012, pp. 760–782.
- [159] V. K. Kukkala, J. Tunnell, S. Pasricha, and T. Bradley, “Advanced Driver-Assistance Systems: A Path Toward Autonomous Vehicles,” *IEEE Consum. Electron. Mag.*, vol. 7, no. 5, pp. 18–25, 2018.
- [160] Y. Wang, Y. Liu, H. Fujimoto, and Y. Hori, “Vision-Based Lateral State Estimation for Integrated Control of Automated Vehicles Considering Multirate and Unevenly Delayed Measurements,” *IEEE/ASME Trans. Mechatronics*, vol. 23, no. 6, pp. 2619–2627, 2018.
- [161] Y. Sun and X. Yu, “An innovative nonintrusive driver assistance system for vital signal monitoring,” *IEEE J. Biomed. Heal. Informatics*, vol. 18, no. 6, pp. 1932–1939, 2014.
- [162] R. N. Scott and P. A. Parker, “Myoelectric prostheses: State of the art,” *J. Med. Eng. Technol.*, 1988.
- [163] N. U. Ahamed, K. Sundaraj, R. B. Ahmad, M. Rahman, and M. A. Islam, “Analysis of right arm biceps brachii muscle activity with varying the electrode placement on three

- male age groups during isometric contractions using a wireless EMG sensor,” *Procedia Eng.*, vol. 41, pp. 61–67, 2012.
- [164] P. D. Neilson, “Frequency-response characteristics of the tonic stretch reflexes of biceps brachii muscle in intact man,” *Med. Biol. Eng.*, vol. 10, no. 4, pp. 460–472, 1972.
- [165] N. Jiang, S. Muceli, B. Graimann, and D. Farina, “Effect of arm position on the prediction of kinematics from EMG in amputees,” *Med. Biol. Eng. Comput.*, vol. 51, no. 1–2, pp. 143–151, Feb. 2013.
- [166] I. Ruhunage, C. J. Perera, K. Nisal, J. Subodha, and T. D. Lalitharatne, “EMG signal controlled transhumeral prosthetic with EEG-SSVEP based approach for hand open/close,” in *2017 IEEE International Conference on Systems, Man, and Cybernetics (SMC)*, 2017, pp. 3169–3174.
- [167] W. D. I. G. Dasanayake, R. A. R. C. Gopura, V. P. C. Dassanayake, and G. K. I. Mann, “Surface EMG signals based elbow joint torque prediction,” in *2013 IEEE 8th International Conference on Industrial and Information Systems*, 2013, pp. 110–115.
- [168] M. B. I. Reaz, M. S. Hussain, and F. Mohd-Yasin, “Techniques of EMG signal analysis: detection, processing, classification and applications,” *Biol. Proced. Online*, vol. 8, no. 1, pp. 11–35, 2006.
- [169] G. A. Bekey, C.-W. Chang, J. Perry, and M. M. Hoffer, “Pattern recognition of multiple EMG signals applied to the description of human gait,” *Proc. IEEE*, vol. 65, no. 5, pp. 674–681, 1977.
- [170] C. J. De Luca, “The Use of Surface Electromyography in Biomechanics,” *J. Appl. Biomech.*, vol. 13, no. 2, pp. 135–163, 1997.
- [171] M. DiCicco, L. Lucas, and Y. Matsuoka, “Comparison of control strategies for an EMG controlled orthotic exoskeleton for the hand,” in *IEEE International Conference on Robotics and Automation, 2004. Proceedings. ICRA '04. 2004*, 2004, vol. 2, pp. 1622–1627 Vol.2.
- [172] P. Westerhoff *et al.*, “In vivo measurement of shoulder joint loads during activities of daily living,” *J. Biomech.*, vol. 42, no. 12, pp. 1840–1849, Aug. 2009.
- [173] O. Benderius and G. Markkula, “Evidence for a fundamental property of steering,” *Proc. Hum. Factors Ergon. Soc. Annu. Meet.*, vol. 58, no. 1, pp. 884–888, Sep. 2014.
- [174] M. Bernardi, F. Felici, M. Marchetti, F. Montellanico, M. . Piacentini, and M. Solomonow, “Force generation performance and motor unit recruitment strategy in muscles of contralateral limbs,” *J. Electromyogr. Kinesiol.*, vol. 9, no. 2, pp. 121–130, Apr. 1999.
- [175] N. U. Ahamed, Z. bin md yusof, M. Alqahtani, O. Altwijri, S. A. M. M. Rahman, and K. Sundaraj, “Gender Effects in Surface Electromyographic Activity of the Biceps Brachii Muscle During Prolonged Isometric Contraction,” *Procedia Comput. Sci.*, vol. 61, pp. 448–453, Jan. 2015.
- [176] O. Plos, S. Buisine, A. Aoussat, F. Mantelet, and C. Dumas, “A Universalist strategy for the design of Assistive Technology,” *Int. J. Ind. Ergon.*, 2012.
- [177] Z. Wang, R. Zheng, T. Kaizuka, and K. Nakano, “Relationship Between Gaze Behavior and Steering Performance for Driver–Automation Shared Control: A Driving Simulator Study,” *IEEE Trans. Intell. Veh.*, vol. 4, no. 1, pp. 154–166, Mar. 2019.

- [178] Z. Wang, R. Zheng, T. Kaizuka, K. Shimono, and K. Nakano, "The effect of a haptic guidance steering system on fatigue-related driver behavior," *IEEE Trans. Human-Machine Syst.*, 2017.
- [179] G. V. Barrett, M. Kobayashi, and B. H. Fox, "Feasibility of Studying Driver Reaction to Sudden Pedestrian Emergencies in an Automobile Simulator," *Hum. Factors J. Hum. Factors Ergon. Soc.*, 1968.
- [180] B. A. Frishberg, "An analysis of overground and treadmill sprinting," *Med. Sci. Sport. Exerc.*, vol. 15, no. 6, pp. 478–485, 1983.
- [181] S. T. Chrysler, O. Ahmad, and C. W. Schwarz, "Creating Pedestrian Crash Scenarios in a Driving Simulator Environment," *Traffic Inj. Prev.*, 2015.
- [182] A. Hac and M. D. Simpson, "Estimation of Vehicle Side Slip Angle and Yaw Rate," *SAE Trans.*, vol. 109, pp. 1032–1038, 2000.
- [183] M. Friedman, "The Use of Ranks to Avoid the Assumption of Normality Implicit in the Analysis of Variance," *J. Am. Stat. Assoc.*, vol. 32, no. 200, pp. 675–701, 1937.
- [184] M. Friedman, "A Comparison of Alternative Tests of Significance for the Problem of m Rankings," *Ann. Math. Stat.*, vol. 11, no. 1, pp. 86–92, 1940.
- [185] "COMS Catalog," 2018. [Online]. Available: http://coms.toyotabody.jp/download/pdf/coms_catalog.pdf. [Accessed: 01-Apr-2019].
- [186] M. I. Ishak, H. Ogino, and Y. Oshinoya, "Introduction on dynamic motion of opposite and parallel steering for electric vehicle," in *2013 IEEE Conference on Systems, Process & Control (ICSPC)*, 2013, pp. 73–78.
- [187] M. I. Ishak, H. Ogino, and Y. Yamamoto, "Numerical Simulation Analysis of an Oversteer In-Wheel Small Electric Vehicle Integrated with Four-Wheel Drive and Independent Steering," *Int. J. Veh. Technol.*, vol. 2016, 2016.
- [188] R. C. Dorf and R. H. Bishop, *Modern Control Systems*, 12th ed. Upper Saddle River: Pearson Education, Inc., 2011.
- [189] P. Jain and M. J. Nigam, "Design of a Model Reference Adaptive Controller Using Modified MIT Rule for a Second Order System," *Adv. Electron. Electr. Eng.*, vol. 3, no. 4, pp. 477–484, 2013.
- [190] A. A. El-samahy and M. A. Shamseldin, "Brushless DC motor tracking control using self-tuning fuzzy PID control and model reference adaptive control," *Ain Shams Eng. J.*, vol. 9, no. 3, pp. 341–352, Sep. 2018.
- [191] M. L. Janssen and G. L. Hall, *Effect of Ambient Temperature on Radial Tire Rolling Resistance*. Society of Automotive Engineers, 1980.
- [192] "National Health and Nutrition Survey." [Online]. Available: https://www.mhlw.go.jp/stf/seisakunitsuite/bunya/kenkou_iryuu/kenkou/eiyuu/h29-houkoku.html. [Accessed: 22-Mar-2019].
- [193] B. Cullinane, D. Smith, and P. Green, "Where, when, and how well people park: a phone survey and field measurements," University of Michigan, Ann Arbor, Transportation Research Institute, Ann Arbor, 2004.
- [194] S. A. Birrell, D. Wilson, C. P. Yang, G. Dhadyalla, and P. Jennings, "How driver behaviour and parking alignment affects inductive charging systems for electric vehicles," *Transp.*

Res. Part C Emerg. Technol., vol. 58, pp. 721–731, Sep. 2015.

- [195] B. L. Welch, “The Generalization of ‘Student’s’ Problem when Several Different Population Variances are Involved,” *Biometrika*, vol. 34, no. 1/2, pp. 28–35, 1947.
- [196] H.-M. Lee, P.-C. Li, S.-K. Wu, and J.-Y. You, “Analysis of Continuous Steering Movement Using a Motor-Based Quantification System,” *Sensors*, vol. 12, no. 12, pp. 16008–16023, 2012.
- [197] F. Kost, “Basic principles of vehicle dynamics,” in *Brakes, brake control and driver assistance systems: function, regulation and components*, R. Konrad, Ed. Wiesbaden: Springer Vieweg, 2014.
- [198] SAE international, “Automated Driving - Levels of Driving Automation Are Defined in New SAE International Standard J3016,” *SAE Int.*, 2016.
- [199] S. P. Marshall, “The Index of Cognitive Activity: measuring cognitive workload,” in *Proceedings of the IEEE 7th Conference on Human Factors and Power Plants*, 2002, p. 7.
- [200] D. Esposito *et al.*, “A Piezoresistive Sensor to Measure Muscle Contraction and Mechanomyography,” *Sensors*, vol. 18, no. 8, 2018.
- [201] T. Roland *et al.*, “An Insulated Flexible Sensor for Stable Electromyography Detection: Application to Prosthesis Control,” *Sensors*, vol. 19, no. 4, p. 961, Feb. 2019.